Final Report

Development of Exploratory Marine Species Density Models in the Mediterranean Sea

Submitted to and prepared for:

Naval Facilities Engineering Command Atlantic, for U.S. Fleet Forces Command, under Contract N62470-15-D-8006 (TO37) issued to HDR

Prepared by:

Laura Mannocci, Jason J. Roberts and Patrick N. Halpin
Marine Geospatial Ecology Lab, Duke University

Submitted by:

San Diego, CA

March 2018

Suggested Citation:

Mannocci L., J.J. Roberts, and P.N. Halpin. 2018. *Development of Exploratory Marine Species Density Models in the Mediterranean Sea.* Final Report. Report prepared for Naval Facilities Engineering Command, Atlantic under Contract No. N62470-15-D-8006, Task Order TO37, by the Duke University Marine Geospatial Ecology Lab, Durham, North Carolina. March 2018.

Table of Contents

Appendices

Figures

Tables

Acronyms and Abbreviations

AFTT	Atlantic Fleet Training and Testing
AIC	Akaike's information criterion
CV	coefficient of variation
ESA	Endangered Species Act
GAM	generalized additive model
km	kilometer(s)
km^2	square kilometer(s)
m	meter(s)
MMPA	Marine Mammal Protection Act
NEMO	Nucleus for European Modelling of the Ocean
NMSDD	Navy Marine Species Density Database
OPFish	ocean productivity index for fish
REML	restricted maximum likelihood
SE	standard error
SST	sea surface temperature
U.S.	United States

1. Introduction

The United States (U.S.) Navy is responsible for compliance with federal laws and regulations that apply to the marine environment and marine species, including but not limited to, the Endangered Species Act (ESA), the Marine Mammal Protection Act (MMPA), the National Environmental Policy Act, and Executive Order 12114. Specifically, and for the purposes of this document, Executive Order 12114 applies to the Global Commons (High Seas), the Foreign Nation Exclusive Economic Zone, and within Foreign Nation Territorial Seas. The ESA and the MMPA apply to the Global Commons (High Seas). As such, U.S. Navy military readiness activities that can occur on the high seas, Foreign Nation Exclusive Economic Zones, and Foreign Nation Territorial Waters throughout the globe necessitate an assessment of risk and potential impact to protected marine mammals and sea turtles.

The Navy Marine Species Density Database (NMSDD) is the authoritative source of marine species density data maintained by the U.S. Navy. These data comprise multiple sources and quality levels and are used as inputs to the Navy Acoustic Effects Model to determine the number of potential incidental "takes" of protected species.

To evaluate potential environmental impacts to marine species in regions where no density estimates exist, the U.S. Navy uses global extrapolations (Department of Navy 2012) derived from relative environmental suitability models (Kaschner et al. 2006). The relative environmental suitability models currently supporting risk assessments in the Mediterranean Sea are coarsely scaled, data deficient, and utilized under a third party license set to expire in 2020. There is a need to begin development of spatially explicit density models of cetaceans in the region to support continued risk assessments on a per-exercise basis and for future environmental compliance efforts in the region.

In a prior Mediterranean gap analysis (Mannocci et al. 2016, 2018), we examined the coverage of cetacean survey effort in geographic space, in time, and in environmental space to explore where, when, and what kind of extrapolations might be required when modeling density of cetacean species from habitat covariates. Our study revealed heterogeneous survey coverage across the Mediterranean Sea. Large data gaps were present in the eastern and southern Mediterranean in all seasons and elsewhere in non-summer months. Survey coverage was also heterogeneous in environmental space. In particular, Mediterranean waters characterized by comparatively warmer temperatures, lower productivity and higher eddy activity were poorly surveyed for cetaceans. This raised the prospect that cetacean density models fitted to environmental covariates would have to be extrapolated in order to provide predictions for the entire Mediterranean Sea.

As the next logical step of the gap analysis study, the present study aimed to develop preliminary habitat-based density estimates of cetaceans in the Mediterranean Sea. We incorporated sightings data for most of the surveys included in the gap analysis, prepared additional habitat covariates, and developed habitat-based density models following a two-stage density surface modeling approach (Miller et al. 2013). We produced density estimates of cetaceans for the entire Mediterranean Sea, along with maps of uncertainty and of the extent of interpolation *versus* extrapolation.

2. Background

2.1 The Mediterranean Sea

The Mediterranean Sea (**Figure 1**) is a semi-enclosed water body connected to the Atlantic Ocean by the Strait of Gibraltar, to the Black Sea by the Bosphorus Strait, and since 1869 to the Red Sea by the Suez Canal. It is divided into a western and an eastern basin by a central ridge between Sicily and the Tunisian-Libyan coast. The Mediterranean Sea is mainly characterized by narrow continental shelves, steep slopes and extensive abyssal plains. It includes a variety of submarine canyons, mostly located along the continental slopes in the north. It also includes approximately one hundred seamounts, known to affect the distribution of pelagic species, including cetaceans (Mussi et al. 2014; Tepsich et al. 2014; Fiori et al. 2014). The Mediterranean is an oligotrophic sea characterized by salty and nutrient-poor waters (Longhurst 2007).

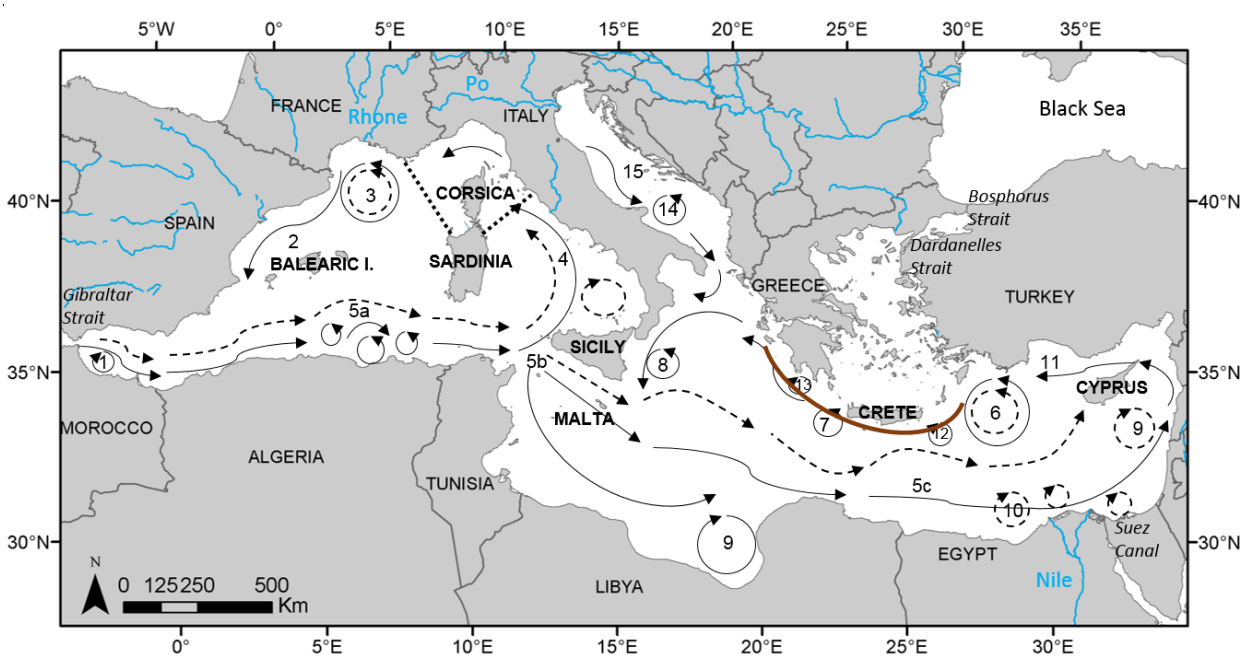

Figure 1. Map of main surface currents and gyres in the Mediterranean Sea. Dashed arrows represent summer circulation; plain arrows represent winter circulation. (1: Western Alborán gyre ; 2: Ligurian-Provençal current; 3: Lions Gyre; 4: Tyrrhenian cyclonic circulation with summer weakening and eastern anticyclone; 5a: Algerian current and eddies, 5b: Atlantic Ionian stream and 5c: mid-Mediterranean jet; 6: Rhodes gyres; 7: Western Cretan gyre; 8: Western Ionian gyre; 9: Gulf of Sirte anticyclone; 10: Shikmona and Mers a-Matruh gyres; 11: Cicilian and Asia Minor current; 12: Iera-Petra gyre; 13: Pelops gyre; 14: Southern Adriatic gyre; 15: Western Adriatic coastal current. This figure was adapted from Pinardi & Masseti (2000). The extent of the Pelagos Sanctuary is represented by black dotted lines. The location of the Hellenic trench is represented by a brown line.

Circulation in the Mediterranean Sea is mainly driven by water flow through the Strait of Gibraltar, freshwater inputs from the main rivers (Nile, and to a lesser extent, Po, Rhone and Ebro), wind stress, and thermohaline and topographic features (Pinardi & Masetti 2000). Atlantic Surface Water flows into the Mediterranean Sea through the Strait of Gibraltar and circulates in a cyclonic (counterclockwise) direction (**Figure 1**). Water flow along the southern coasts generates short-lived mesoscale anticyclonic eddies (e.g., the eddy field off Algeria). To the north, water flow creates persistent cyclonic gyres (e.g., the Lions gyre) associated with upwelling of nutrient-rich waters that result in enhanced primary productivity (Pinardi & Masetti 2000). As it moves eastward, surface water evaporates and becomes saltier, warmer and poorer in nutrients, resulting in a gradual decline in phytoplankton biomass and productivity from west to east (Bethoux & Gentili 1999; Bethoux et al. 1999). As it becomes saltier and denser, the Atlantic Surface Water sinks in the Levantine Sea, returning westward as Levantine Intermediate Water before exiting into the Atlantic through the Strait of Gibraltar. During winter, water sinks in the Aegean, Adriatic and Ligurian seas and goes to the very bottom, creating the Mediterranean Deep Water (Pinardi & Masetti 2000).

Phytoplankton biomass and primary production have marked seasonal cycles in the Mediterranean Sea (Bosc et al. 2004; D'Ortenzio & Ribera d'Alcalà 2009). Phytoplankton blooms are primarily initiated in winter and spring by wind stress, causing mixing and nutrient upwelling to surface layers. Upwelling of nutrients also occurs at cyclonic eddies. While blooms are markedly seasonal and intense in the northwestern basin (e.g., in the Gulf of Lions), they are often sporadic and subject to significant inter-annual variability in the eastern basin. Stratification occurs in summer, resulting in a lower and more homogeneous phytoplankton biomass across the Mediterranean Sea.

2.2 Mediterranean Marine Mammal Species

Eleven cetacean species and one pinniped species are known to regularly occur in the Mediterranean Sea (Notarbartolo di Sciara 2016). These species are fin whale *Balaenoptera physalus*, sperm whale *Physeter macrocephalus*, Cuvier's beaked whale *Ziphius cavirostris*, short-beaked common dolphin *Delphinus delphis*, long-finned pilot whale *Globicephala melas*, Risso's dolphin *Grampus griseus*, killer whale *Orcinus orca*, striped dolphin *Stenella coeruleoalba*, rough-toothed dolphin *Steno bredanensis*, common bottlenose dolphin *Tursiops truncatus*, the Black Sea harbor porpoise *Phocoena phocoena relicta,* and the Mediterranean monk seal *Monachus monachus*. It is likely that the Black Sea common dolphin (*Delphinus delphis ponticus*) and the Black Sea bottlenose dolphin (*Tursiops truncatus ponticus*) do not regularly enter the Mediterranean Sea, as the Turkish straits system forms a strong ecological barrier that precludes gene flow between Black Sea and Mediterranean populations (Natoli et al. 2005, 2008). All these species form Mediterranean subpopulations that are genetically distinct from their North Atlantic relatives. The Mediterranean subpopulations of four species (sperm whale, short-beaked common dolphin, the Black Sea harbor porpoise and Mediterranean monk seal) are currently listed as endangered by the International Union of Conservation of Nature.

3. Material and Methods

3.1 Study Area

At the project's inception, the U.S. Navy provided a shapefile that delineated the extent of the Mediterranean Sea and defined a polygon representing the desired study area for the project. The U.S. Navy also provided a point shapefile that identified four ports of critical interest to the Navy: Augusta Bay (Sicily), Gaeta (Italy), Gibraltar (United Kingdom), and Souda Bay (Crete). Starting with these features, we defined the spatial extent of our analysis, as follows.

First, we manually edited the study area polygon to split off gulfs, estuaries, and other inshore areas where the literature (or our expert judgment, when no literature was available) suggested either that cetaceans were absent or that distinct populations were likely present that should not be modeled from surveys conducted in broader Mediterranean waters. For these "specially handled" areas in the NMSDD, we either set density to zero (based on the literature or expert opinion), to null (when it was not tractable to obtain density estimates within the scope of this project, e.g., for the Sea of Marmara), or to an estimate derived from an external study. For example, the U.S. Sounds Navy's polygon included the Gulf of Corinth, an area reported to be inhabited by genetically distinct populations of striped and short-beaked common dolphins (Bearzi et al. 2016). We split the Gulf of Corinth from the broader Mediterranean and obtained species density estimates from a recent photographic capture-recapture analysis specifically for this area (Bearzi et al. 2016). External estimates such as these are 'stitched' into the density surface for a given species, rather than combined with the predicted density surface. This is consistent with density modeling for other regions within the NSMDD, and with the U.S. Navy's hierarchical approach to data inclusion in the NMSDD (**Figure 2**). Any uncertainty reported is from the study cited.

Figures 3 through **8** show the areas that were spatially extrapolated or handled specially. For the specially handled areas, the polygon attributes of the NMSDD specify how density was assigned for each area.[1]

[1] In the NMSDD, for each polygon, the MODEL_TYPE attribute indicates whether density was predicted by a model ("Habitat-based density model"), extrapolated spatially ("Spatial extrapolation"), or handled specially for that area (e.g., "Assumed absent" or "External study"). When predicted by a model, the UNCER_QUAL attribute indicates whether all environmental covariates at that location and time were within the sampled ranges used to fit the model, or whether one or covariates fell outside the sampled ranges, requiring an "environmental extrapolation". In subsequent sections of this document, we refer to these two cases as "interpolation" vs. "extrapolation". But when a polygon was predicted by "spatial extrapolation", a focal mean statistic was used obtain the mean density of nearby polygons predicted by a habitat-based model. Similarly, UNCER_QUAL was computed by a focal majority statistic; thus for spatially-extrapolated polygons, it indicates whether the majority of nearby model-predicted polygons required environmental extrapolation.

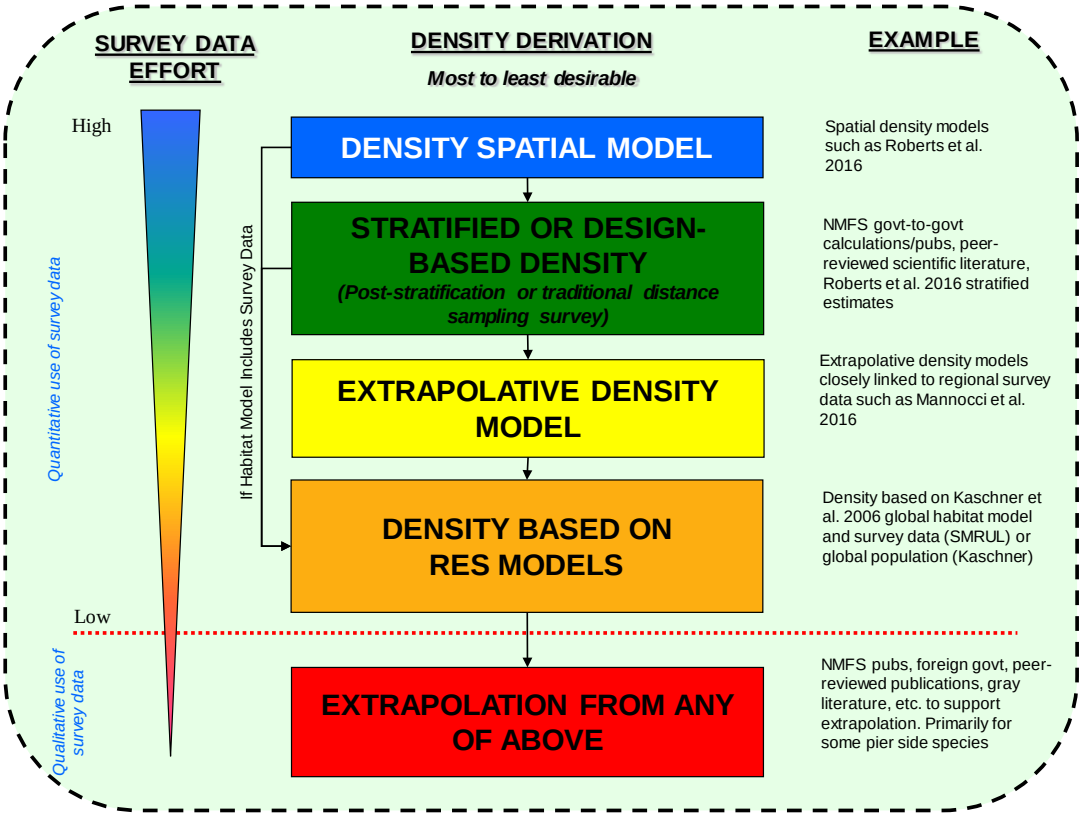

Figure 2. Phase II NMSDD hierarchy for data inclusion.

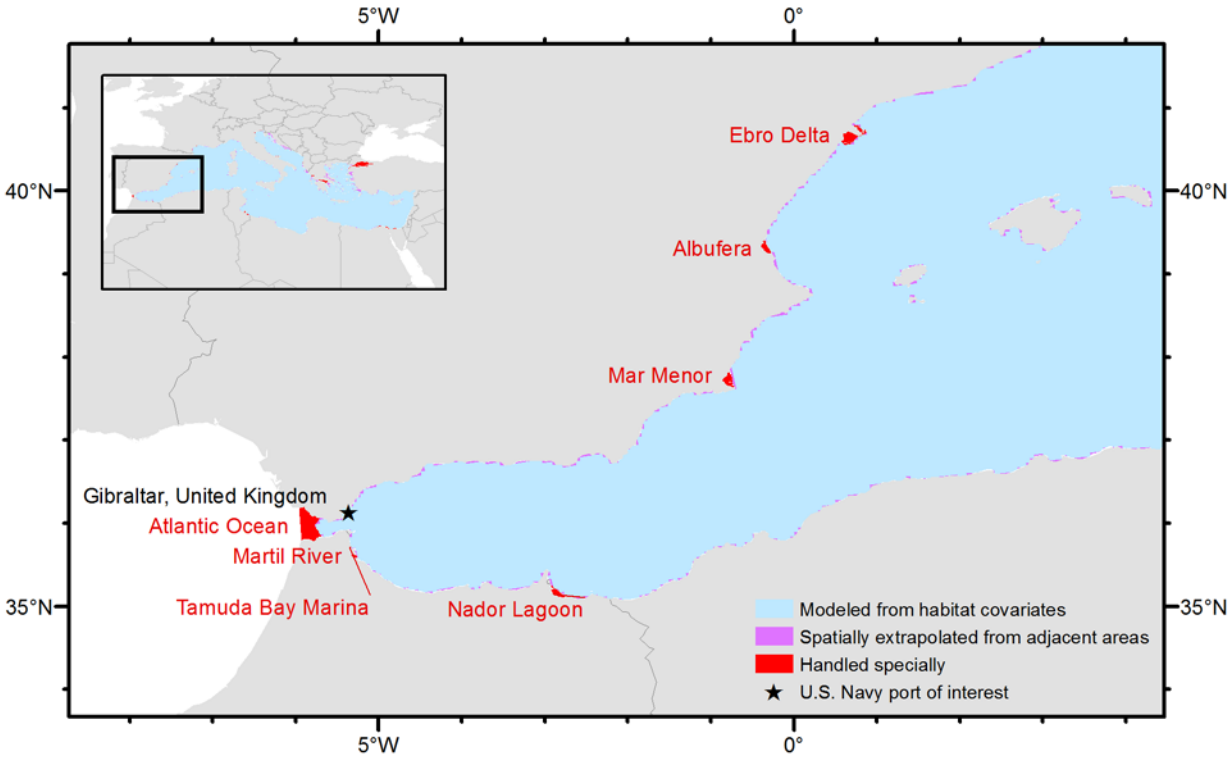

Figure 3. Areas in the southwest part of the original U.S. Navy Mediterranean study area that were modeled from habitat covariates, handled specially, or spatially extrapolated.

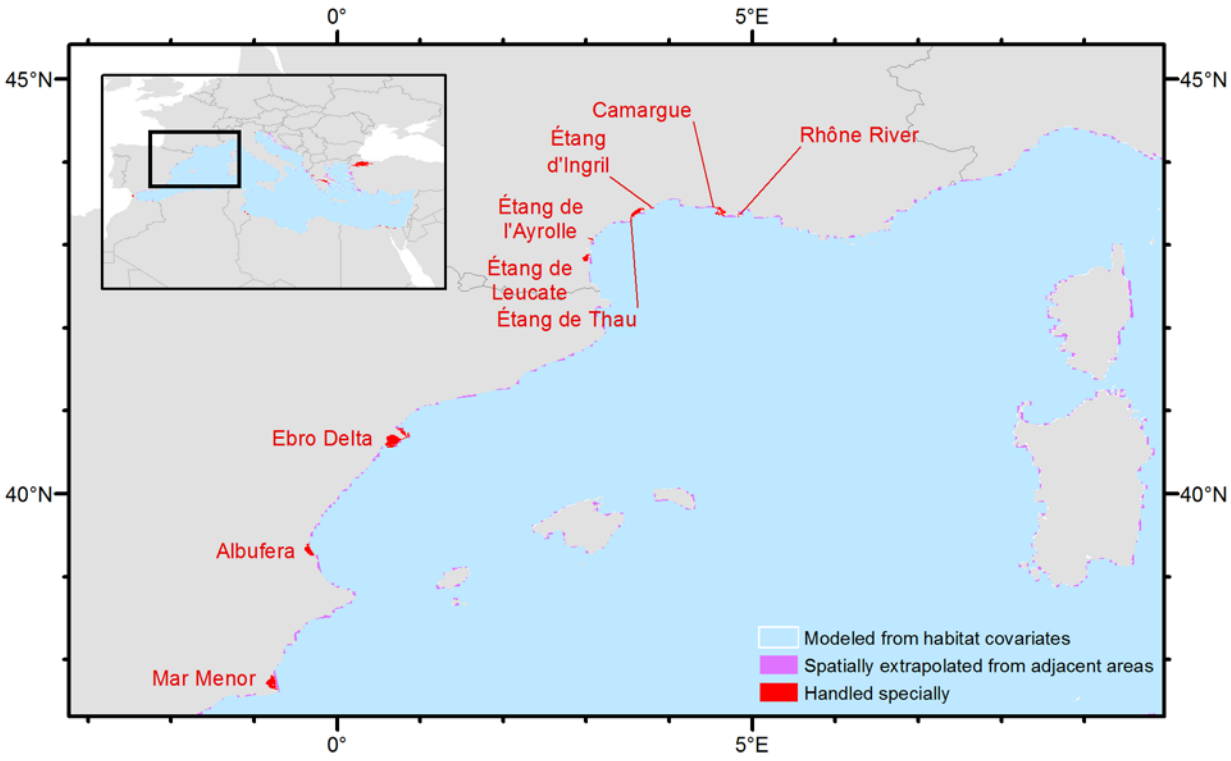

Figure 4. Areas in the northwest part of the original U.S. Navy Mediterranean study area that were modeled from habitat covariates, handled specially, or spatially extrapolated.

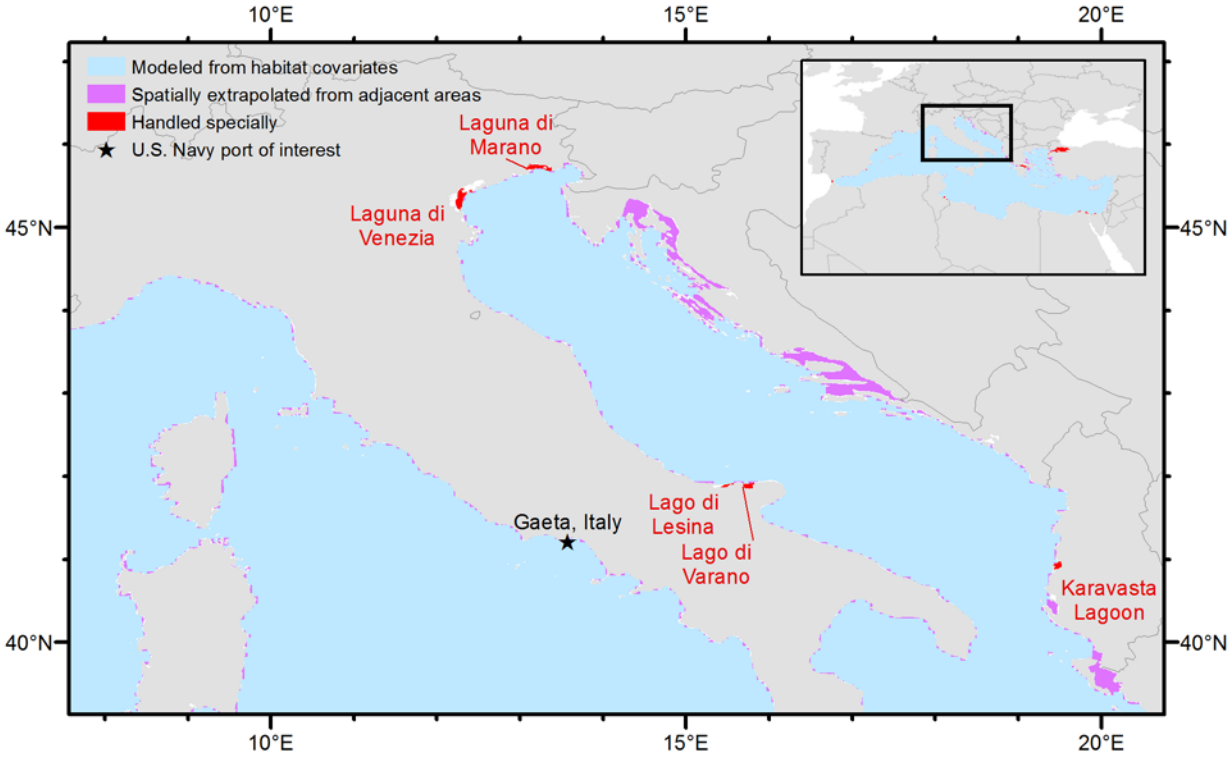

Figure 5. Areas in the north-central part of the original U.S. Navy Mediterranean study area that were modeled from habitat covariates, handled specially, or spatially extrapolated.

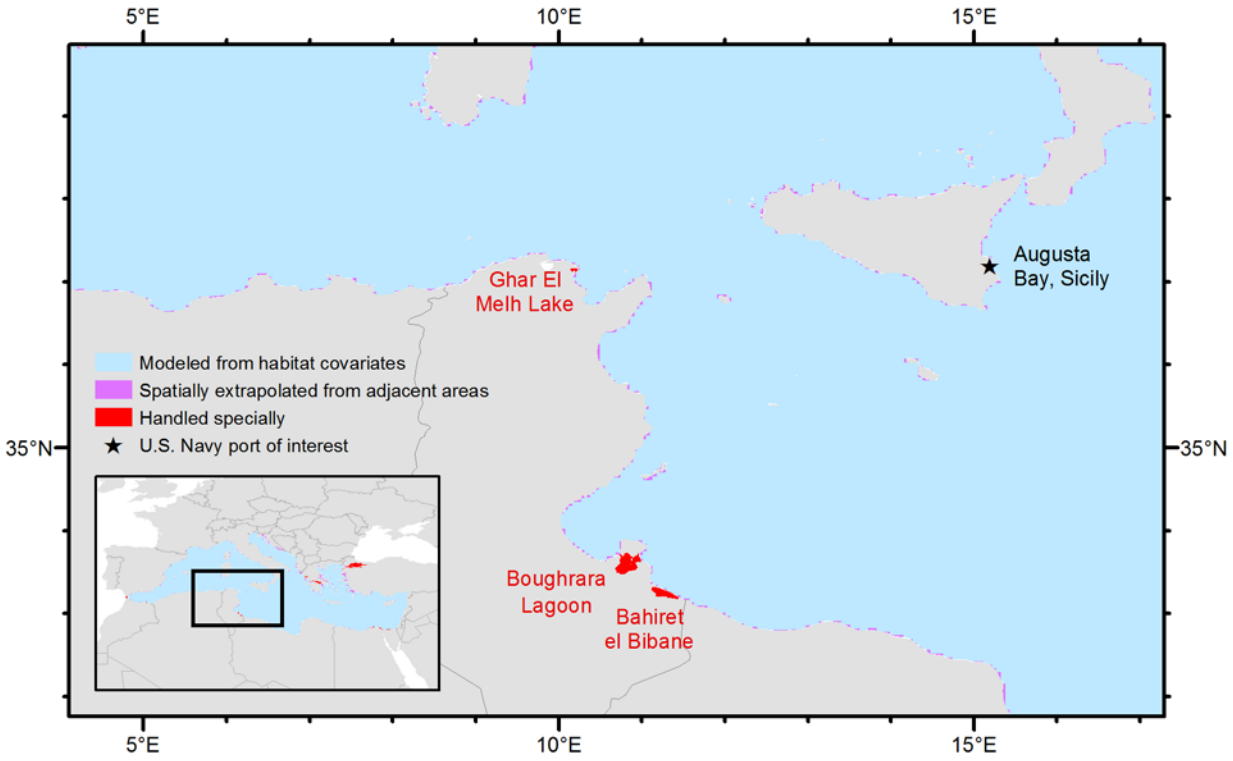

Figure 6. Areas in the south-central part of the original U.S. Navy Mediterranean study area that were modeled from habitat covariates, handled specially, or spatially extrapolated.

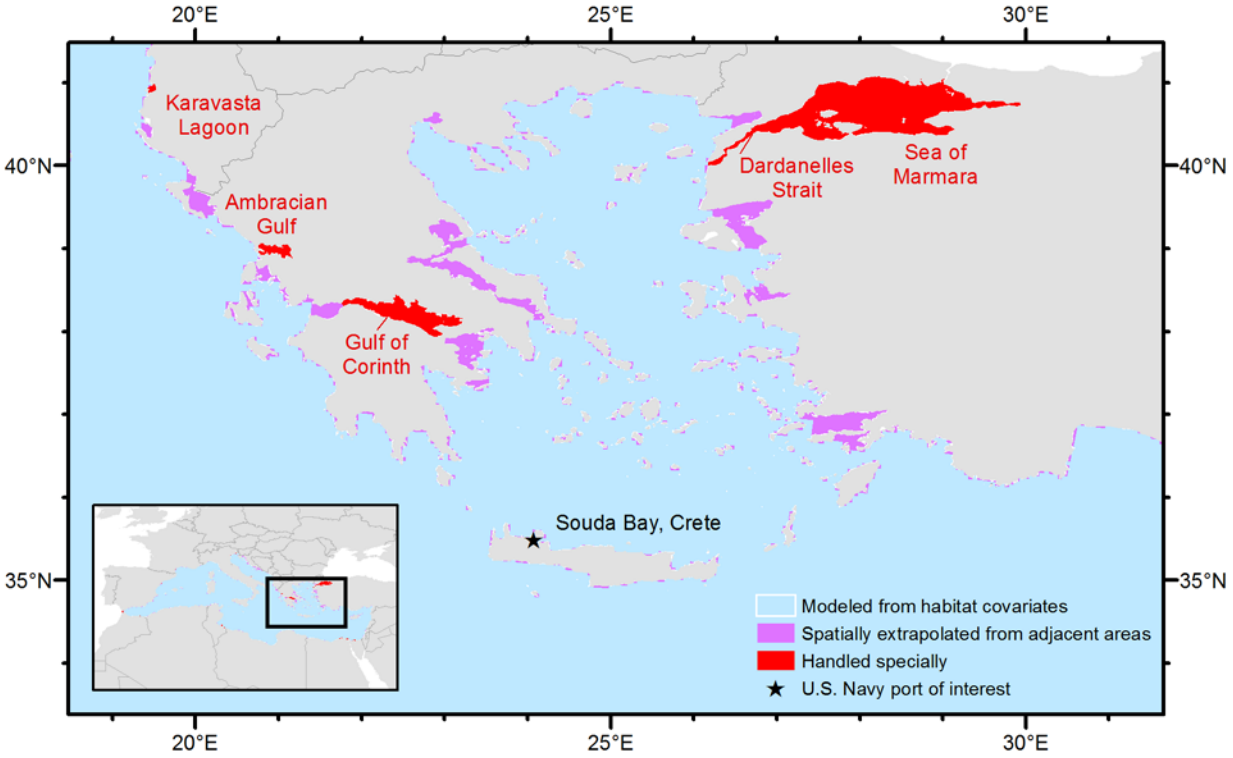

Figure 7. Areas in the northeast part of the original U.S. Navy Mediterranean study area that were modeled from habitat covariates, handled specially, or spatially extrapolated.

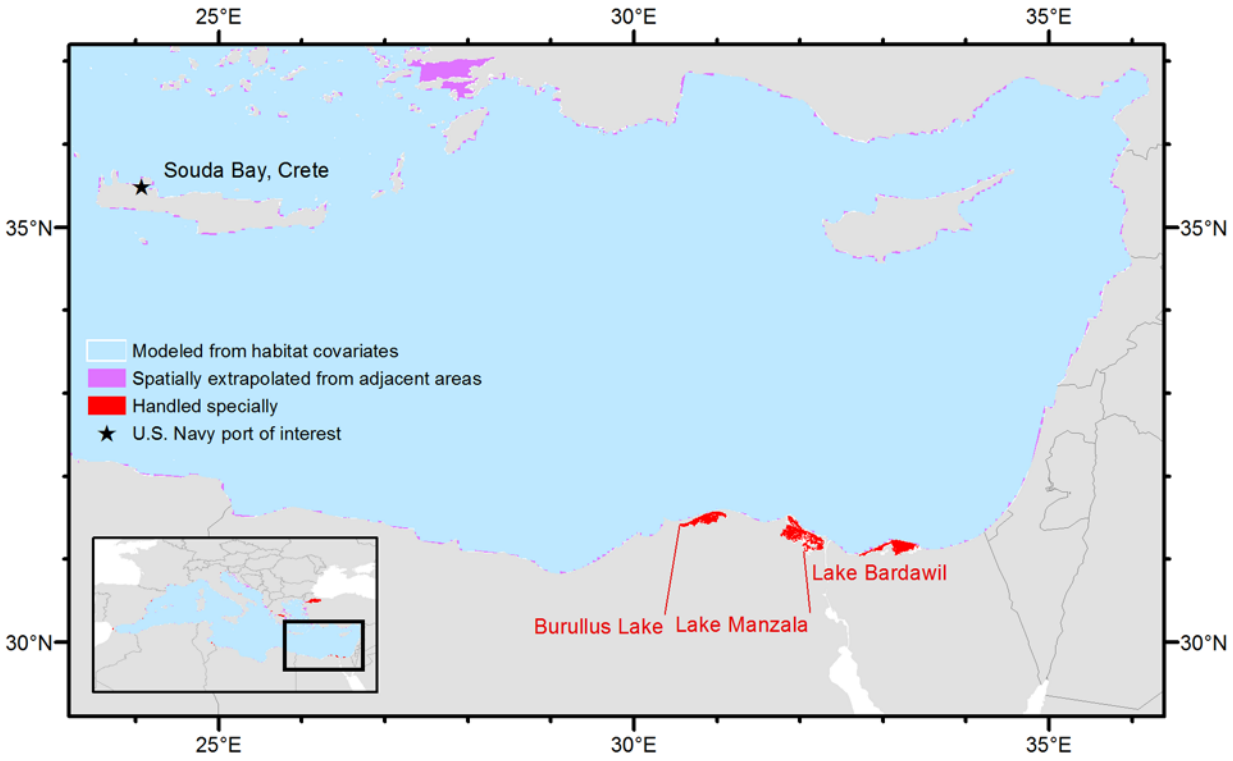

Figure 8. Areas in the southeast part of the original U.S. Navy Mediterranean study area that were modeled from habitat covariates, handled specially, or spatially extrapolated.

Next, after reviewing the available environmental covariates suitable for building habitat-based cetacean density models, we further split the remaining Mediterranean Sea polygon into areas where habitat covariates were available and areas where they were not. In general, habitat covariates were available throughout the Mediterranean Sea except for inshore areas of the northeastern Adriatic Sea (**Figure 5**), and the coastlines of Albania, Greece, and Turkey (**Figure 7**). (We suspect that the complex topography of these areas makes satellite remote sensing and oceanographic modeling of these areas particularly difficult.) Unable to predict density in these areas due to a lack of habitat covariates, we instead extrapolated density estimates from adjacent cells using a focal mean statistic (a 3 × 3 moving window), as was done for similar areas for the Navy's Atlantic Fleet Training and Testing (AFTT) study area (Roberts et al. 2015).

Finally, we projected the subdivided study area to a custom Lambert Azimuthal Equal Area coordinate system and gridded it into 5 × 5 kilometer (km) square cells. This 5 km spatial resolution represented a compromise between resolutions of available covariate products, which ranged from 30 arc seconds (approximately 500 meters [m]) to 0.2°(approximately 20 km), and allowed resolution of the complex topography of the Mediterranean Sea.

3.2 Survey Data Processing

The Mediterranean Sea has never been comprehensively surveyed with line-transect methods by a single organization. Prior to modeling, we performed a gap analysis that identified aerial and shipboard line-transect surveys conducted in the Mediterranean Sea since 1997 (Mannocci et al. 2016, 2018). This study identified 302,481 km of line-transect effort conducted by many

teams under the auspices of 12 surveyor organizations with whom we established collaborations. Following the gap analysis, we proposed to pool the surveys and build basin-wide density models. Most collaborators agreed and submitted the additional data required for density modeling. Ultimately we were able to utilize data from seven organizations, comprising roughly two-thirds of the survey effort identified in the gap analysis (see **Section 3.3** [Survey Data Summary] for details).

Starting from provider-specific text files, spreadsheets, and databases, we transformed all survey data into a common format, imported it into a single geodatabase, and manually reviewed and cleaned each day of survey effort. While all collaborators utilized generally similar survey protocols, the data collected by and format used by each collaborator differed, requiring provider-specific treatments in all cases. All data providers utilized satellite global positioning systems, and in most cases we were able to reconstruct survey tracklines, but the degree of precision depended on how frequently data providers reported positions. In general, most aerial surveys reported positions several times per minute, with some as frequently as every 4 seconds. Most shipboard surveys reported positions several times per hour, with some as frequently as once per minute.

All collaborators reported the minimum information necessary to estimate density via distance sampling methodology (Buckland et al. 2001), including the time, location, species, and group size of the sighting, as well as the perpendicular distance to the animal(s) from the trackline or the information needed to calculate this distance. Most collaborators also reported one or more covariates related to the probability of making a sighting, such as an assessment of the sea state, presence of sun glare, water turbidity, and so on. When such covariates were reliably recorded, we retained them and utilized them in detection modelling (described in the following sections).

After all surveys were processed, we aggregated all survey transects where observers were reported to be “on effort” and split them into segments. We sought to obtain segments of 5 km in length, matching the spatial resolution of the analysis, following the procedure of Roberts et al. (2016). That is, for each survey, we first iterated through the sequence of points that defined the transects, finding sections of continuous survey effort, defined as a sequence of effort points for which there were no off-effort gaps of 1 hour or more and no stretch of 7.5 km for which one-third or more of it was off-effort. We then split each continuous section into equal-length on-effort segments, as follows.

First, we computed the number of segments, n, for the continuous section by dividing its length by 5 km using integer division. Then, if the remainder was less than 2.5 km, we split the continuous section into n equal-length segments slightly longer than 5 km. Otherwise, we increased the number of segments by 1, resulting in n+1 equal-length segments slightly shorter than 5 km. For example, a 22 km continuous section would be split into 4 segments of 5.5 km, while a 23 km continuous section would be split into 5 segments of 4.6 km.

For the Alnitak/Alnilam surveys, our collaborators provided already-constructed segments which could not be decomposed and reconstructed into new segments using the information provided to us. For these surveys, we did not apply our segmenting procedure but instead utilized the already-constructed segments.

For the period for which spatial models were fitted, 1999–2016, the segmenting procedure applied to surveys other than Alnitak/Alnilam yielded 31,317 segments, with a mean length of 4.997 km (SD=0.194 km), a maximum length of 7.468 km, and a minimum length of 0.260 km. Of these, 8 were less than 1 km long. For the same period, the Alnitak/Alnilam surveys contributed 11,865 already-constructed segments, with a mean length of 3.548 km (SD=0.806 km), a maximum length of 9.217 km, and a minimum length of 0.035 km. Of these, 188 were less than 1 km long. Combining all surveys yielded 43,182 segments with a mean length of 4.598 km (SD=0.790 km).

3.3 Survey Data Summary

3.3.1 Overview of effort data

We incorporated line-transect surveys from seven survey organizations (**Table 1**). Line-transect surveys represented 166,333 km of effort, of which 117,929 km were achieved by aerial surveys and 80,644 km, by shipboard surveys. Survey effort was concentrated in the northwestern and central Mediterranean and was patchy in the eastern and southern Mediterranean (**Figure 9**).

Table 1. Total effort of line-transect surveys incorporated in density models of cetaceans

Surveyor	Platform	Surveyed subregion	Surveyed years	Effort (km)
PELAGIS	Aerial	Algero-Provençal basin, Tyrrhenian Sea/eastern Ligurian Sea	2011, 2012	32,240
TETHYS/ISPRA	Aerial	Algero-Provençal basin, Tyrrhenian Sea/eastern Ligurian Sea, Ionian Sea	2009–2011, 2013, 2014, 2016	61,996
BWI/ISPRA	Aerial	Adriatic Sea	2010, 2013	16,595
University of Valencia	Aerial	Algero-Provençal Basin	2010, 2011, 2013	7,098
Alnitak/Alnilam	Shipboard	Alborán Sea/Strait of Gibraltar	1999–2011	42,094
EcoOcean Institute	Shipboard	Algero-Provençal Basin	1999–2001, 2005-2015	31,537
IFAW/MCR	Shipboard	All subregions but the Adriatic Sea	2003, 2004, 2005, 2007, 2013	7,013
			TOTAL:	**166,333**

BWI: Blue World Institute; ISPRA = Italian National Institute for Environmental Protection and Research; IFAW = International Fund for Animal Welfare; MCR = Marine Conservation Research; U = University

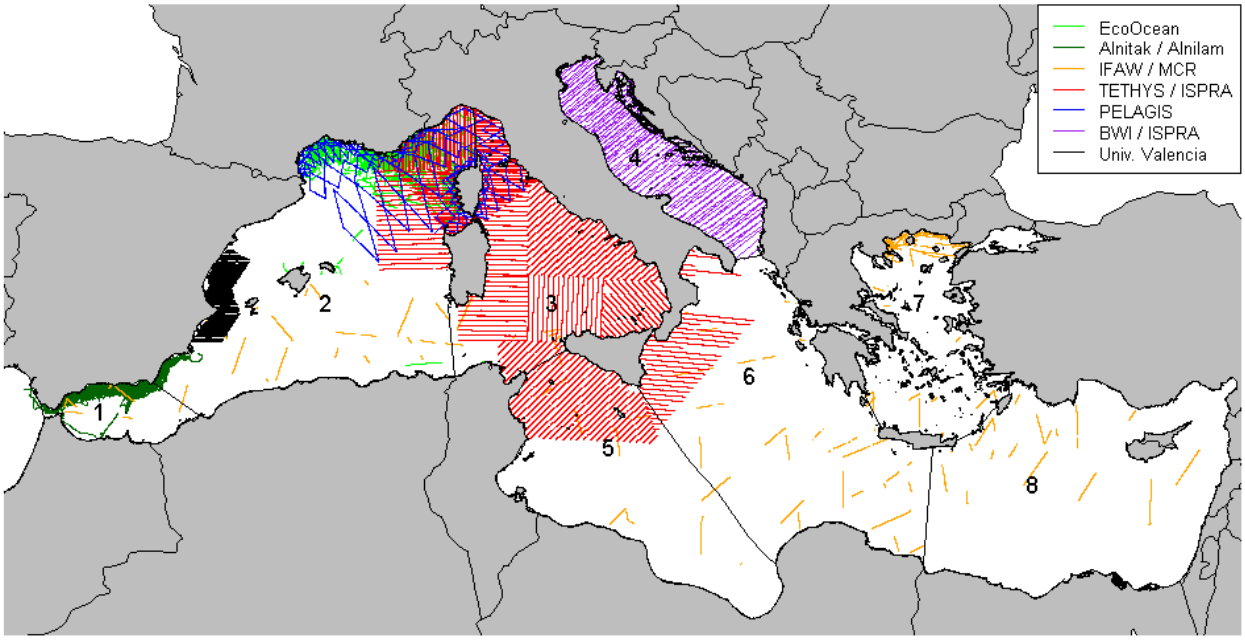

Figure 9. Line-transect surveys incorporated in cetacean density models color-coded by surveyor. Numbered subregions are overlaid: (1) Alborán Sea/Strait of Gibraltar, (2) Algero-Provençal Basin, (3) Tyrrhenian Sea/eastern Ligurian Sea, (4) Adriatic Sea, (5) Strait of Sicily/Tunisian Plateau/Gulf of Sirte, (6) Ionian Sea/Central Mediterranean, (7) Aegean Sea, and (8) Levantine Sea.

In terms of inter-annual survey coverage, survey effort increased in 2009 when aerial surveys were initiated (**Figure 10**). Survey effort was exceptionally low in 2015. The northern Alborán Sea and western Ligurian Sea received coverage in multiple years owing to long-term shipboard survey efforts (**Figure 11**).

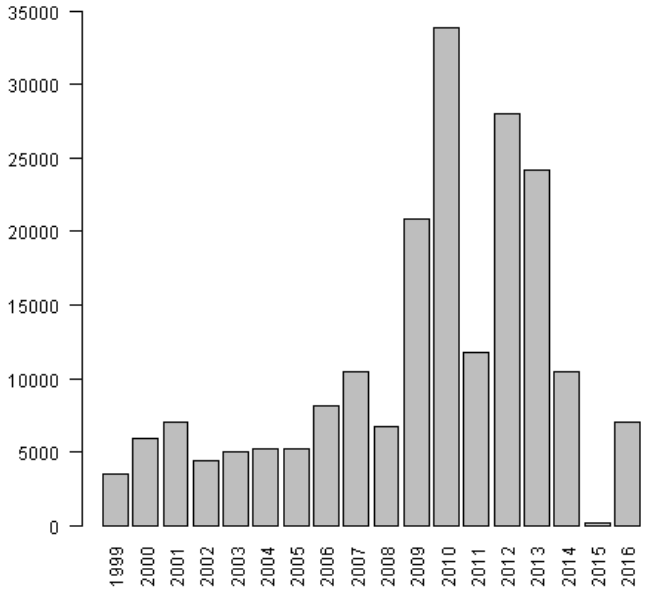

Figure 10. Total survey effort (kilometers) per year available in the entire Mediterranean Sea for the 1999–2016 study period.

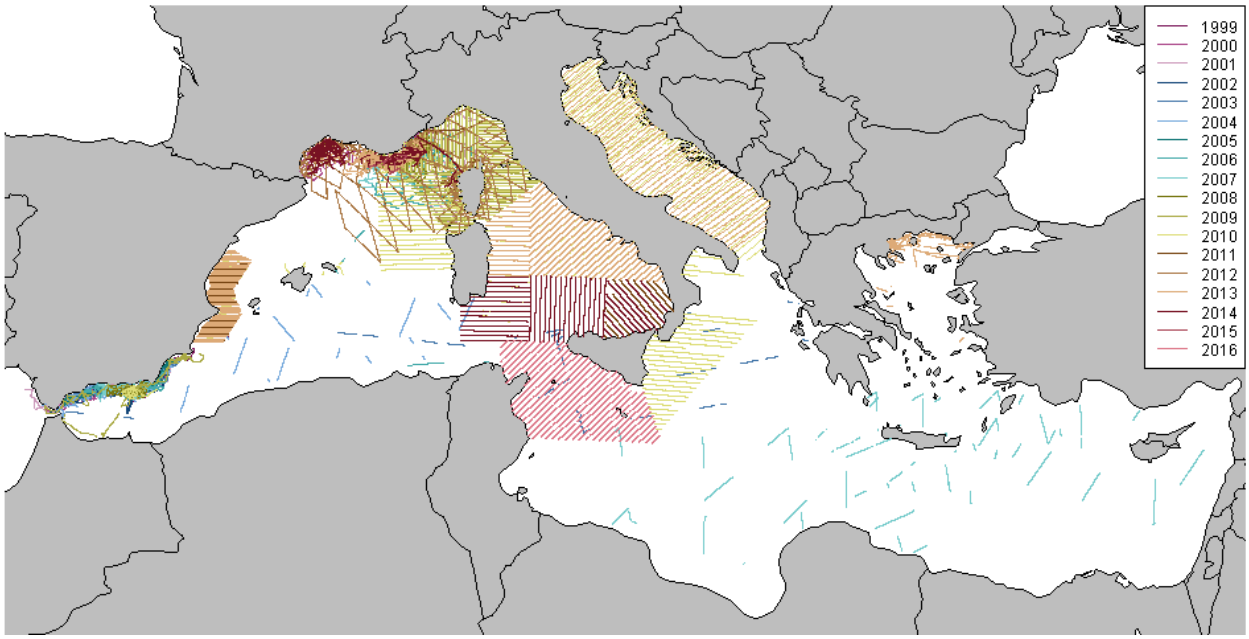

Figure 11. Line-transect surveys incorporated in cetacean density models color-coded by year.

In terms of seasonal survey coverage, the amount of survey effort was larger in summer (maximum in July) with a secondary peak in January (**Figure 12**). Survey effort was comparatively low in the spring and fall. The eastern basin was only surveyed in summer and fall (**Figure 13**). The Adriatic Sea was only surveyed in summer.

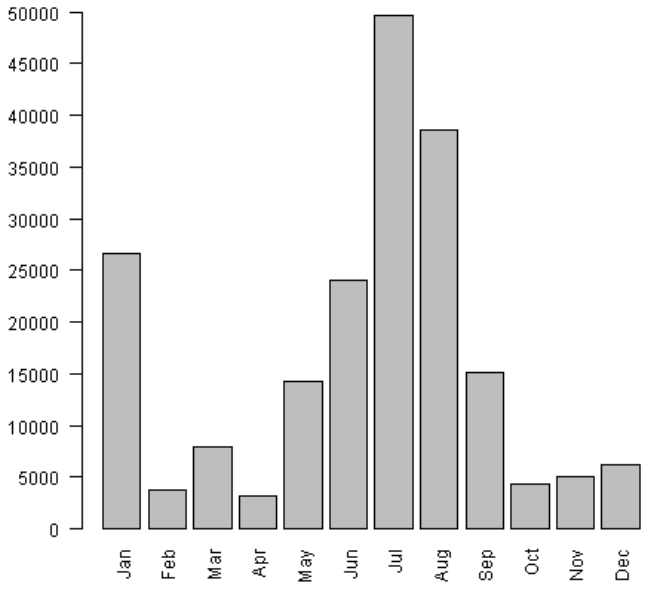

Figure 12. Total survey effort (kilometers) per month available in the entire Mediterranean Sea for the 1999–2016 study period.

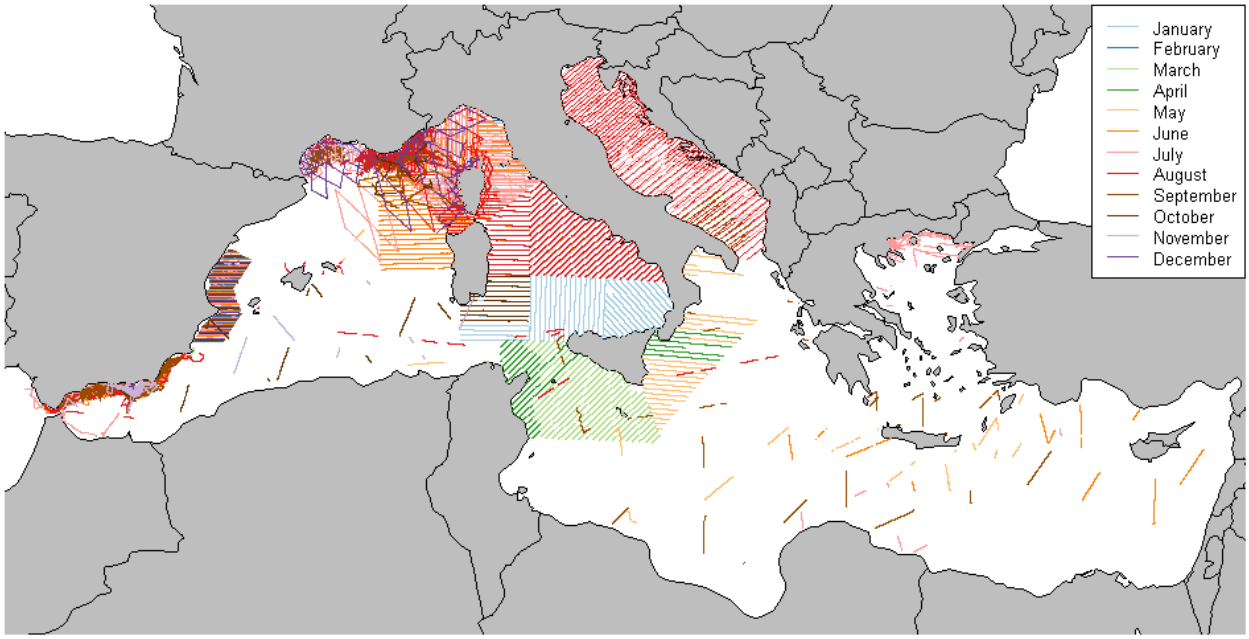

Figure 13. Line-transect surveys incorporated in cetacean density models color-coded by month.

Surveys from five other survey organizations that were incorporated in the gap analysis could not be incorporated in density models because sightings data were unavailable or missed important information. These surveys are listed in **Table 2**.

Pelagos Cetacean Research Institute, SUBMON and the University of Malta contributed partial (effort-only) data for this gap analysis. The Pelagos Cetacean Research Institute surveys span the eastern Ionian Sea (including the Hellenic Trench), an area that has not been surveyed by other organizations. The SUBMON surveys encompass areas of the Ligurian-Provençal current and the Balearic Islands that have been poorly surveyed by other organizations. The University of Malta surveys span the Maltese Islands in all seasons. In the data we incorporated (one TETHYS-ISPRA survey), the majority of survey effort in the Maltese Islands occurred in the spring of 2016. Incorporating these datasets in future density models, if and when the data become available, would therefore improve coverage in underrepresented areas and seasons.

INSTM and IMMRAC contributed sightings but the associated data lacked important information for density modeling. Given this, the comparatively small amount of effort represented by these surveys, and the lack of sufficient sightings to model detectability well for the vessels they used (small motor boats), we decided to defer them to future modelling efforts.

Table 2. Total effort of line-transect surveys that could not be incorporated in density models of cetaceans.

Surveyor	Platform	Surveyed subregion	Years	Effort (km)
Pelagos Cetacean Research Institute	Shipboard	Ionian Sea/Central Mediterranean and Aegean Sea	2001–2014	16,742
SUBMON	Shipboard	Algero-Provençal Basin	2010, 2011, 2015	2,951
University of Malta	Shipboard and aerial	Strait of Sicily/Tunisian Plateau/Gulf of Sirte	1998–2015	24,704
INSTM	Shipboard	Strait of Sicily/Tunisian Plateau/Gulf of Sirte	2001, 2003, 2005	2,352
IMMRAC	Shipboard	Levantine Sea	2005	1,458
			TOTAL:	**48,207**

IMMRAC = Israel Marine Mammal Research and Assistance Center; INSTM = Institut National des Sciences et Technologies de la Mer ; U = University

3.3.2 Overview of Sightings Data

The incorporated line-transect surveys provided sightings for 10 species of cetaceans (**Table 3**). Ambiguous sightings (i.e., sightings that were not identified to the species level) were not used in the density models, except in two cases: (1) three sightings of unidentified Balaenopterids were assigned to the fin whale group following advice of the PELAGIS Observatory, and (2) all 51 sightings of unidentified Ziphiidae were assigned to Cuvier's beaked whale, which is the most frequently observed beaked whale species in the Mediterranean Sea. Ambiguous sightings of dolphins could not be incorporated in the density models, causing a downward bias in density estimation (in the future we propose to classify these sightings to the species level; see **Section 5.3**, Future work).

Striped dolphin was by far the most frequently sighted species, followed by common bottlenose dolphin. Sightings were generally most numerous in summer months, reflecting the large amount of effort in these months (**Table 4**). Maps of sighting distributions and group sizes for each species are provided in **Figures 14 through 23**.

Habitat-based density models were developed for all species except killer whale and the Black Sea harbor porpoise for which 10 or fewer sightings were recorded by the incorporated surveys.

Table 3. Number of usable sightings for density modeling. Ambiguous sightings not identified to the species level appear in bold at the end of the table. For density modeling, 3 sightings of unidentified Balaenopterids were assigned to fin whale and all 51 sightings of unidentified Ziphiidae were assigned to Cuvier's beaked whale.

Species or species group	Sighting number
Striped dolphin	3,364
Common bottlenose dolphin	743
Short-beaked common dolphin	902
Killer whale	2
Risso's dolphin	150
Long-finned pilot whale	452
Black Sea harbor porpoise	10
Fin whale	384
Sperm whale	113
Cuvier's beaked whale	17
Short beaked common dolphin or striped dolphin	**126**
Short beaked common dolphin or striped dolphin or common bottlenose dolphin	**112**
Unidentified Delphinid	**402**
Unidentified Balaenopterid	**14**
Unidentified Ziphiid	**51**
Unidentified cetacean	**9**

Table 4. Number of usable sightings for density modeling per month.

Species or species group	Jan	Feb	Mar	Apr	May	Jun	Jul	Aug	Sep	Oct	Nov	Dec
Striped dolphin	421	63	111	45	153	462	889	606	440	79	57	38
Common bottlenose dolphin	68	1	47	14	21	49	199	196	100	10	17	21
Short-beaked common dolphin	26	0	24	5	2	138	304	143	197	3	60	0
Killer whale	0	0	0	0	0	1	1	0	0	0	0	0
Risso's dolphin	22	2	4	3	8	17	30	33	19	7	1	4
Long-finned pilot whale	19	0	15	1	1	77	123	85	111	4	14	2
Black harbor porpoise	0	0	0	0	0	0	10	0	0	0	0	0
Fin whale	8	3	3	5	25	75	127	99	29	8	3	5
Sperm whale	2	1	2	0	1	18	40	34	9	2	0	4
Cuvier's beaked whale	6	0	0	0	1	11	17	12	15	2	4	0

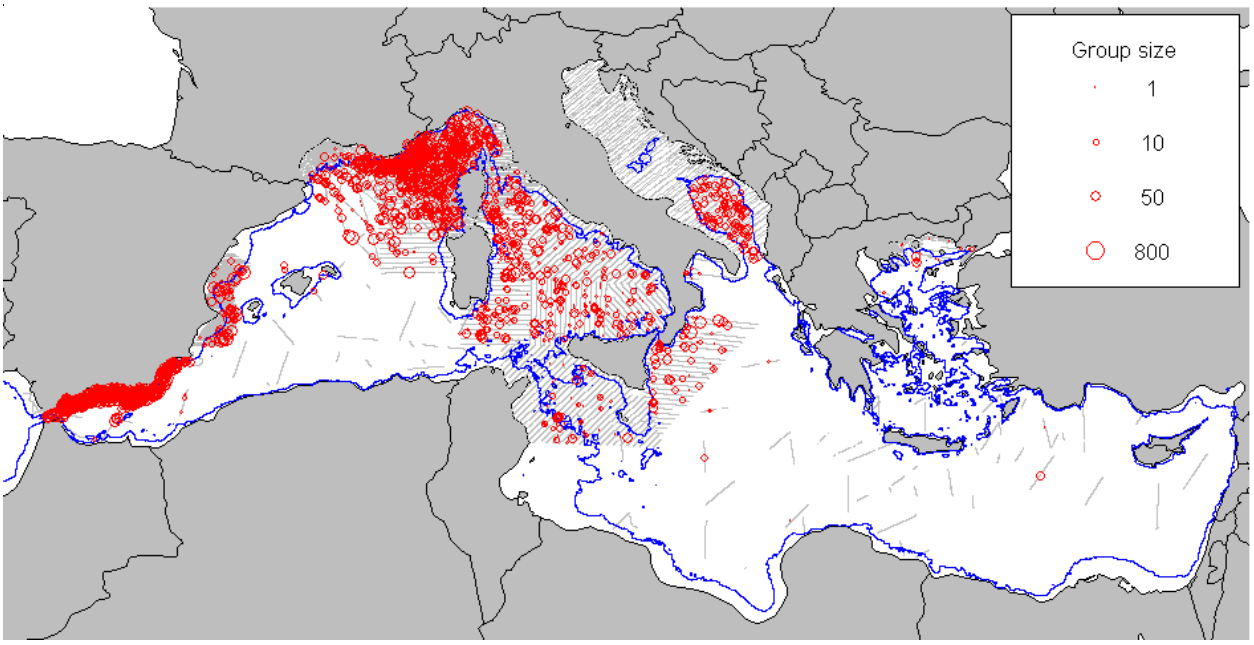

Figure 14. All usable sightings of striped dolphins reported from the incorporated surveys in the Mediterranean study area. Survey tracklines are shown in grey. The 200 m isobath is shown in blue. Striped dolphins were seen in offshore and slope waters throughout surveyed areas.

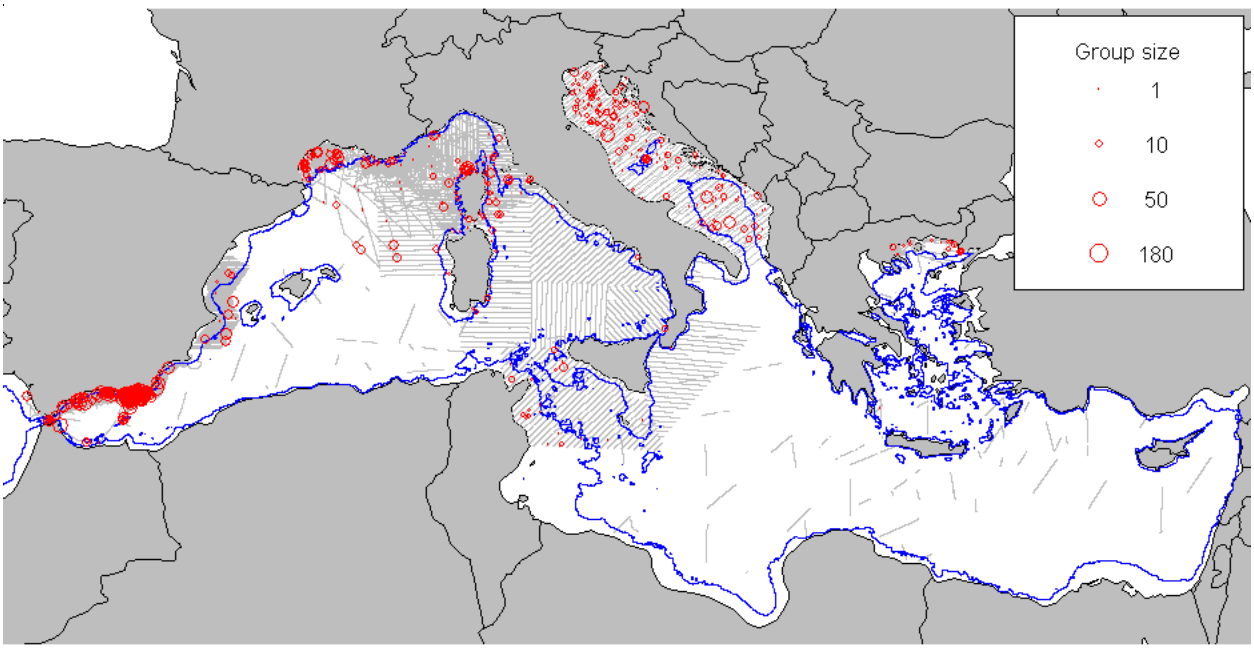

Figure 15. All usable sightings of common bottlenose dolphins reported from the incorporated surveys in the Mediterranean study area. Survey tracklines are shown in grey. The 200 m isobath is shown in blue. Common bottlenose dolphins were seen on the continental shelf throughout surveyed regions. Sightings were rarest offshore.

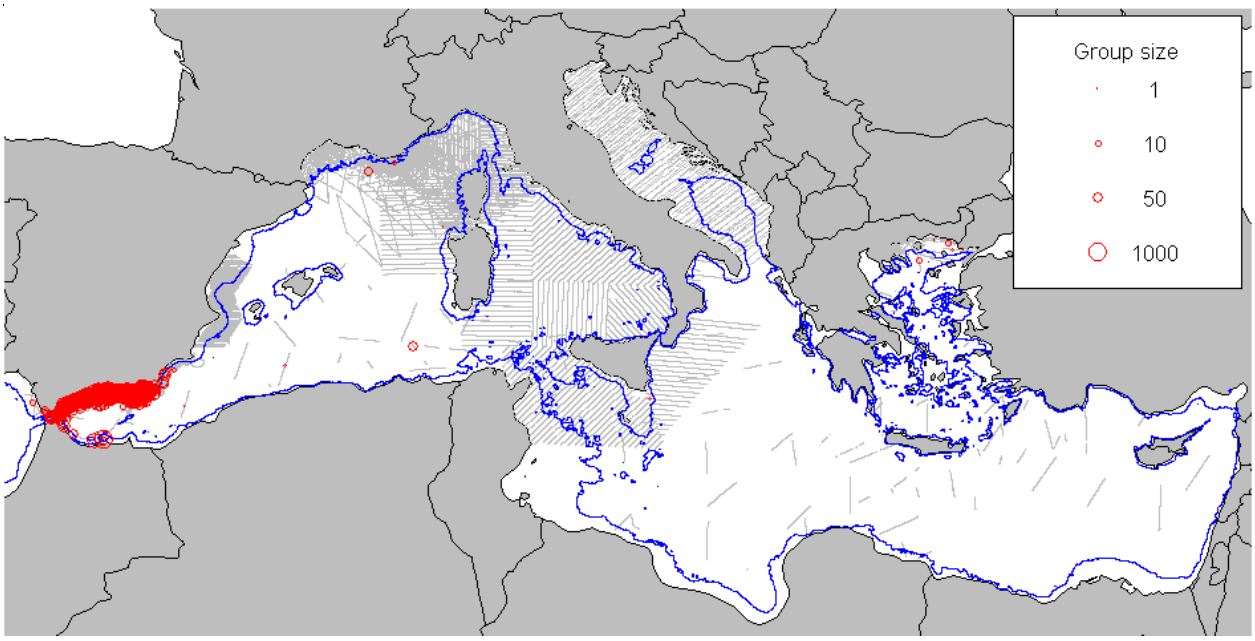

Figure 16. All usable sightings of short-beaked common dolphins reported from the incorporated surveys in the Mediterranean study area. Survey tracklines are shown in grey. The 200 m isobath is shown in blue. Short-beaked common dolphins were seen primarily in the Alborán Sea, and northern Aegean Sea. Rare sightings were made in offshore waters of the western basin.

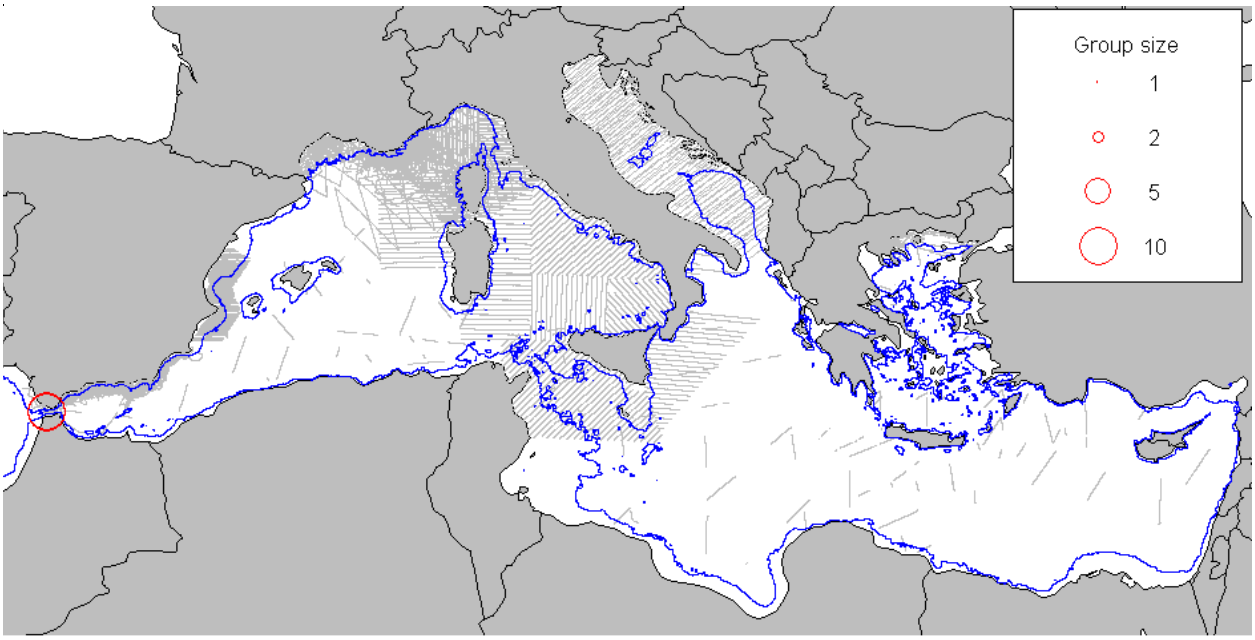

Figure 17. All usable sightings of killer whales reported from the incorporated surveys in the Mediterranean study area. Survey tracklines are shown in grey. The 200 m isobath is shown in blue. Killer whales were sighted only in the strait of Gibraltar. This species was not modeled.

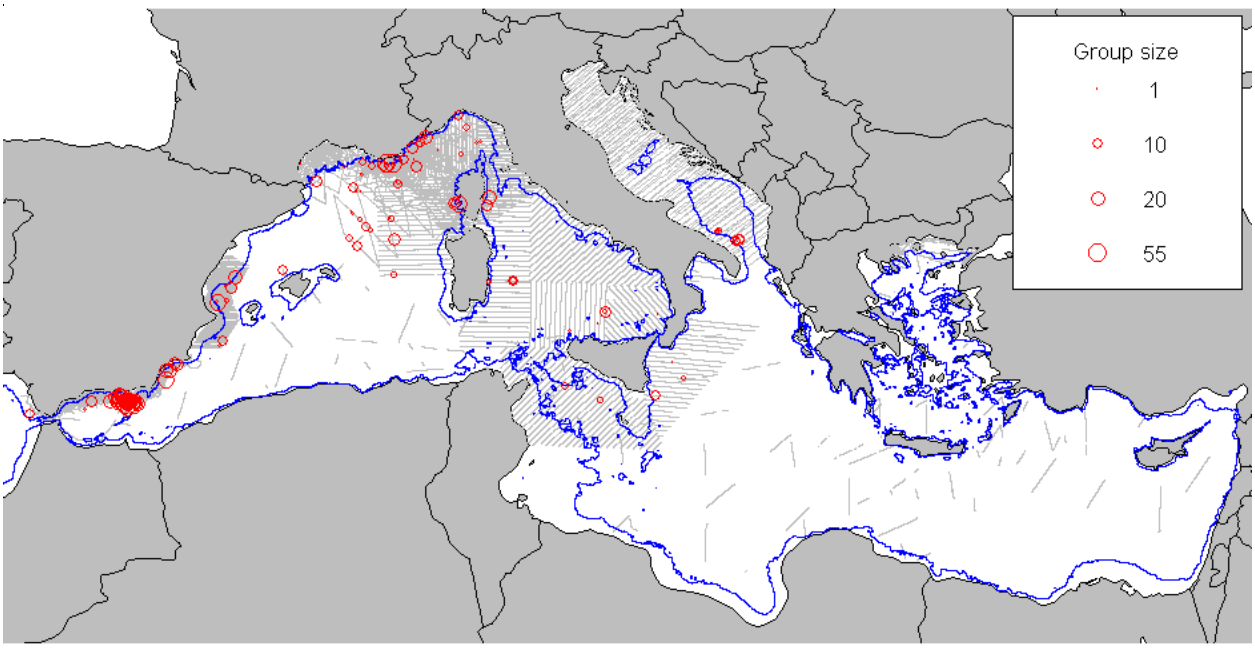

Figure 18. All usable sightings of Risso's dolphins reported from the incorporated surveys in the Mediterranean study area. Survey tracklines are shown in grey. The 200 m isobath is shown in blue. Risso's dolphins were seen on the continental slope and farther offshore in the western and central Mediterranean. No sightings were reported east of the Adriatic Sea by available surveys.

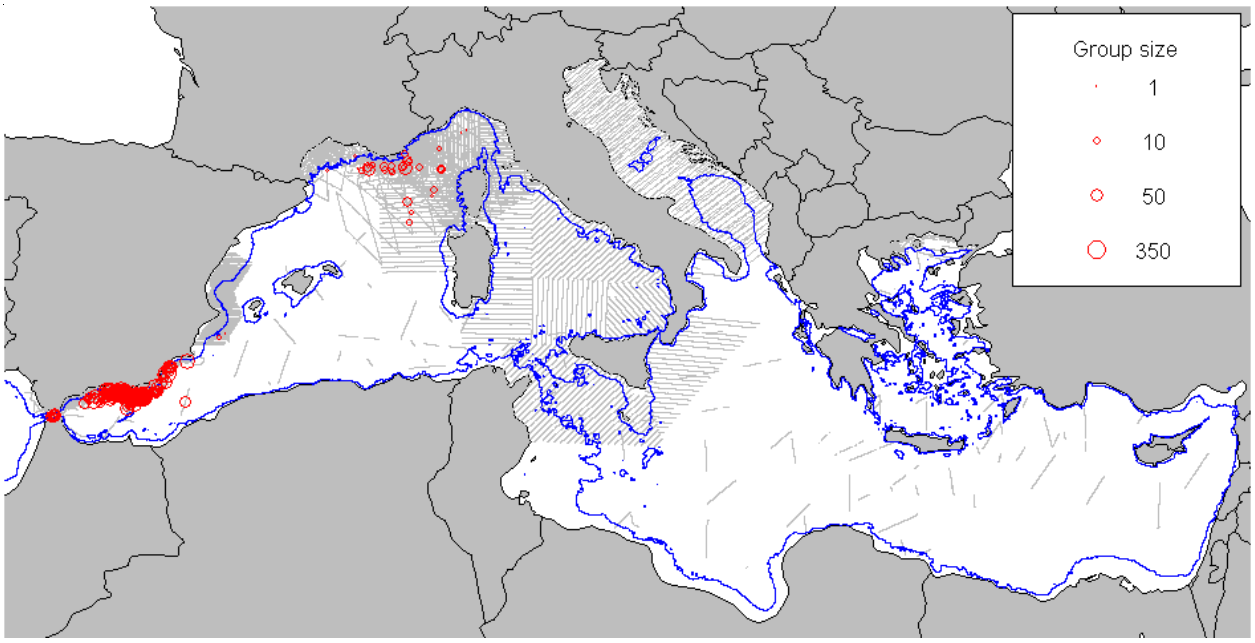

Figure 19. All usable sightings of long-finned pilot whales reported from the incorporated surveys in the Mediterranean study area. Survey tracklines are shown in grey. The 200 m isobath is shown in blue. Long-finned pilot whales were seen most frequently in offshore waters of the Alborán Sea and occasionally in the Ligurian Sea. No sightings were reported in the eastern Mediterranean.

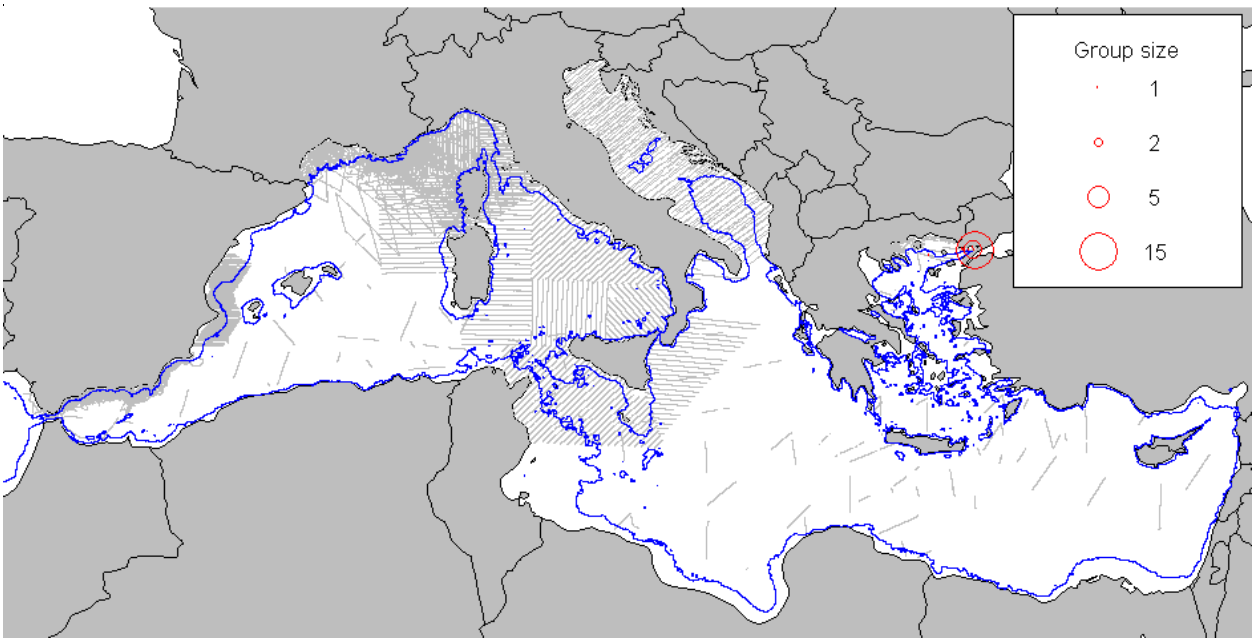

Figure 20. All usable sightings of Black Sea harbor porpoise reported from the incorporated surveys in the Mediterranean study area. Survey tracklines are shown in grey. The 200 m isobath is shown in blue. Harbor porpoises were sighted exclusively in the northeastern Aegean Sea. This species was not modeled.

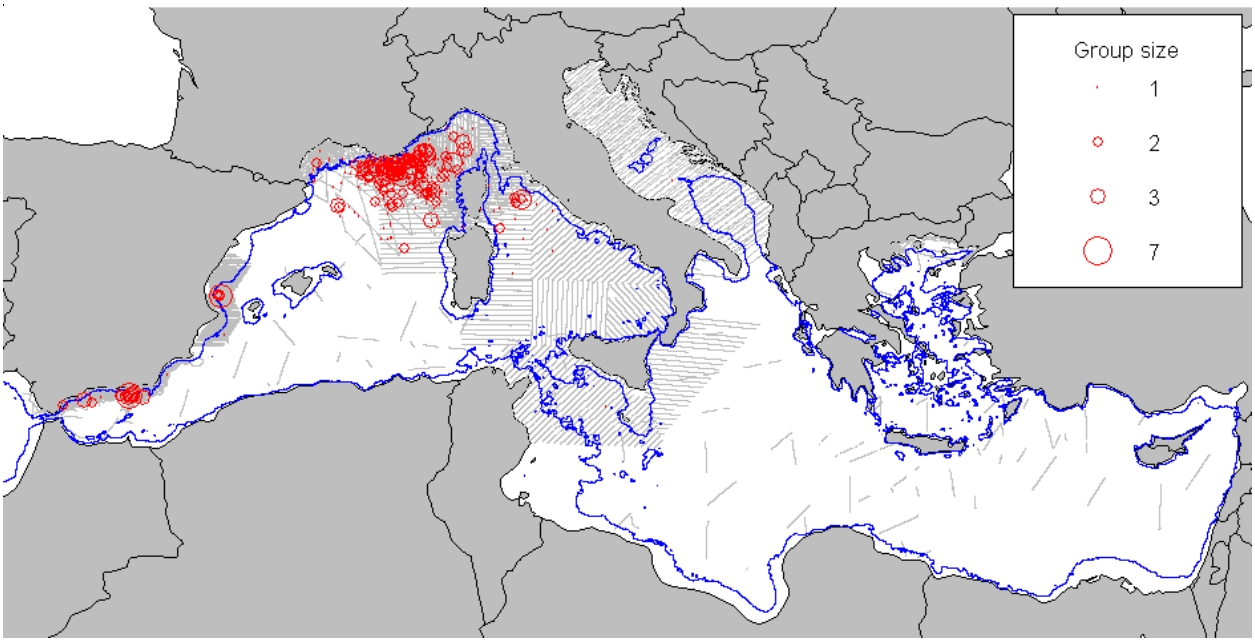

Figure 21. All usable sightings of fin whales reported from the incorporated surveys in the Mediterranean study area. Survey tracklines are shown in grey. The 200 m isobath is shown in blue. Fin whales were primarily seen in offshore waters beyond the continental shelf of the Ligurian Sea. They were also reported, rarely, in the northern Tyrrhenian Sea and northern Alborán Sea. No sightings in the eastern Mediterranean were reported by available surveys.

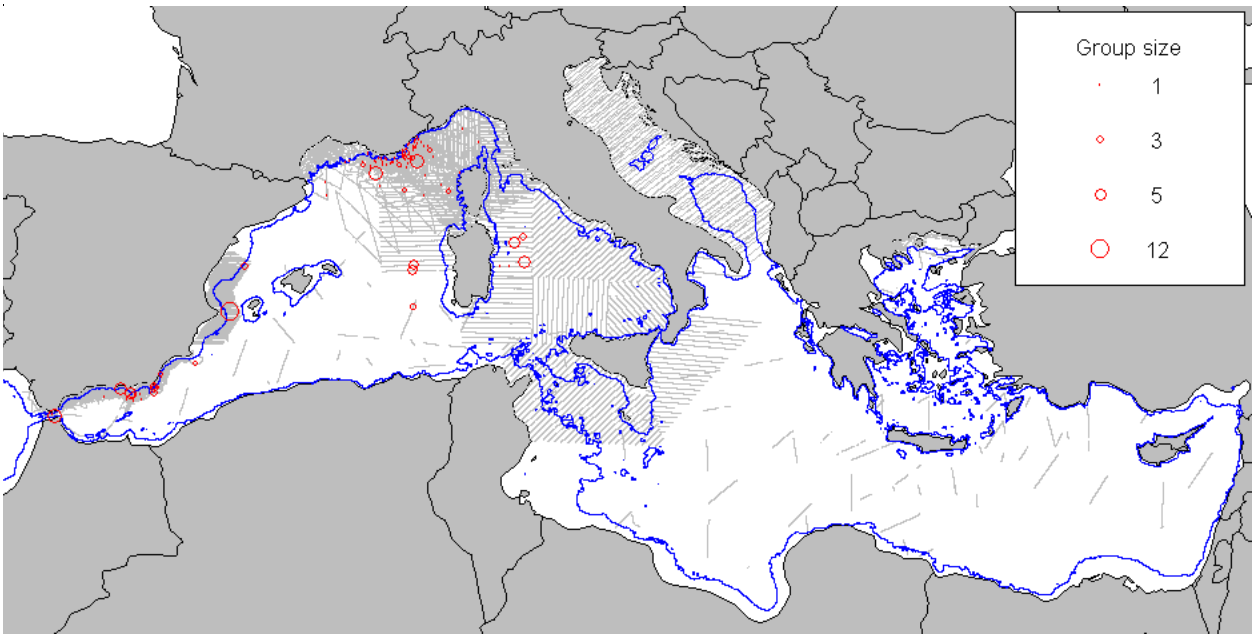

Figure 22. All usable sightings of sperm whales reported from the incorporated surveys in the Mediterranean study area. Survey tracklines are shown in grey. The 200 m isobath is shown in blue. Sperm whales were sighted infrequently, mostly in offshore waters of the Ligurian, Tyrrhenian and Alborán seas. No sightings in the eastern Mediterranean were reported by available surveys.

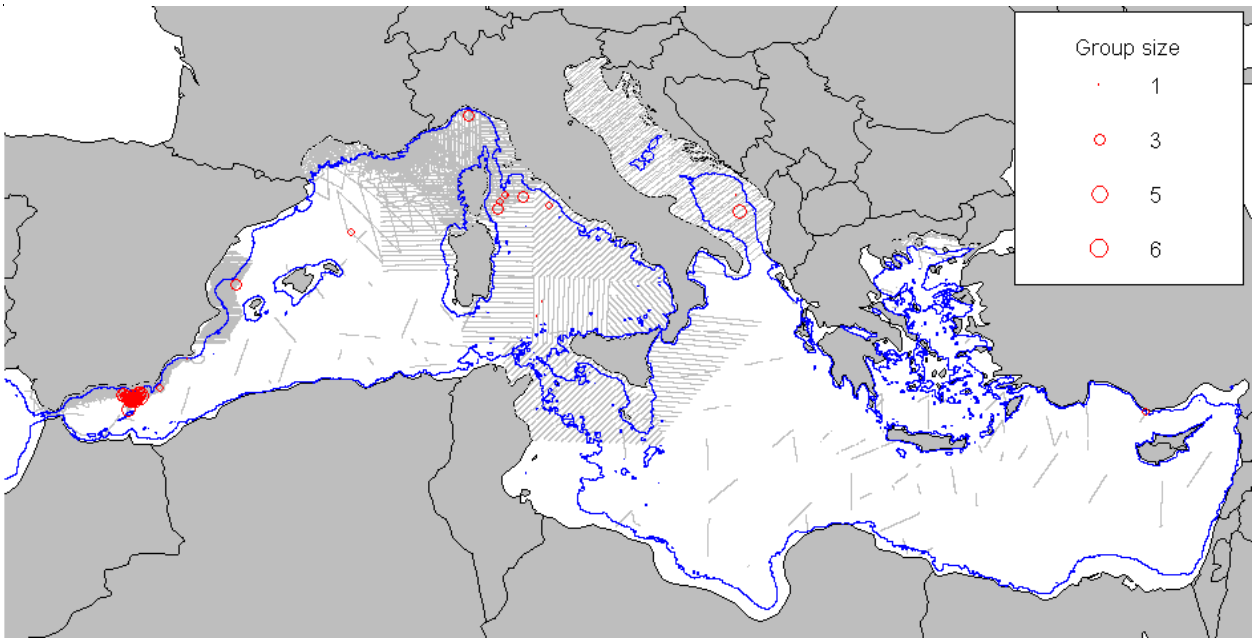

Figure 23. All usable sightings of Cuvier's beaked whales reported from the incorporated surveys in the Mediterranean study area. Survey tracklines are shown in grey. The 200 m isobath is shown in blue. Cuvier's beaked whales were seen in offshore waters. Sightings were most numerous in the Alborán Sea.

3.4 Detection Modeling

Detection modeling was the first stage of the two-stage density surface modeling approach (Miller et al. 2013). Detection modeling was performed using single-team "distance sampling" methodology (Buckland et al. 2001), following the five steps described below.

3.4.1 Distance exploration and truncation

In distance sampling, detectability is modeled from the perpendicular distances to the sightings from the survey trackline. As the first step, perpendicular distances were explored and truncation distances were chosen. Right truncation distance was chosen such that the minimum probability of detection (which occurred at the right truncation distance) was approximately 0.15 (Buckland et al. 2001). However, this practice was occasionally relaxed to alleviate situations with low sample sizes.

Left truncation was necessary for University of Valencia surveys, which used flat windows and consequently had an inadequate view of the line. To determine the left truncation distance, we first estimated the declination angle at which visibility became impaired, as follows: (1) we pooled declination angles for all dolphin sightings in University of Valencia surveys (we used all species of dolphins sighted during both surveys, 2010-2011 and 2013, to maximize sample size) (2) we calculated perpendicular distances for all sightings; (3) we produced and inspected a histogram of perpendicular distances and identified the distance at which the sighting frequency started to decrease as distance decreased (**Figure 24**); (4) we converted this distance back to the declination angle at which left truncation should occur.

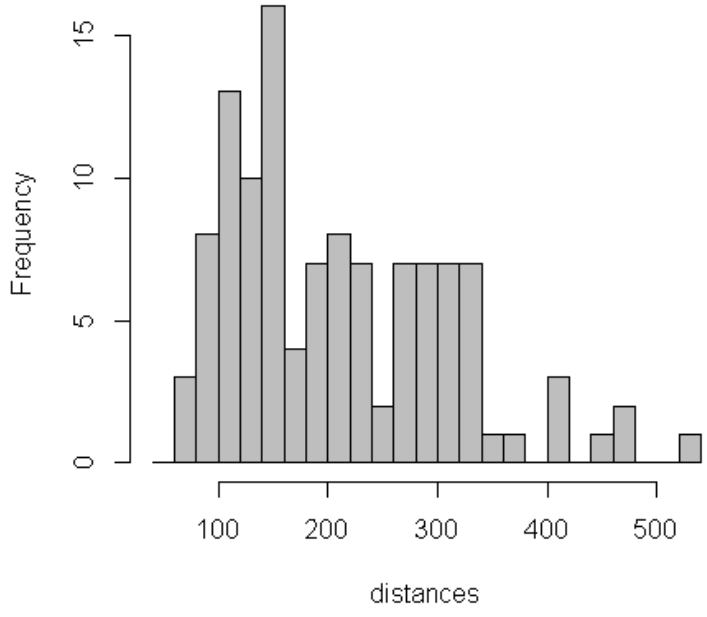

Figure 24. Histogram of perpendicular distances for the University of Valencia flat windows surveys for an altitude of 190.5 m (625 feet). This histogram was inspected to derive a declination angle of 61.4 decimal degrees, corresponding to 104 m on the histogram, below which the view was inadequate.

A complicating factor was that the 2010-2011 survey and the 2013 survey were carried out at different altitudes (**Table 5**). Because of this, we typically fitted separate detection functions to the two surveys (see next section for details). Thus, the left truncation distances for the detection functions were different (because altitude was different) even though the declination angle of left truncation was the same. In order to fit detection functions, we kept the sightings separate for the two surveys, and fitted detection functions that used left truncation distances derived from the common declination angle, but different altitudes.

Table 5. Characteristics of aerial surveys used in density models of cetaceans. Subjective conditions refer to the observers' overall qualitative assessment of survey conditions (usually bad, medium, good and excellent).

Survey	Aircraft	Altitude (feet)	Mean speed (knots)	Covariates collected
PELAGIS	Britten Norman equipped with bubble windows	600	90	Beaufort sea state, cloud cover, glare, turbidity, subjective conditions
TETHYS/ISPRA	Partenavia P-68 equipped with bubble windows	700	100	Beaufort sea state, cloud cover, glare, turbidity, subjective conditions
BWI / ISPRA	PartenaviaP-68 equipped with bubble windows	650	100	Beaufort sea state, cloud cover, glare, turbidity, subjective conditions
University of Valencia 2010/2011	Cessna 337 equipped with flat windows	500	90	Beaufort sea state, visibility
University of Valencia 2013	Cessna 337 equipped with flat windows	750	90	Beaufort sea state, visibility

3.4.2 Survey grouping and sightings hierarchies

There were five types of aerial surveys and three types of shipboard surveys available for density modeling. Aerial surveys were conducted by four survey organizations and differed by aircraft type, survey altitude and mean speed (**Table 5**). Shipboard surveys were conducted by three different organizations and differed by vessel type, observation height and mean speed (**Table 6**). All shipboard surveys were conducted from motor sailboats.

Table 6. Characteristics of shipboard surveys used in density models of cetaceans. We note that Alnitak/Alnilam surveys had two observation configurations depending on swell: (1) in the presence of swell, observers were located on the deck; (2) in the absence of swell, observers were located both on the deck and in the crow's nest at the base of the mast. Thus, wherever possible, separate detection functions were fitted for either observer configuration. Shipboard surveys from EcoOcean institute and IFAW/MCR only had observers on the deck.

Survey	Boat	Observation platform height (m)	Mean speed (knots)	Covariates collected
Alnitak/Alnilam	Motor sailboat R/V Toftevaag with length 18 m	-deck 3.5 -crow's nest (mast) 11	4.5	Douglas sea state, swell, sightability
EcoOcean Institute	29 different motor sailboats with length 10–32m	-deck 2.6–3.3	5.5	Douglas sea state, Beaufort sea state, cloud cover
IFAW/MCR	Motor sailboats with length 21 m and 14 m	-"A frame" 5.3 (treated as a deck)	6.5	Beaufort sea state, cloud cover, glare, swell, wave height, visibility

For each species, separate detection hierarchies were generated for aerial and shipboard surveys (examples are shown in **Figures 25 and 26**). Surveys were pooled based on similarity until at least 60 sightings (ideally) were obtained, and a detection function was fitted to these sightings (however, in some data poor situations, detection functions were fitted with as few as 30 sightings following (Miller & Thomas 2015)). Although Buckland et al. (2001) advised to use at least 60 sightings to fit a detection function, the true minimum depends on the data and question. Shipboard surveys were only pooled with shipboard surveys, and similarly for aerial surveys.

To increase sample size for aerial surveys, sightings from PELAGIS aerial surveys in the Atlantic that used the same protocol as PELAGIS surveys in the Mediterranean Sea were incorporated.

We first considered pooling sightings of similar species (e.g., bottlenose dolphin with striped dolphin, long-finned pilot whale with Risso's dolphin) to increase sample size for detection function fitting. At the workshop, data providers expressed concern about pooling species with potentially different detectabilities, so we considered species-specific detection functions only in the updated models.

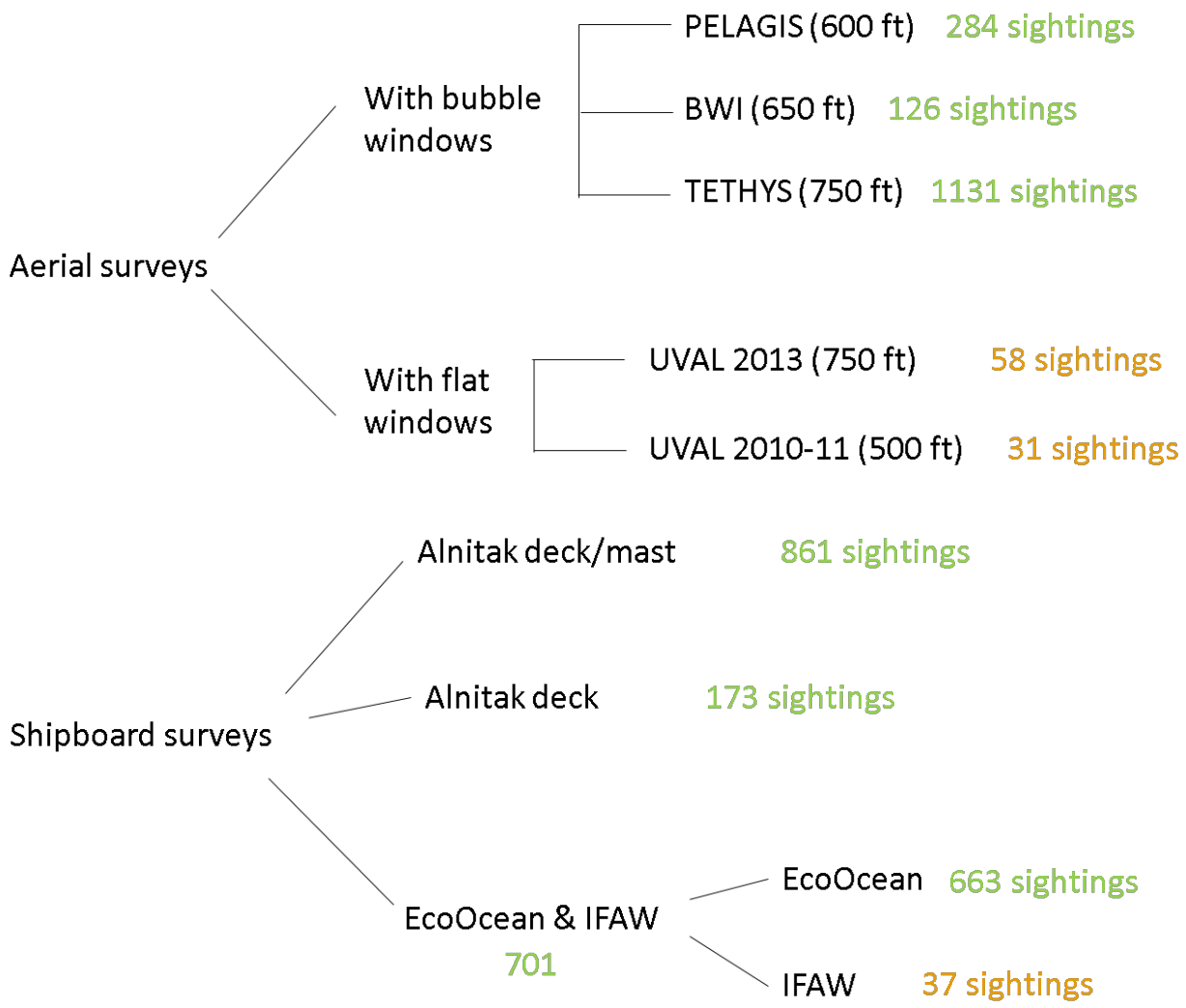

Figure 25. Example sightings hierarchies for a large sample size situation (species: striped dolphin). Color-coding: ≥60 sightings: green; 31–59 sightings: orange; ≤30 sightings: red. Refer to Appendix A for details.

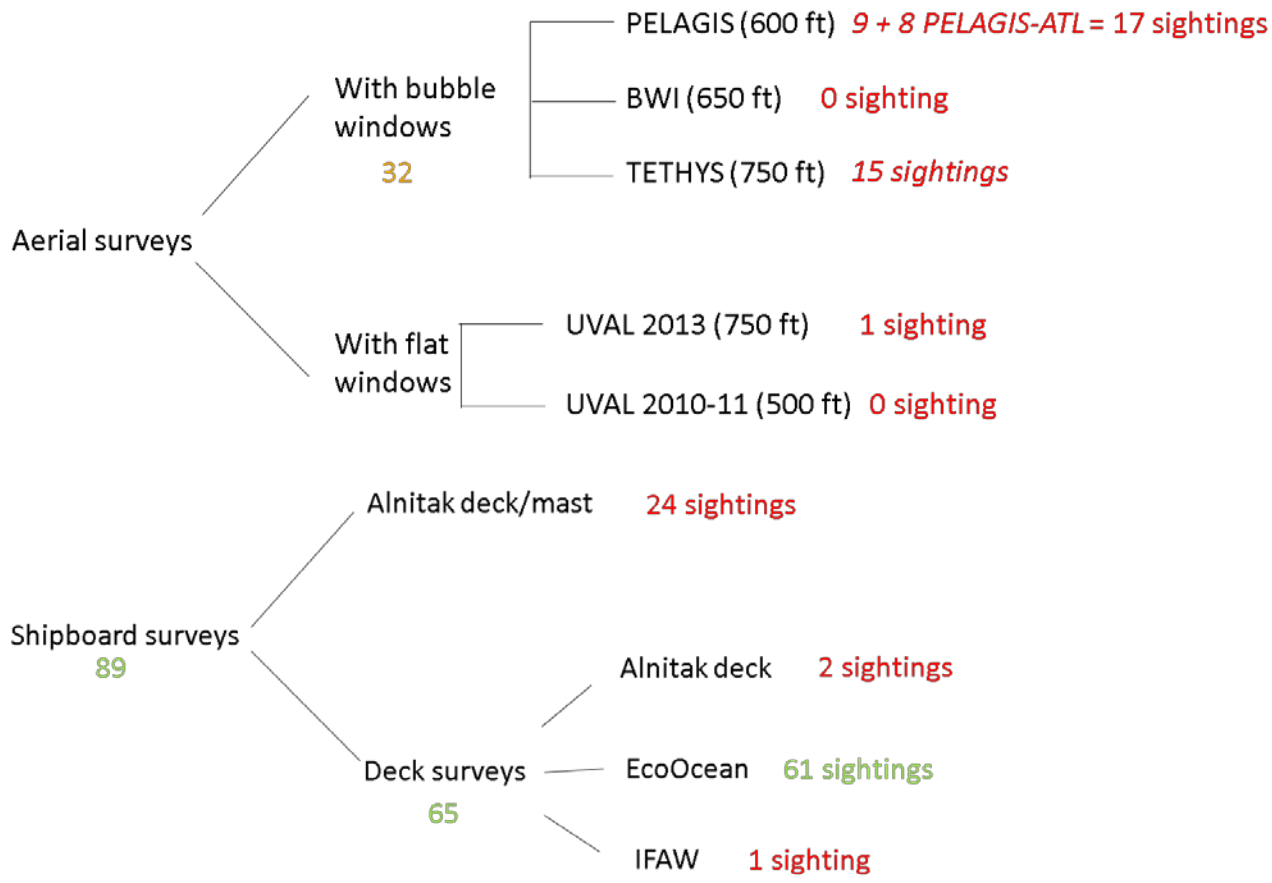

Figure 26. Example sighting hierarchies for a low sample size situation (species: sperm whale). Color-coding: ≥60 sightings: green; 31–59 sightings: orange; ≤30 sightings: red. Refer to Appendix A for details.

3.4.3 Detection Function Fitting

When fewer than 60 sightings were available, we fitted detection functions following the conventional distance sampling framework (Buckland et al. 2001), i.e., with no covariates.

When more sightings were available, we fitted detection functions following the multiple covariate distance sampling framework (Marques & Buckland 2004). Candidate covariates included those related to survey conditions, e.g., Beaufort Sea state, cloud coverage, visibility and swell. The availability of these covariates differed by survey (**Tables 5 and 6**). Candidate covariates also included survey ID, surveyor organization, year, season, observer, presence of a mast observer (for shipboard surveys only) and group size (tested with and without log-transformation). Ordinal covariates (e.g., Beaufort sea state) were tested both as continuous covariates and as factors. For factor covariates, categories were reclassified after inspection of plots of perpendicular distances versus covariate values in order to increase available sample size per category (we sought to obtain at least 15 sightings per category). When sample size was large (in general, 300 sightings or more), combinations of covariates were tested in addition to individual covariates.

We tested half normal, hazard rate and uniform key functions with various adjustment terms for extra flexibility. However, when less than 30 sightings were available, we only tested half normal and hazard rate models with no adjustment terms.

After all candidate detection models were fitted, we ranked them according to the Akaike information criterion (AIC). The model with the lowest AIC was selected after inspection of the detection function plot, quantile-quantile (q-q) plot and goodness of fit tests.

3.4.4 g(0) Correction for availability bias

The probability of detecting an animal on the trackline (i.e., at perpendicular distance of 0), or g(0), is affected by both availability bias (i.e., observers fail to detect animals because they are submerged) and perception bias (i.e., observers fail to detect animals present at the surface) (Pollock et al. 2006). Distance sampling assumes that g(0)=1, but one or both of these biases is usually present, invalidating this assumption and leading to a g(0) that is less than 1. If g(0) is nonetheless assumed to be 1, density and abundance will be underestimated, as detectability will be assumed to be higher than it actually is. This problem may be corrected by estimating g(0) with various techniques, which usually require additional data to be collected during surveying (typically by the platform circling back to resample a sighting, or by using double-platform experiments). In the absence of data available for quantifying perception bias in Mediterranean surveys, we were unable to estimate g(0)s that corrected for perception bias.

To provide more realistic estimates of abundance (rather than assuming g[0]=1), we did estimate g(0)s that corrected for availability bias, as follows. First, for each species, we searched the literature and extracted mean dive duration and surfacing times in the Mediterranean Sea (**Table 7**). For Risso's dolphin, there were no published estimates in the Mediterranean Sea so we used estimates from the western North Atlantic For short-beaked common dolphin, mean surface and dive time were unavailable in the literature, so dive parameters for striped dolphin were used.

Then, for aerial surveys that used bubble windows, we applied the Carretta et al. (2000) formula:

$$g(0)_{availability} = \frac{E[s] + t}{E[s] + E[d]}$$

where E[s] was the mean time spent at or near the surface, t was the window of time during which an animal was within visual range of the aerial observer, and E[d] was the mean dive duration. This approach is appropriate when the observer's view of the trackline is unimpeded, as is afforded by bubble windows, and the viewing area can be assumed to be square. Following Carretta et al. (2000), we used t = 10s which corresponded to the time an aircraft flying at a speed of 100 knots would have travelled approximately 500 m. Species-specific g(0)s for bubble-window surveys are presented in **Table 8**.

Table 7. Dive parameters used to derive g(0) estimates that corrected for availability bias.

Species	Dive duration (s)	Surfacing time (s)	Source
Striped dolphin	66.4	132.8	Gomez de Segura et al. (2006): focal follows in the Balearic Sea (n=24 groups)
Common bottlenose dolphin	68.7	231.3	Forcada et al. (2004): focal follows in the Balearic Sea (n=12 groups)
Short-beaked common dolphin	66.4	132.8	Same dive parameters as striped dolphin
Risso's dolphin	175.07	322.05	Palka et al. (in review): DTAGs deployed in the Western North Atlantic
Long-finned pilot whale	218.6	299	Cañadas (2011): DTAGs deployed in the Alborán Sea (n=16 individuals)
Fin whale	336	137	David et al. (personal communication): focal follows in the NW Med (n=63 individuals)
Sperm whale	2686.2	548.4	Drouot et al. (2004): focal follows in the NW Med
Cuvier's beaked whale	1578	120	Cañadas and Vázquez (2014): focal follows in the Alborán Sea (n=57 groups)

Table 8. Species-specific g(0)s used to correct estimated abundances for availability bias in aerial surveys with bubble windows. These g(0)s were derived by applying the formula of Carretta et al. (2000) with dive parameters from Table 7.

Species	g(0)	Source
Striped dolphin	0.717	Caretta et al. 2000 formula with dive parameters from Gomez de Segura et al. (2006)
Common bottlenose dolphin	0.804	Caretta et al. 2000 formula with dive parameters from Forcada et al. (2004)
Short-beaked common dolphin	0.717	Caretta et al. 2000 formula with dive parameters from Gomez de Segura et al. (2006)
Risso's dolphin	0.668	Caretta et al. 2000 formula with dive parameters from Palka et al. (in review)
Long-finned pilot whale	0.597	Caretta et al. 2000 formula with dive parameters from Cañadas et al. (2011)
Fin whale	0.311	Caretta et al. 2000 formula with dive parameters from David et al. (personal communication)
Sperm whale	0.173	Caretta et al. 2000 formula with dive parameters from Drouot et al. (2004)
Cuvier's beaked whale	0.076	Caretta et al. 2000 formula with dive parameters from Cañadas and Vázquez (2014)

For aerial surveys that used flat windows, visibility was assumed to be impeded by optical distortion or the aircraft itself, both looking down, ahead, and behind. Forcada et al. (2004) and Gomez de Segura et al. (2006), who utilized similar aircraft to those analyzed here, reported on

this effect and the angles at which visibility became obstructed in these three directions. Following these studies, we applied the Laake et al. (1997) equation (7) on a per-sighting basis:

$$g(0)_{availability} = \frac{E[s]}{E[s]+E[d]} + \frac{w(x) - w(x)^2 0.5(\frac{1}{E[d]})}{E[s]+E[d]}$$

where E[s] was the mean time spent at or near the surface, E[d] was the mean dive duration and the w(x) parameter was the amount of time the ocean was in the observer's view at a perpendicular distance x, given the vertical and lateral angles of obstruction. The w(x) parameter was calculated based on the aircraft properties reported in Gomez de Segura et al. (2006) for the Cessna 337 aircraft (the same aircraft used in the University of Valencia flat windows surveys):

$$w(x) = x/s \frac{1}{\tan\left(\frac{40\pi}{180}\right)} + \frac{1}{\tan\left(\frac{35\pi}{180}\right)}$$

where s was the mean aircraft speed and 40 and 35 corresponded to the lateral angles (in decimal degrees) forward and backward, respectively, at which the horizontal scan field became obstructed on the Cessna 337 aircraft.

For shipboard surveys, we applied Laake et al. (1997) equation (4) to derive g(0) for each species and survey following Cañadas and Vázquez (2014):

$$g(0)_{availability} = \frac{E[s]}{E[s]+E[d]} + E[d](\frac{1-\exp\left(-\frac{1}{E[d]}r/s\right)}{E[s]+E[d]})$$

where E[s] was the mean time spent at or near the surface, E[d] was the mean dive duration, r was the maximum forward distance at which animals were expected to be detected (which was taken as the 90th percentile of radial distances, as in Cañadas and Vázquez 2014) and s was the mean vessel speed. Species- and survey-specific g(0)s for shipboard surveys are presented in **Table 9**.

Table 9. Species- and survey-specific g(0)s used to correct estimated abundances for availability bias in shipboard surveys. These g(0)s were derived by applying the formula of Laake et al. (1997) with dive parameters from Table 7.

Species	EcoOcean Institute	IFAW / MCR	Alnitak deck/mast	Alnitak deck
Striped dolphin	0.999	0.996	1.000	1.000
Common bottlenose dolphin	1.000	1.000	1.000	1.000
Short-beaked common dolphin	0.967	0.996	1.000	1.000
Risso's dolphin	0.989	-	1.000	0.999
Long-finned pilot whale	0.986	0.947	1.000	0.979
Fin whale	0.948	-	0.998	0.530
Sperm whale	0.385	0.471	0.614	0.313
Cuvier's beaked whale	-	0.156	0.559	0.262

3.4.5 Per-segment Abundance Estimation

For each species, we estimated the abundance in segment *j*, $\widehat{N}_j$, using a Horvitz-Thompson-like estimator:

$$\widehat{N}_j = \sum_{r=1}^{R_j} s_{jr}/\hat{p}(z_{jr})g(0)$$

where R_j was the number of observed groups in segment *j*, s_{jr} was the size of the r^{th} group in segment *j* , and $\hat{p}(z_{jr})$ was the estimated probability of detection given observation level covariates, z_{jr}, and g(0) was the probability of detection on the track line (Marques et al. 2007).

3.5 Spatial Modeling

Spatial modeling was the second stage of the two-stage density surface modeling approach (Miller et al. 2013).

3.5.1 Environmental covariates

We derived covariates from remote sensing and ocean models (**Table 10**) and projected them to the 5 × 5 km grid of the study area. For dynamic covariates, we prepared monthly rasters by aggregating and summarizing the available time series. We obtained covariate values for the survey segments by interpolating the 5 × 5 km grid at the segment centroids. We used ArcGIS (version 10.5), the Marine Geospatial Ecology Tools software (Roberts et al. 2010) and custom Python scripts to prepare and sample all covariates.

Table 10. List of environmental covariates included in cetacean density models. We note that other covariates (distance to the closest shore, eddy kinetic energy, and bottom temperature) were prepared but dropped from the model selection procedure as they were insufficiently sampled by the surveys or led to aberrant predictions. The common availability period to all covariates was January 1999 to December 2016.

Covariate category	Covariate (abbreviation)	Availability period	Source
Static	Depth	-	Depth of the seafloor (m), derived from SRTM30-PLUS global bathymetry (Becker et al. 2009).
	Slope	-	Slope of the seafloor (%), derived from SRTM30-PLUS global bathymetry (Becker et al. 2009).
	DistToCan	-	Distance to the closest submarine canyon (m), derived from (Harris et al. 2014).
	DistToSmt	-	Distance to the closest seamount (m), derived from Rovere and Würtz (2015)
Physical	SSTMonthly	Jan 1992-Dec 2016	Monthly SST (°C), derived from GHRSST Level 4 CMC daily 0.2° SST observations (Brasnett 2008)
	NemoSST Monthly	Jan 1992-Dec 2016	Monthly mean SST (°C), derived from daily predictions from the Mediterranean Forecasting System 1/16° and 1/24° ocean models (NEMO) (Simoncelli et al. 2014).

Covariate category	Covariate (abbreviation)	Availability period	Source
	SalinityMonthly	Jan 1992-Dec 2016	Monthly mean salinity (psu), derived from daily predictions from the Mediterranean Forecasting System 1/16° and 1/24° ocean models (Simoncelli et al. 2014).
Biological	VGPM Monthly	Oct 1997-Aug 2017	Monthly net primary production across the water column (mg C m^{-2} day^{-1}), estimated from SeaWiFS and Aqua by the Vertically Generalized Production Model (VPGM) (Behrenfeld & Falkowski 1997).
	ChlMonthly	Jan 1999-Dec 2016	Monthly mean chlorophyll concentration at the ocean surface (mg m^{-3}), derived from daily predictions from the Mediterranean Sea Biogeochemical Reanalysis 1/16° ocean model (Teruzzi et al. 2016)
	NPPMonthly	Jan 1999-Dec 2016	Monthly mean primary production at the ocean surface (mol m^{-3} s^{-1}), derived from daily predictions from the Mediterranean Sea Biogeochemical Reanalysis 1/16° ocean model (Teruzzi et al. 2016)
	PCBMonthly	Jan 1999-Dec 2016	Monthly mean phytoplankton carbon biomass at the ocean surface (mol m^{-3}), derived from daily predictions from the Mediterranean Sea Biogeochemical Reanalysis 1/16° ocean model (Teruzzi et al. 2016)
	VertIntChl Monthly	Jan 1999-Dec 2016	Depthwise integration of ChlMonthly, giving monthly mean chlorophyll concentration across the water column (mg m^{-2}).
	VertIntNPP Monthly	Jan 1999-Dec 2016	Depthwise integration of NPPMonthly, giving monthly mean primary production across the water column (mol m^{-2} s^{-1}).
	VertIntPCB Monthly	Jan 1999-Dec 2016	Depthwise integration of PCBMonthly, giving monthly mean phytoplankton carbon biomass across the water column (mol m^{-2}).
	OPFish Monthly	Jan 1998-Dec 2016	Monthly mean Ocean Productivity index for Fish (OPFish) (unitless), derived from fronts in 1/24° ocean color observations (Druon 2017).
	OPFishMonthly3	Jan 1998-Dec 2016	OPFishMonthly smoothed with a 3 x 3-cell moving window (the 3 × 3 focal mean).
	OPFishMonthly5	Jan 1998-Dec 2016	OPFishMonthly smoothed with a 5 x 5-cell moving window (the 5 × 5 focal mean).

Key: NEMO = Nucleus for European Modelling of the Ocean; SST = sea surface temperature

Because the Mediterranean Sea is characterized by a strong inter-annual variability of oceanographic processes (Pinardi & Masetti 2000; Bosc et al. 2004; D'Ortenzio & Ribera d'Alcalà 2009), we used a contemporaneous resolution for dynamic covariates (climatological covariates would smooth out the strong inter-annual variability). We initially considered both 8-day and monthly covariates. However, certain covariates were only available at a monthly resolution so we performed the final analysis with just the monthly resolution.

3.5.2 Generalized additive models

We fitted generalized additive models (GAMs) with the following structure:

$$E[] = A_j \exp\left[\beta_0 + \sum_k f_k(z_{jk})\right]$$

where $\widehat{N}_j$ was the estimated abundance in segment j (response variable assumed to follow a Tweedie distribution (Foster & Bravington 2013)) and *E* indicated expectation; A_j was the model offset, the area of segment *j* calculated as $2(w_R - w_L)l_j$, where w_R was the right-truncation distance, w_L was the left-truncation distance (0 if data were not left truncated), and l_j was the segment length; f_k were smooth functions of the sampled environmental covariates z_k; and β_0 was the model intercept.

Model fitting was restricted to the segments from 1999 to 2016, which were the segments for which all covariates were available.

We fitted year-round models for all eight species because the literature provided no clear evidence of differing relationships between abundance and the environment in different seasons (e.g., feeding in summer and breeding in winter) across the Mediterranean Sea. We note that contrary to other fin whale populations, Mediterranean fin whales calve and breed year-round (Notarbartolo di Sciara et al. 2016), supporting the use of a year-round model.

Consistent with our objective of producing density estimates in the entire Mediterranean Sea, we developed simple habitat models that captured dominant abundance-environment relationships but did not reproduce details present in the data (Elith et al. 2010). Simple models can achieve higher transferability and are highly recommended for extrapolation (Wenger & Olden 2012; Merow et al. 2014). To fit simple models and limit the extent of extrapolation, we limited the number of covariates to 4. We therefore fitted GAMs with all possible combinations of 1, 2, 3 and 4 covariates, after eliminating the pairs of covariates for which the Spearman's rank correlation coefficient (Hollander & Wolfe 1975) calculated on segments was ≥0.6 or ≤-0.6. We used thin-plate regression splines with shrinkage to allow smooth term effects to be removed from the model during fitting. To model simple abundance-environment relationships and mitigate overfitting, which is known to limit model transferability (Wenger & Olden 2012), we restricted the basis size to 4 for each smooth term. We used restricted maximum likelihood (REML) as the criterion for estimating smooth parameters because it penalizes overfitting and leads to more pronounced optima (Wood 2011). We computed and compared AIC values of all candidate (1, 2, 3 and 4-covariate) models and selected the model with the lowest AIC as the best model. Model selection based on AIC effectively reduces overfitting by penalizing models with excessive complexity (Wenger & Olden 2012). We fitted all GAMs in R with the mgcv package (version 1.8.17) (Wood 2014).

3.5.3 Density predictions

For all species, densities (individuals per 25 square kilometers [km^2]) were predicted at a monthly time step for the 1999–2016 period during which all covariates were available (i.e., 17 × 12 = 204 rasters were generated). The 12 predicted monthly density maps were averaged across all modeled years to obtain 12 monthly densitologies.

Given the strong spatiotemporal heterogeneity of the survey effort, and insufficient knowledge of monthly variations in cetacean distributions within the Mediterranean Sea, we did not offer monthly predictions of density. Instead, we averaged monthly densitologies on a seasonal or annual basis, as follows.

For fin whale, monthly densitologies were averaged into two seasonal surfaces because monthly predictions were compatible with the contraction-dispersion of fin whale distribution in the western Mediterranean, presumably following the distribution of krill (Notarbartolo di Sciara et al. 2016; Panigada et al. 2017a). We started the winter season in September because six tagged fin whales started to disperse from the Ligurian Sea to the northwestern Mediterranean in September (Panigada et al. 2017a). Two other tagged whales moved from the Strait of Sicily to the northwestern Mediterranean in April (Panigada et al. 2017a). However, we chose to start the summer season in March because this was the month in which monthly predicted densities started to concentrate in the Ligurian Sea.

For all other species, information about large-scale animal movements within the Mediterranean Sea was insufficient to offer confident predictions at a seasonal resolution. We therefore averaged monthly densitologies into a single annual surface predicting mean density across all modeled months and years.

3.5.4 Uncertainty from the spatial model

To visualize parameter uncertainty from the spatial stage of the model, we produced maps of the mean coefficient of variation (CV). Similarly to how we generated density predictions, we generated monthly maps of standard errors (SEs) and averaged them across all modeled years. We then divided these 12 monthly maps of SEs by the 12 monthly maps of densities for every grid cell to obtain 12 monthly maps of CVs. Lastly, we averaged the monthly maps of CVs into a single year-round surface or two seasonal surfaces (for fin whale only).

We caution that these maps of CVs underestimate the true uncertainty of our models, as they do not account for uncertainty in detection functions or g(0) estimates. Current statistical tools do not allow incorporation of these sources of uncertainty when more than one detection function or g(0) estimate is used, which was the case with all our models. The only way to incorporate these sources of uncertainty is to perform a nonparametric bootstrap, which is extremely intensive computationally.

In addition to mapping CVs, we mapped the extent of interpolation *versus* extrapolation throughout the Mediterranean Sea. We only characterized univariate extrapolation, i.e., extrapolation beyond individual covariate ranges (not combinations of covariates). On these maps, a grid cell was flagged as extrapolation when it had at least one covariate (among selected covariates) that fell beyond the sampled range in a monthly prediction. In future analyses, it would be useful to characterize extrapolation in multivariate space (see 5.3 Future Work).

3.5.5 Total predicted abundance

For each species, total predicted abundances were obtained by summing predicted abundances across all cells of the Mediterranean study area. CVs associated with these abundance estimates were obtained by averaging CVs across all cells of the Mediterranean study area.

4. Results

4.1 Detection Functions

Sightings hierarchies and detailed summaries of detection functions for each species are provided in **Appendix A**.

4.2 Spatial Models

The most commonly selected covariates were Depth (selected for all eight species) and SalinityMonthly (selected for five species) (**Table 11**). We note that other ecologically relevant covariates such as distance to canyons, chlorophyll concentration and VertIntNPPMonthly were never selected in the final models. It is also interesting to note that covariates derived from global models (VGPMMonthly and SSTMonthly) were sometimes selected rather than equivalent covariates derived from Mediterranean regional models (NPPMonthly and NemoSSTMonthly). Only the smoothed versions of the OPFishMonthly covariate (OPFishMonthly5 and OPFishMonthly3) were selected, suggesting that the unsmoothed covariate exhibited excessive noise.

Table 11. Selected GAMs based on lowest AIC for each species.

Species	Selected covariates (ordered with in decreased order of importance following F-scores)	Explained deviance (%)
Striped dolphin	Depth NemoSSTMonthly VGPMMonthly SalinityMonthly	17.9
Common bottlenose dolphin	Depth Slope SalinityMonthly	17.3
Short-beaked common dolphin	SalinityMonthly SSTMonthly OPFishMonthly5 Depth	48.3
Risso's dolphin	Depth	11.5
Long-finned pilot whale	Depth SalinityMonthly VGPMMonthly SSTMonthly	44.5
Fin whale	Depth OPFishMonthly5 Slope SalinityMonthly	23.8
Sperm whale	Depth OPFishMonthly3 NPPMonthly	22.0
Cuvier's beaked whale	Depth Slope	36.2

Explained deviances ranged from 11.5 percent for Risso's dolphin (modeled with depth only) to 48.3 percent for short-beaked common dolphin. **Appendix B** provides detailed GAM summaries and GAM term plots for each species.

4.3 Predicted Densities and Uncertainty

4.3.1 Striped dolphin

The selected covariates for striped dolphin were depth, SST derived from the NEMO ocean model, net primary production derived from the Vertically Generalized Production Model, and salinity, and the explained deviance was 17.9 percent (**Table 11**). Striped dolphin predicted densities were higher on the continental slope and offshore (**Figure 27a**), consistent with the distribution of sightings (**Figure 14**). Predicted densities were higher in the Western Mediterranean than in the eastern Mediterranean. In the western Mediterranean, predicted densities concentrated on the continental slope (notably off Algeria) and in the Alborán Sea, which is characterized by relatively lower SST, higher primary production and lower salinity than the rest of the Mediterranean Sea. Maps of monthly densitologies show highest densities along the western Mediterranean continental slope in March and June (see **Appendix C**).

CVs were higher in the eastern Mediterranean and peaked in low salinity coastal areas (particularly at the mouth of the Po River in the northern Adriatic Sea) (**Figure 27b**). Extrapolation occurred in a large part of the eastern Mediterranean (characterized by higher SST, higher salinity and lower primary production in summer and fall), in the northern Adriatic Sea and Gulf of Lions (lower SST in winter), and east of the Balearic Islands and in the central Tyrrhenian Sea (higher SST in summer) (**Figure 27c**). Predicted densities are thus more speculative and should be interpreted with caution in these areas.

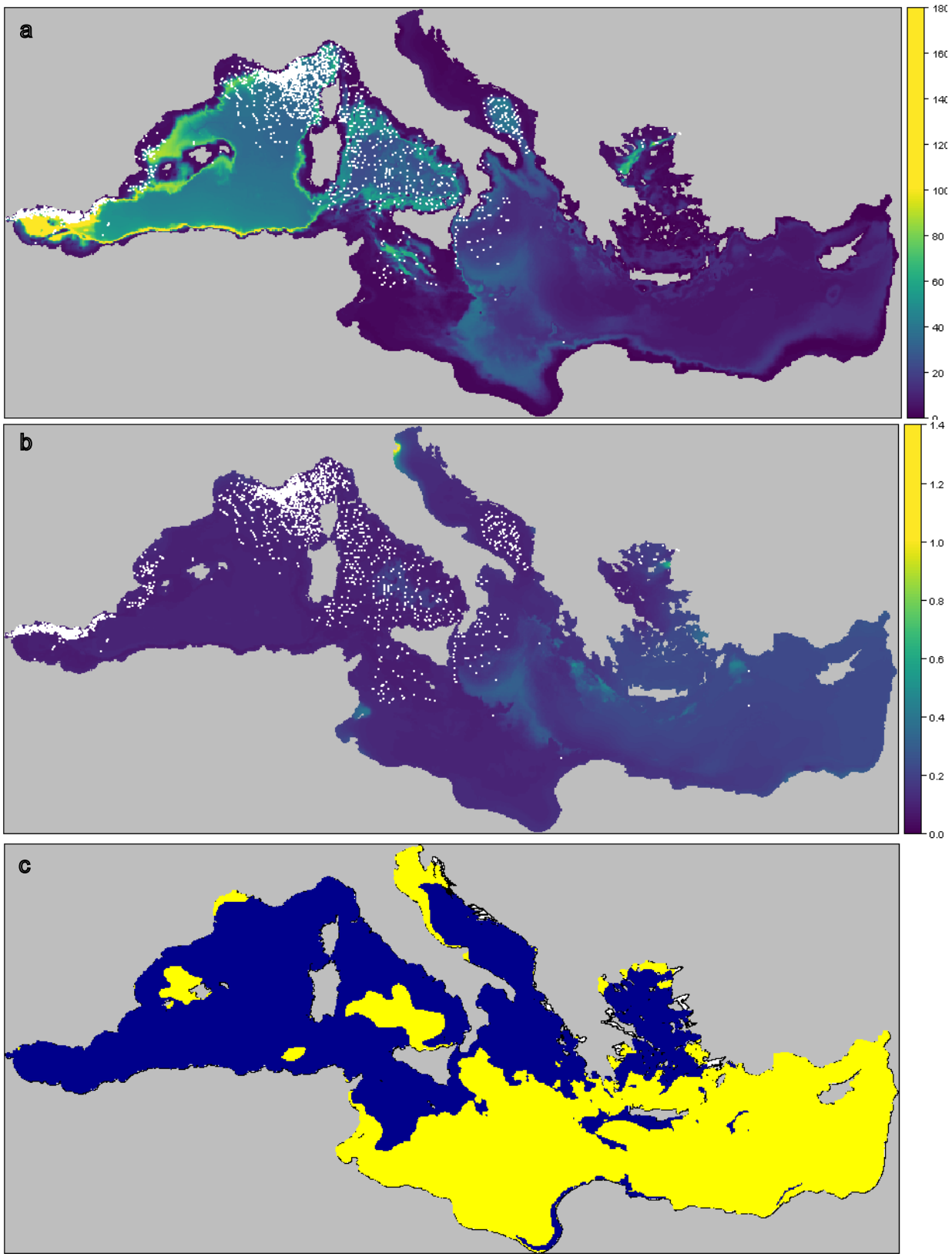

Figure 27. Maps of (a) mean annual predicted densities (individuals per 25 km^2), (b) mean annual coefficients of variation (unit-less) and (c) interpolation (dark blue) versus extrapolation (yellow) for striped dolphin. Sightings are overlaid in white on figures (a) and (b).

4.3.2 Common bottlenose dolphin

The selected covariates for common bottlenose dolphin were depth, slope, and salinity, and the explained deviance was 17.3 percent (**Table 11).** Densities of common bottlenose dolphin were predicted to be higher on the continental shelf and inner slope throughout the Mediterranean Sea (**Figure 28a**), where most sightings were concentrated (**Figure 15**). Predicted densities were relatively low in offshore waters. Highest densities were predicted in two nearshore areas with very low salinity: the mouth of the Po River (northern Adriatic Sea) and the mouth of the Dardanelles (which receives low salinity water outflow from the Black Sea). These density hotspots should not be trusted as they are due to extrapolation to poorly sampled lower salinity areas (see below). Maps of monthly predicted densities showed little between-month variation (see **Appendix C**).

CVs were highest in low salinity areas and deep areas in the central Mediterranean where predictions were extrapolated (**Figure 28b**). Extrapolation occurred in deeper areas (particularly in the central Mediterranean), shallower areas on the Tunisian Plateau, higher salinity areas in the eastern Mediterranean in summer and fall, and low salinity areas (**Figure 28c**). We urge caution when considering predicted densities in these extrapolated areas.

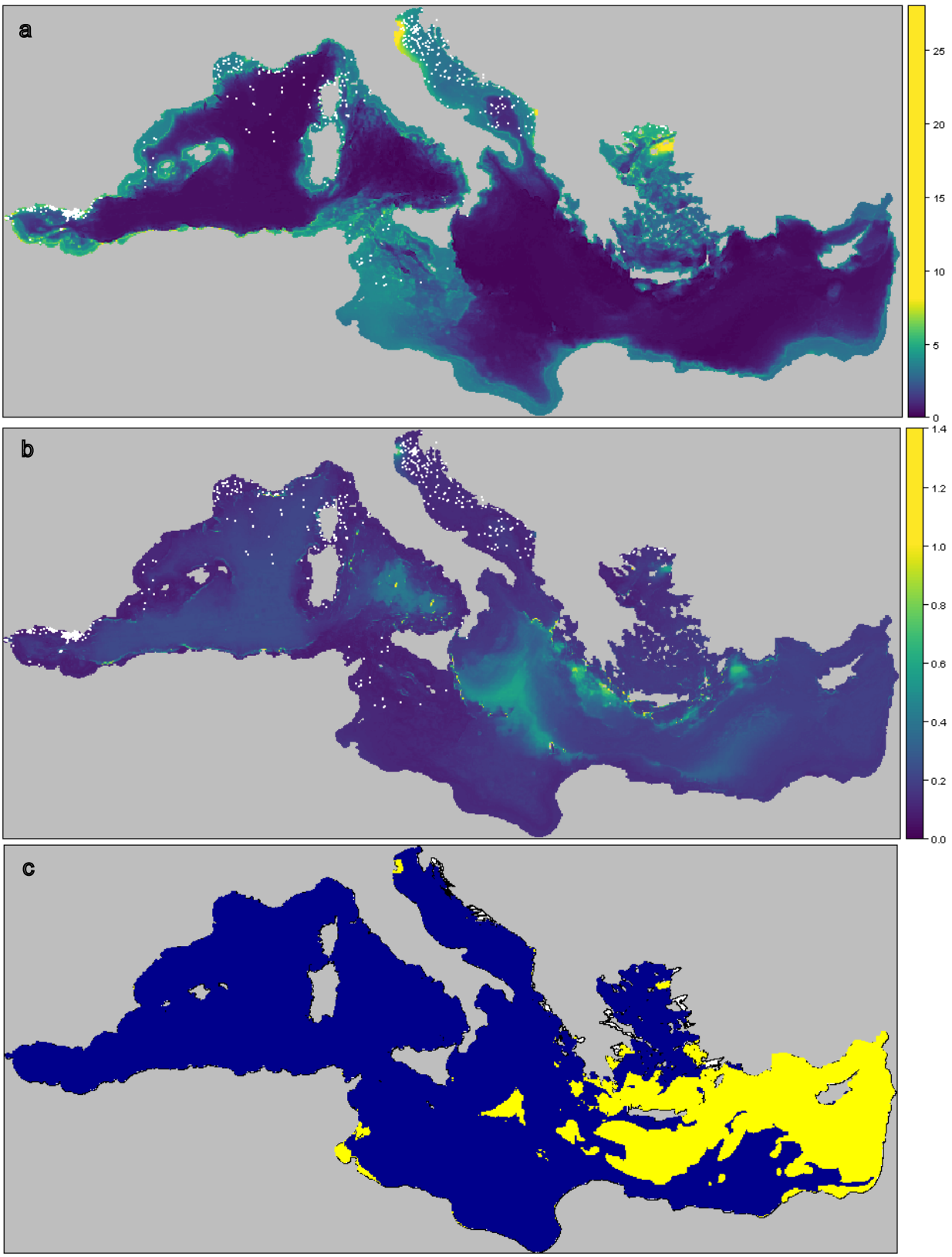

Figure 28. Maps of (a) mean annual predicted densities (individuals per 25 km^2), (b) mean annual coefficients of variation (unit-less) and (c) interpolation (dark blue) versus extrapolation (yellow) for common bottlenose dolphin. Sightings are overlaid in white on maps (a) and (b).

4.3.3 Short-beaked common dolphin

The selected covariates for short-beaked common dolphin were salinity, sea surface temperature derived from GHRSST, ocean productivity for fish smoothed with a 5 × 5-cell moving window, and depth, and had an explained deviance of 48.3 percent (**Table 11).** Highest densities of short-beaked common dolphin were predicted in the Alborán Sea (where most sightings were reported [**Figure 16**]), and on the Algerian continental shelf (**Figure 29a**). Intermediate densities were predicted in nearshore waters of the Adriatic and northern Aegean seas (consistent with sightings reported by a shipboard survey of the Aegean Sea). The predicted density hotspot in the Gulf of Lions is most likely an artifact, probably related to the occurrence of low salinity values at the mouth of the Rhone River. Predicted densities were low in the rest of the Mediterranean Sea. Maps of monthly predicted densities showed highest densities in the Alborán, Adriatic and northern Aegean seas from May to October (see **Appendix C**).

CVs were largest in the Levantine Sea where predicted densities were very low (**Figure 29b**). Extrapolation occurred in most of the eastern Mediterranean (higher SST, higher salinity and lower OPFish in summer and early fall), in the northern Adriatic Sea, northern Aegean Sea and Gulf of Lions (lower SST in winter), and east of the Balearic Islands and in the central Tyrrhenian Sea (higher SST in summer) (**Figure 29c**). Predicted densities are thus more speculative and should be interpreted with caution in these areas.

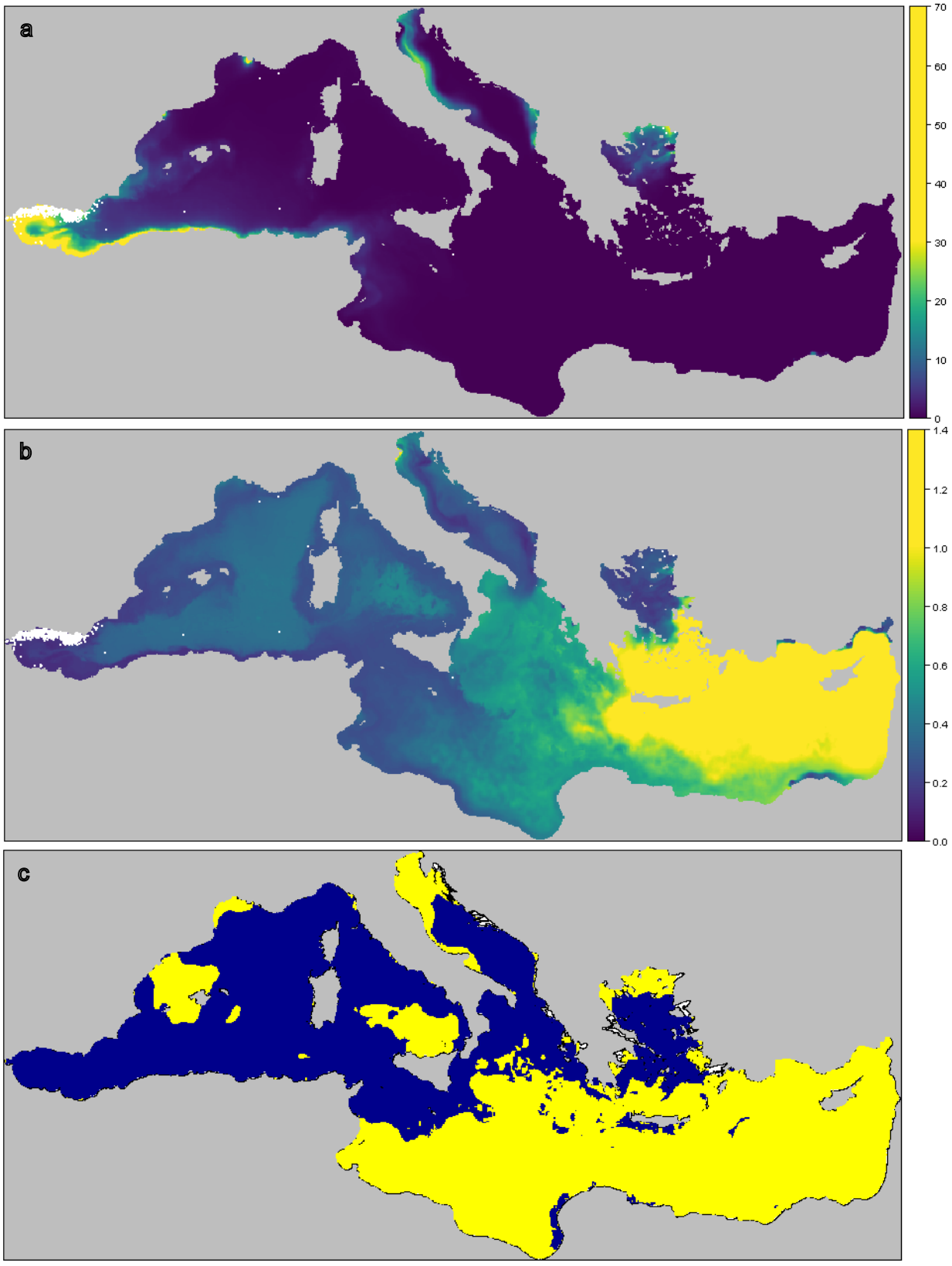

Figure 29. Maps of (a) mean annual predicted densities (individuals per 25 km^2), (b) mean annual coefficients of variation (unit-less) and (c) interpolation (dark blue) versus extrapolation (yellow) for short-beaked common dolphin. Sightings are overlaid in white on maps (a) and (b).

4.3.4 Risso's dolphin

For Risso's dolphin the final model only included depth and had an explained deviance of 11.5% (**Table 11**). All other covariates were non-significant and dropped during model selection. Risso's dolphin densities were predicted to peak at intermediate depth values (from 800 to 1,400 m) (**Figure 30a**). Risso's dolphins were predicted to occur throughout the Mediterranean with highest densities predicted on the continental slope (in concordance with the occurrence of sightings on the continental slope in the western Mediterranean [**Figure 18**]).

CVs were largest in the deep waters of the central Mediterranean where low densities were predicted (**Figure 30b**). Extrapolation occurred to deeper waters in the central Mediterranean and the Hellenic Trench, and to shallower waters on the Tunisian plateau (**Figure 30c**). Predicted densities should be interpreted with caution in these areas.

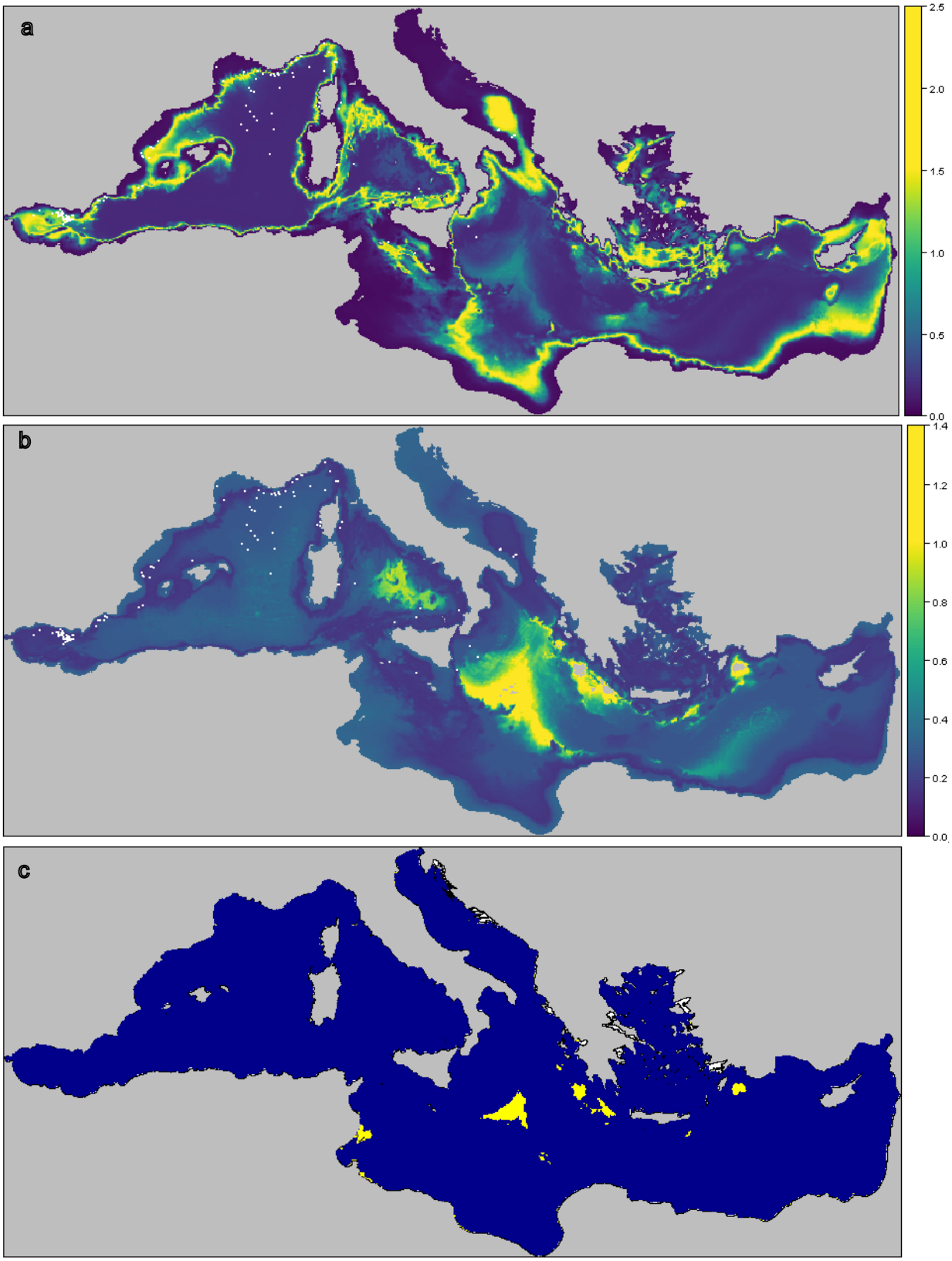

Figure 30. Maps of (a) mean annual predicted densities (individuals per 25 km^2), (b) mean annual coefficients of variation (unit-less) and (c) interpolation (dark blue) versus extrapolation (yellow) for Risso's dolphin. Sightings are overlaid in white on maps (a) and (b).

4.3.5 Long-finned pilot whale

The selected covariates for long-finned pilot whale were depth, salinity, net primary production derived from the VGPM, and sea surface temperature derived from GHRSST, and the explained deviance was 44.5 percent (**Table 11**). Highest densities of long-finned pilot whale were predicted in offshore waters of the Alborán Sea (**Figure 31a**), consistent with sightings concentrations (**Figure 19**). High densities were also predicted along the continental slope off the Algerian coast where conditions were similar but surveying was limited. Low densities were predicted in the central and eastern Mediterranean Sea where no sightings of long-finned pilot whales were reported from the incorporated surveys. We note that intermediate densities were predicted in the Hellenic Trench where extrapolation to deeper waters occurred (see below). Maps of monthly predicted densities showed highest densities in the Alborán Sea in summer months (see **Appendix C**).

CVs were highest in the eastern Mediterranean and in shallow waters of the Tunisian Plateau (**Figure 31b**). Extrapolation occurred in most of the eastern Mediterranean (higher SST, higher salinity and lower primary production in summer and early fall), in the northern Adriatic Sea, northern Aegean Sea and Gulf of Lions (lower SST in winter), and east of the Balearic Islands and in the central Tyrrhenian Sea (higher SST in summer) (**Figure 31c**). We urge caution for the interpretation of predicted densities in these extrapolated areas.

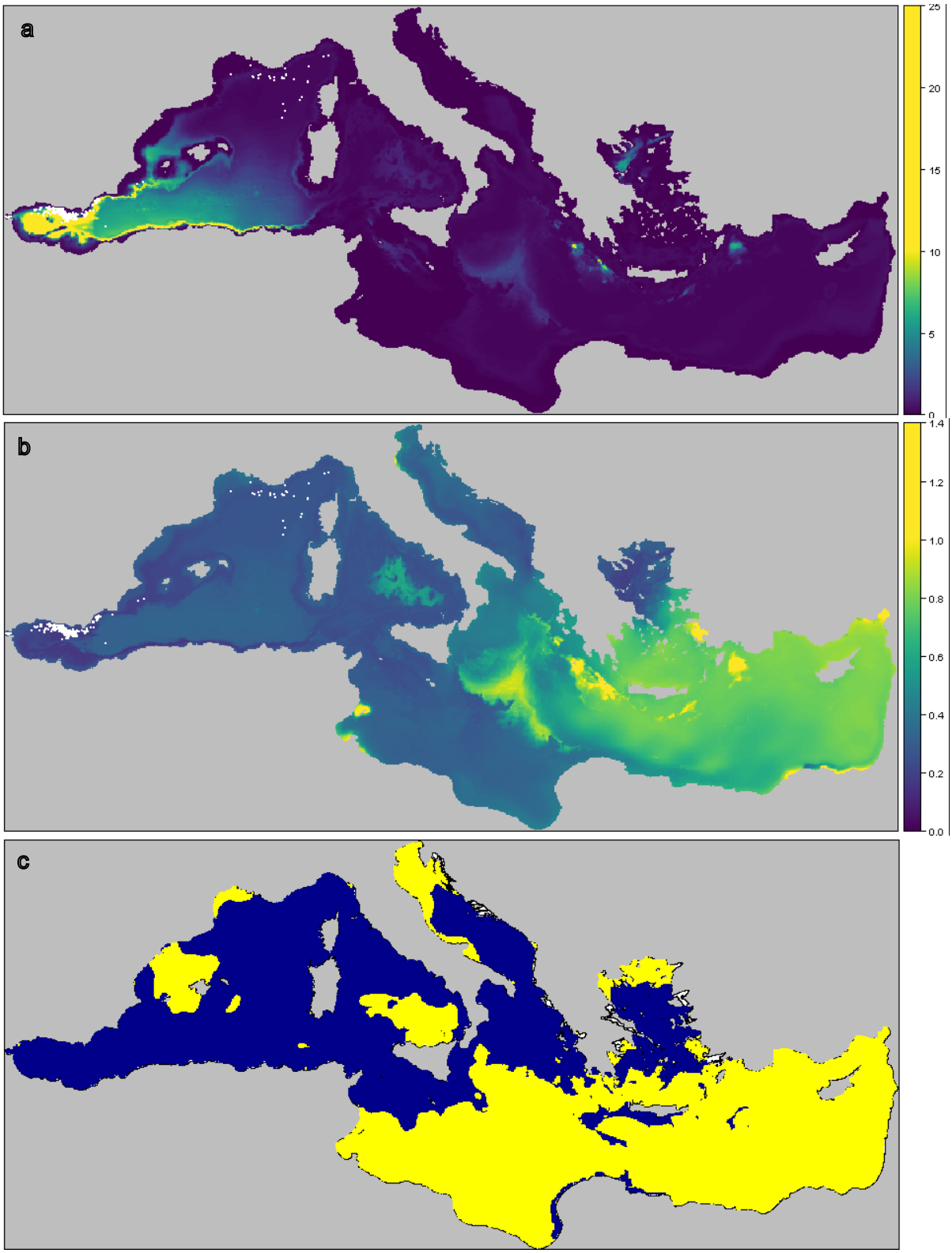

Figure 31. Maps of (a) mean annual predicted densities (individuals per 25 km^2), (b) mean annual coefficients of variation (unit-less) and (c) interpolation (dark blue) versus extrapolation (yellow) for long-finned pilot whale. To improve visibility of the color scale, high CVs (up to 27) obtained near the mouth of the Po River (where predicted density approached zero) were not shown. Sightings are overlaid in white on maps (a) and (b).

4.3.6 Fin whale

The selected covariates for fin whale were depth, ocean productivity for fish smoothed with a 5 × 5-cell moving window, slope, and salinity, and the explained deviance was 23.8 percent (**Table 11**). In summer, highest fin whale densities were predicted in offshore waters of the Ligurian Sea (**Figure 32a**) where sightings were concentrated (**Figure 21**). Predicted densities were lower in the eastern Mediterranean than in the western Mediterranean, albeit intermediate densities were predicted in the western Ionian Sea, southern Adriatic Sea and northern Levantine Sea. Predicted densities were low on the continental shelf throughout the Mediterranean Sea. Maps of monthly predicted densities showed a decrease from March to August (see **Appendix C**).

CVs were highest in deep waters of the central Mediterranean and Hellenic Trench, as well as in the northern Adriatic Sea (**Figure 32b**). Extrapolation occurred in areas of the southeastern Mediterranean characterized by higher salinity and lower OPFish as well as in the northern Adriatic Sea (lower salinity) (**Figure 32c**). Predicted densities should be interpreted with caution in these areas.

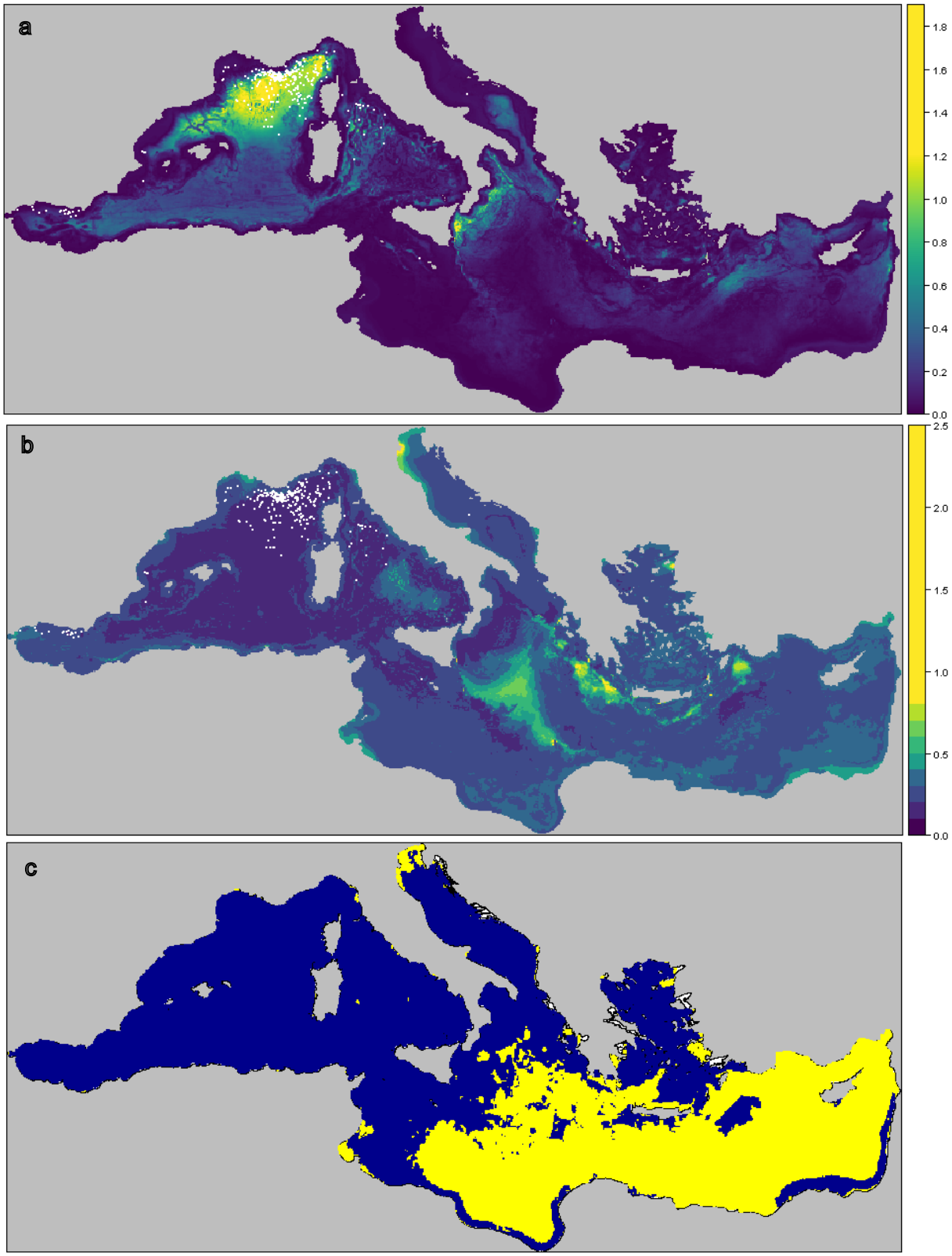

Figure 32. Maps of (a) mean summer predicted densities (individuals per 25 km^2), (b) mean summer coefficients of variation (unit-less) and (c) interpolation (dark blue) versus extrapolation (yellow) for fin whale. The summer season was defined from March to August (see Materials and Methods). Sightings are overlaid in white on maps (a) and (b).

Predicted densities were lower in winter than in summer throughout the Mediterranean Sea (**Figure 33a**). Although predicted densities remained highest in the Ligurian Sea, they were more homogeneous across the Algero-Provencal basin. In the eastern basin, fin whales were predicted to occur in offshore waters in low densities, with a few higher density areas in the western Ionian Sea and Levantine Sea. Maps of monthly predicted densities showed highest densities in September and February (see **Appendix C**).

As in summer, CVs were highest in deep waters of the central Mediterranean and Hellenic Trench and in the northern Adriatic Sea (**Figure 33b**). Extrapolation occurred in areas of the southeastern Mediterranean characterized by higher salinity and lower OPFish, and in the northern Adriatic Sea characterized by lower salinity (**Figure 33c**). Again, predicted densities should be interpreted with caution in these extrapolated areas.

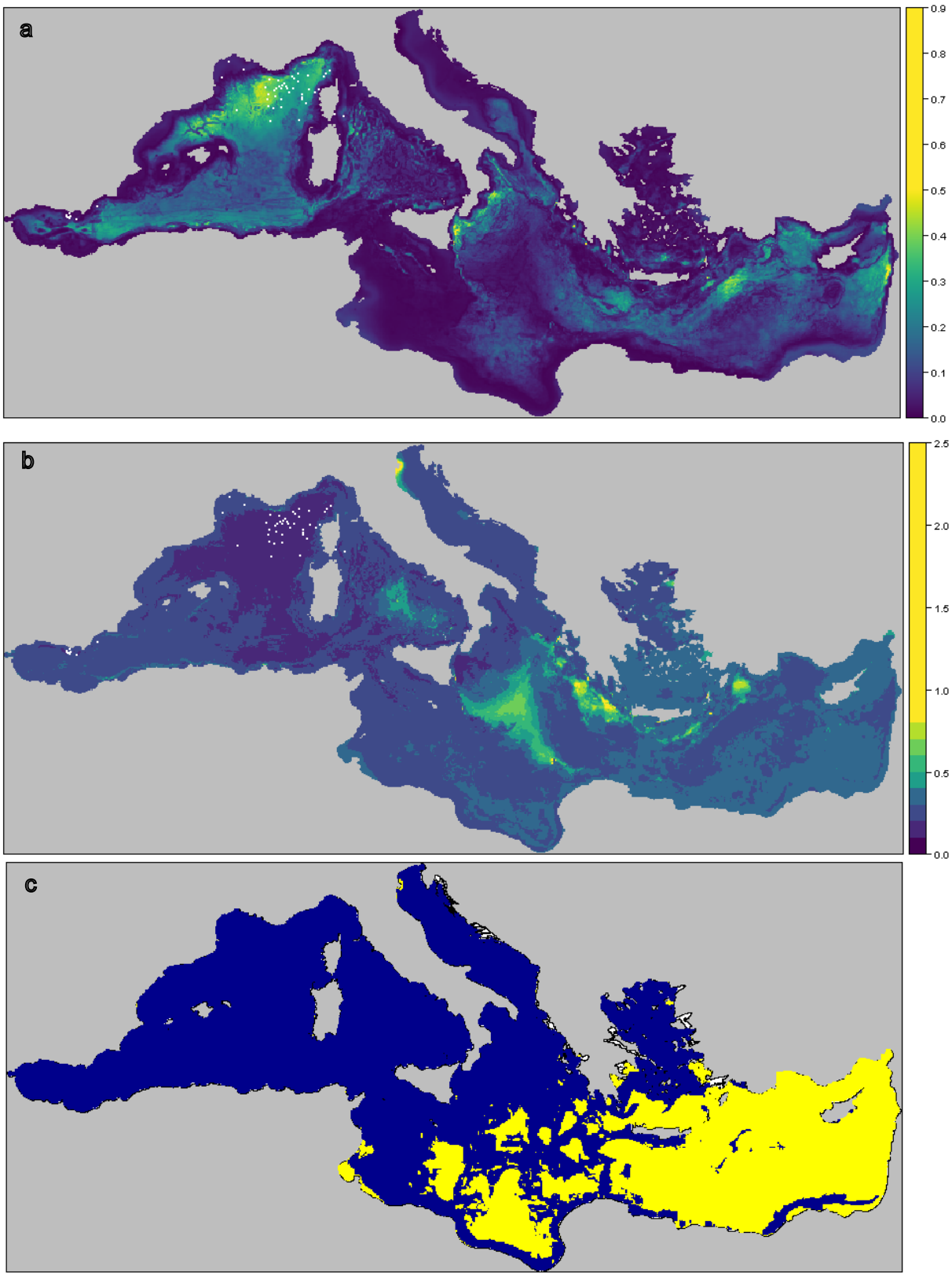

Figure 33. Maps of (a) mean winter predicted densities (individuals per 25 km^2), (b) mean winter coefficients of variation (unit-less) and (c) interpolation (dark blue) versus extrapolation (yellow) for fin whale. The winter season was defined from September to February (see Materials and Methods). Sightings are overlaid in white on figures (a) and (b).

4.3.7 Sperm whale

The selected covariates for sperm whale were depth, ocean productivity for fish smoothed with a 3 × 3-cell moving window, and net primary production derived from the Mediterranean Sea Reanalysis, and the explained deviance was 22.0 percent (**Table 11**). Sperm whale predicted densities were overall higher in the western Mediterranean than in the eastern Mediterranean (**Figure 34a**). Densities were highest on the continental slope in the western Mediterranean. High densities were also predicted in the western Ionian Sea (probably related to the intermediate values of OPFish). Low predicted densities on the continental shelf throughout the Mediterranean Sea were consistent with the absence of sightings on the shelf (**Figure 22**). Maps of monthly predicted densities showed highest densities in the western Mediterranean and the western Ionian Sea from May to September (see **Appendix C**).

CVs were highest in deepest areas of the central Mediterranean as well as nearshore where productivity was highest (**Figure 34b**). Extrapolation occurred in central and eastern Mediterranean waters characterized by deeper depth and lower OPFish and primary production in summer (**Figure 34c**). Limited extrapolation also occurred in some productive nearshore areas. We warn that predicted densities should be interpreted with caution in these areas.

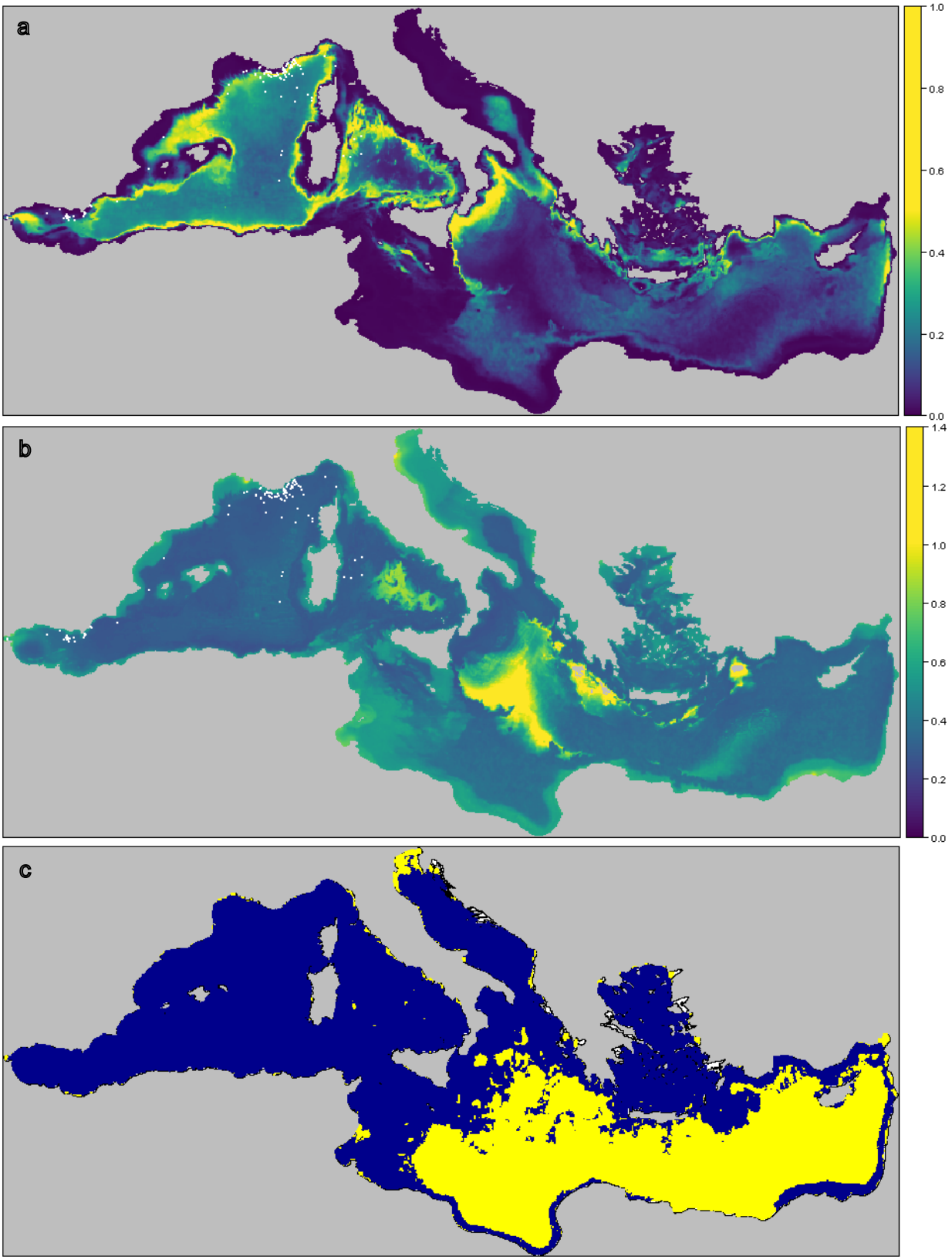

Figure 34. Maps of (a) mean annual predicted densities (individuals per 25 km^2), (b) mean annual coefficients of variation (unit-less) and (c) interpolation (dark blue) versus extrapolation (yellow) for sperm whale. Sightings are overlaid in white on maps (a) and (b).

4.3.8 Cuvier's beaked whale

For Cuvier's beaked whale, the final model included depth and slope only, and explained 36.2% of the deviance (**Table 11**). Densities were predicted to increase with depth values between 1,000 and 2,000 m and gentle slopes, consistent with the distribution of sightings, mainly located in the Alborán Sea (**Figure 23**). Predicted densities were highest in deep waters of the Alborán Sea, the northern Balearic Sea, the southern Adriatic Sea, the Gulf of Sirte and the Levantine Sea (**Figure 35a**).

CVs were highest in deepest waters and some nearshore areas (**Figure 35b**). Extrapolation occurred to deeper waters in the central Mediterranean and in the Hellenic Trench, and to shallower waters on the Tunisian plateau (extrapolation areas corresponded to high CVs) (**Figure 35c**). Predicted densities should be considered with caution in these areas.

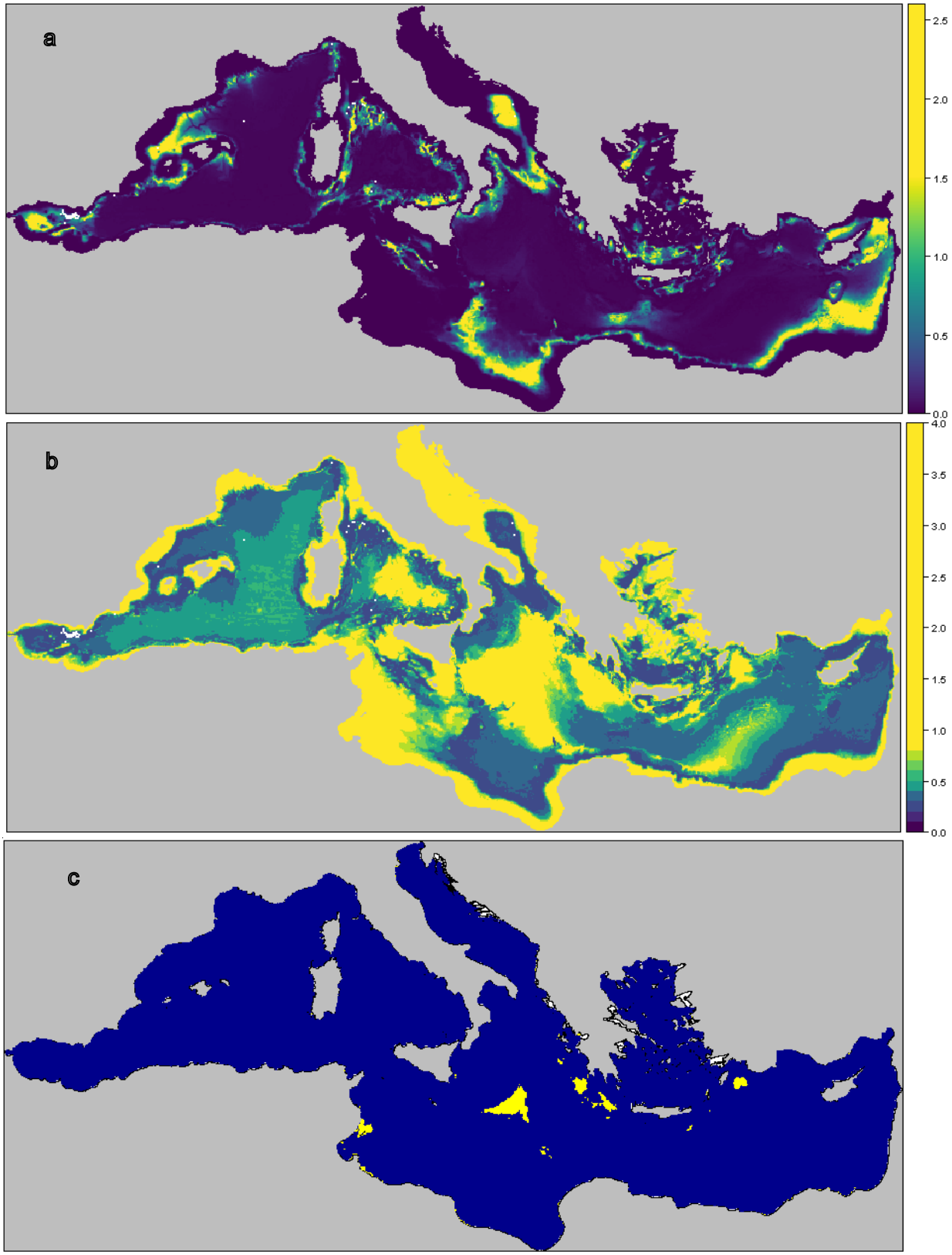

Figure 35. Maps of (a) mean annual predicted densities (individuals per 25 km^2), (b) mean annual coefficients of variation (unit-less) and (c) interpolation (dark blue) versus extrapolation (yellow) for Cuvier's beaked whale. Sightings are overlaid in white on maps (a) and (b).

4.4 Total Predicted Abundances

Total predicted abundances in the entire Mediterranean Sea, associated CVs and extents of extrapolation are presented in **Table 12** for each species. Total predicted abundances should be interpreted with substantial caution because (1) they were not corrected for perception bias, (2) for some species, producing predictions for the entire Mediterranean Sea required substantial extrapolation. The increased uncertainty related to extrapolation is not reflected in the CVs, which currently only account for uncertainty in the spatial model. As a result, we are presently unable to evaluate the reliability of these estimates.

Table 12. Total predicted abundance in the entire Mediterranean Sea, along with associated CV and extent of extrapolation for each species. Predicted abundances are annual means for all species except fin whale for which predicted abundances are summer and winter means. Note that mean predicted abundances are not corrected for perception bias, and CVs only incorporate spatial uncertainty. Total predicted abundances and CVs are also provided per month in Appendix C.

Species	Total predicted abundance (individuals)	CV	Extent of extrapolation (%)
Striped dolphin	1,950,345	0.15	49.5
Common bottlenose dolphin	165,320	0.19	20.3
Short-beaked common dolphin	164,512	0.55	53.4
Risso's dolphin	43,889	0.31	1.0
Long-finned pilot whale	81,830	0.47	52.3
Fin whale (summer / winter)	14,153 / 8,073	0.26 / 0.28	37.8 / 31.5
Sperm whale	12,704	0.43	34.4
Cuvier's beaked whale	19,587	0.64	1.0

5. Discussion

5.1 General

We developed habitat-based density models for eight cetacean species incorporating major surveys since 1999 and a variety of static, physical and biological covariates. We then predicted these models across the entire Mediterranean Sea, offering the first density predictions for most of these species in the region.

The coverage of surveys was heterogeneous throughout the Mediterranean Sea, and eastern and southern waters were sparsely surveyed compared to northwestern waters. Because of their relative oligotrophy, eastern Mediterranean waters are thought to host relatively low abundances of cetaceans relative to more productive regions (e.g., the eastern North Atlantic) (Notarbartolo di Sciara 2016). Thus, developing models from surveys conducted primarily in western waters, which encompass known high concentrations of cetaceans (e.g., the Ligurian Sea), and predicting them across the entire Mediterranean Sea may lead to an overestimation of densities in eastern waters. Furthermore, using survey data that is up to 17 years old for modeling average densities may be problematic if cetacean populations have increased or

decreased during this period (as seems to be the case for short-beaked common dolphin [Bearzi et al. 2003]). To document the uncertainty associated with our predictions, we mapped coefficients of variation from the spatial stage of the model, as well as the extent of interpolation *versus* extrapolation. Density predictions should always be viewed together with these associated uncertainty maps. We discuss modeling results and assess predictions against ecological knowledge for each species below.

5.2 Species-specific Considerations

5.2.1 Striped dolphin

The predicted distribution of striped dolphin was in accordance with its known distribution in deep waters from the Gibraltar Strait to the Levantine Sea (Notarbartolo di Sciara 2016). Predicted densities appeared remarkably high in the Alborán Sea compared to other areas of the northwestern Mediterranean. Despite the careful treatment we applied to the Alnitak surveys, a possible overestimation of abundances in the Alborán Sea cannot be ruled out.

A shipboard line-transect survey across the western Mediterranean in 1991-1992 estimated a density of 0.09 individuals km^{-2} (2.25 individuals 25 km^{-2}) in the Balearic Sea, 0.20 individuals km^{-2} (5 individuals 25 km^{-2}) in the Alborán Sea and 0.30 individuals km^{-2} (7.5 individuals 25 km^{-2}) in the Ligurian Sea (Forcada & Hammond 1998). The between-region differences in densities reported by this study do not seem to hold with those in our predictions; densities predicted by our model were several factors higher in the Alborán Sea than the Ligurian Sea. However, we advise caution in comparing our predicted densities to those of Forcada and Hammond (1998) because this survey was conducted in the early 1990s when oceanographic conditions may have been different and the striped dolphin population suffered mortality from a viral epizootic disease and incidental catch in driftnet fisheries. We will further investigate between-regions differences in predicted densities in the future.

In the northwest Mediterranean, Panigada et al. (2017b) and Laran et al. (2017) reported lower densities of striped dolphins in the winter than in the summer. In contrast in the Balearic Sea, Gomez de Segura et al. (2006) reported no significant changes in densities throughout the year. Although some seasonal variations in densities were apparent from our monthly predictions, there was insufficient evidence of seasonal variations across the region reported in the literature for us to recommend our monthly predictions be used for management purposes, so we provided a year-round mean density prediction.

Although it may appear high, the predicted abundance of close to 2 million individuals for the entire Mediterranean does not seem unrealistic considering that 98,000 individuals (uncorrected for perception and availability bias) and 130,000 individuals (uncorrected for perception bias) were estimated by other studies for parts of the northwestern Mediterranean in summer (Panigada et al. 2017b; Laran et al. 2017), and that the striped dolphin is by far the most abundant cetacean species in the Mediterranean Sea (Notarbartolo di Sciara 2016).

5.2.2 Common bottlenose dolphin

Our model predicted a widespread distribution of common bottlenose dolphin in continental shelf waters throughout the Mediterranean Sea. The predicted distribution is compatible with the

known occurrence of the species on the continental shelf from the Gibraltar Strait to the Levantine Sea (with possible habitat fragmentations in parts of its range due to human activities) (Notarbartolo di Sciara 2016).

As noted above, the highest densities predicted in the northern Adriatic Sea and the eastern Aegean Sea should be considered with care as extrapolation occurred in these low salinity areas that were poorly sampled by the surveys. Low confidence in these predictions is reflected in the high CVs. If these areas are of critical interest to the Navy, future revisions to this model should seek to control for this effect, e.g., by introducing additional surveys of low salinity areas, manually limiting the lower bound of the salinity covariate, or excluding the covariate from the model.

The predicted abundance of 165,320 individuals for the entire Mediterranean Sea appeared high but not implausible when compared to design-based estimates available for some of the surveyed areas. Cañadas and Hammond (2006) reported an uncorrected estimate of 584 individuals (95% CI = 278–744) in the northern Alborán Sea between 2000 and 2003. Lauriano et al. (2014) estimated 2,095 individuals in the Ligurian Sea, Corsican and Sardinian Seas, and Tyrrhenian Sea after correction for availability bias. Forcada et al. (2004) estimated 7,654 individuals (95% CI = 1,608–15,766) in the western Balearic Sea. In the PELAGIS survey area, Laran et al. (2017) reported that common bottlenose dolphins were distributed in coastal waters of the Gulf of Lions and Corsica in summer but found primarily in oceanic and slope strata in winter. They estimated abundances of 3,860 individuals (95% CI= 1,000–15,000) in summer and 13,412 individuals (95% CI = 5,500–32,600) in winter. We may build separate summer and winter models in the future, although there is limited evidence that common bottlenose dolphins have different relationships to their environment between seasons.

5.2.3 Short-beaked common dolphin

The predicted distribution of short-beaked common dolphin was consistent with the known distribution of the species in the Mediterranean Sea. Widespread and abundant throughout the Mediterranean in the mid-20th century, the population of short-beaked common dolphin is now abundant only in the westernmost portion of the basin, with sparse records in Algeria and Tunisia, concentrations around Maltese Islands and parts of the Aegean Sea, and isolated groups in the southeastern Tyrrhenian Sea and eastern Ionian Sea (Bearzi et al. 2003). Incorporating survey data from areas where short-beaked common dolphins are known to concentrate (e.g., Maltese Islands) would increase the reliability of predictions.

Our model predicted that densities of short-beaked common dolphin were higher in the western than in the eastern Alborán Sea, consistent with a prior density modeling study of the Alborán Sea (Cañadas & Hammond 2008). Two of the covariates selected in the prior study, SST and depth, were also retained in our final model. A more recent study by Cañadas and Vázquez (2017) suggested a contraction of short-beaked common dolphin habitat from east to west in the Alborán Sea following the global increase of water temperatures.

Our predicted abundance of 164,512 individuals in the entire Mediterranean Sea is likely an overestimate, considering that others estimated 19,428 individuals (95% CI = 15,277–22,804) in the surveyed part of the Alborán Sea (Cañadas & Hammond 2008). In addition, Forcada and

Hammond (1998) estimated 14,736 individuals (95% CI = 6,923–31,366) in the western Mediterranean from the 1991-1992 shipboard survey. However, these estimates were uncorrected for availability and perception biases. In the future, we will examine density relationships with covariates in more detail to investigate possible causes of overestimation.

5.2.4 Risso's dolphin

Our model predicted a widespread distribution of Risso's dolphin throughout the Mediterranean Sea with higher densities on the continental slope, in accordance with the species known distribution. The Risso's dolphin is known to occur widely in the Mediterranean Sea where it concentrates in continental slope waters as well as around islands and archipelagos (Bearzi et al. 2011). Although no sightings were reported east of the Adriatic Sea from the incorporated surveys, Risso's dolphin records exist for Greece (Frantzis et al. 2003), Turkey and Israel (Bearzi et al. 2011).

Our model highlighted Risso's dolphin's preferences for outer continental slope waters (the modeled relationship showed optimum densities at 800 to 1,400 m), as found by Azzellino et al. (2016) in the western Ligurian Sea. The modeled relationship increased with depth values > 3,000 m owing to sightings reported offshore by surveys in the Algero-Provencal basin and Tyrrhenian Sea. The modest explained deviance (11.5 percent) could increase with the incorporation of additional covariates that are ecologically meaningful for this species (e.g., physiographic covariates).

Our predicted abundance of 43,889 individuals in the entire Mediterranean Sea appeared high given the presumed low abundance of Risso's dolphin in the Mediterranean Sea (Bearzi et al. 2011). However, abundance estimates are scarce for Risso's dolphins in the Mediterranean Sea, providing few comparison points. We note that 2,000 individuals (95% CI = 700–5,900) were estimated in summer for the PELAGIS survey area in the Ligurian Sea and northern Algero-Provencal basin (Laran et al. 2017).

5.2.5 Long-finned pilot whale

Our model predicted the distribution of long-finned pilot whale to be restricted to the westernmost part of the Mediterranean Sea, in accordance with the literature. Long-finned pilot whales are found almost exclusively in the western basin (Verborgh et al. 2016). Densities are thought to be highest in the Strait of Gibraltar, Alborán Sea and Gulf of Vera (Cañadas et al. 2005). The species is present in the Balearic Sea, Provençal basin and Ligurian Sea, albeit in small numbers. Rare records are also available for the Adriatic Sea, Maltese islands, Morocco and Algeria.

Few abundance estimates exist for long-finned pilot whales in the Mediterranean Sea. The genetically isolated resident population of the Gibraltar Strait was estimated around 213 individuals (95% CI = 142–352) between 1999 and 2005 based on photo-identification data (Verborgh et al. 2009). In the Alborán Sea and Gulf of Vera, at least 1,569 individuals are known from photo-identification data (Verborgh et al. 2016). An unpublished density modeling study derived an abundance of 2,888 individuals (95% CI = 2,565–3,270) (uncorrected for availability and perception biases) in the Strait of Gibraltar, northern Alborán Sea and Gulf of Vera. A comparison of our predicted abundance of 81,830 individuals in the entire Mediterranean Sea

with the aforementioned local abundance estimates suggests a possible overestimation by our model. We will investigate this possible overestimation in more detail in the future.

5.2.6 Fin whale

The predicted distribution of fin whale throughout the Mediterranean Sea, with higher densities in the western Mediterranean, was consistent with general knowledge on Mediterranean fin whales. Fin whales occur throughout the Mediterranean Sea, but most sightings have been recorded between the Gulf of Lions and southern Italy, and in the Strait of Sicily. Small numbers of sightings have been recorded in the Ionian Sea and the southern Adriatic Sea. Sightings are rare farther east because of limited effort (Notarbartolo di Sciara et al. 2016). Two distinct populations of fin whales are known, one resident in the Mediterranean Sea and the other a seasonal visitor to the western Mediterranean from the North Atlantic Ocean. Individuals from the latter population likely cross the Strait of Gibraltar in winter and remain in the Mediterranean Sea until summer (Notarbartolo di Sciara et al. 2016).

Our summer and winter predictions concurred with the presumed contraction / dispersion of fin whale distribution according to the seasonal availability of their prey (Notarbartolo di Sciara et al. 2016). Our modeling results generally agreed with those of Druon et al. (2012) who modeled potential fin whale feeding habitat from presence-only data and four environmental covariates (depth, chlorophyll concentration, chlorophyll fronts and sea surface temperature). We note that the OPFish derived from chlorophyll fronts (Druon 2017) was selected in our fin whale density model. When extrapolated to the eastern Mediterranean, the Druon et al. (2012) model predicted fin whale aggregations in the western Ionian Sea, southern Adriatic Sea, Aegean Sea, and Levantine Sea in winter, and a disappearance of feeding habitat in summer. Our model predicted high densities in these same areas but in both winter and summer.

Our predicted summer abundance of 14,153 individuals in the entire Mediterranean Sea appeared plausible when compared to design-based estimates derived in surveyed areas of the northwestern Mediterranean. Laran et al. (2017) estimated 2,500 individuals (95% CI = 1,472–4,310) (corrected for availability bias only) in the Pelagos Sanctuary, Gulf of Lions and western seas of Corsica. Panigada et al. (2017b) estimated 665 individuals (95% CI = 350–1,263) (uncorrected for perception and availability bias) in the Pelagos Sanctuary, central Tyrrhenian Sea and western seas of Corsica and Sardinia. However, we believe the difference between our predicted summer and winter abundances (14,153 and 8,073 individuals, respectively) is probably larger than it should be. Although fin whales from the seasonal visitor population exit the Mediterranean Sea between May and October (Gauffier et al. 2018), it is unlikely that the departure of these individuals would lead to such a large drop in the overall abundance.

5.2.7 Sperm whale

The predicted distribution of sperm whale was overall consistent with its known occurrence over slope and offshore waters throughout the Mediterranean Sea (Notarbartolo di Sciara 2016). However, it is possible that our model underestimated sperm whale densities in the Hellenic trench, where sperm whales are known to concentrate (Rendell and Frantzis 2016). Incorporating line-transect surveys from the Hellenic Trench would increase the reliability of predictions in this presumed important area. We found no evidence in the literature supporting

the higher density area predicted by our model in the western Ionian Sea. We will examine this predicted density hotspot in greater detail in the future.

Our model predicted higher sperm whale densities in water depths between 1,000 and 2,000 m, corresponding to the continental slope. Similarly, a habitat modeling study in the northwestern Mediterranean predicted suitable sperm whale habitat over the continental slope and adjacent offshore waters (Praca and Gannier 2008). Distances to the nearest seamount or canyon were not retained in our final model, although higher probabilities of occurrence were predicted near these features in the Pelagos sanctuary by Fiori et al. (2014).

Our predicted abundance estimate of 12,704 individuals in the entire Mediterranean appeared high compared to existing abundance estimates. Based on photo-identification data, Rendell and Frantzis (2016) estimated 250 individuals in the Greek seas, and suggested an abundance in the low hundreds in the eastern basin. Lewis et al. (2017) derived abundance and density estimates from acoustic line-transect surveys conducted by IFAW/MCR (visual sightings of these surveys were incorporated in the present density models). They found that density in the surveyed part of the southwestern Mediterranean was 17 times higher than in the surveyed part of the eastern Mediterranean. A higher density in the southwestern Mediterranean compared to the eastern Mediterranean was also apparent in our predicted map (between-region differences in densities have not been quantified yet). After extrapolating to unsurveyed areas, Lewis et al. (2017) estimated 1,678 individuals in the western basin and 164 individuals in the eastern basin, summing up to 1,842 individuals in the entire Mediterranean Sea. Laran et al. (2017) estimated a few hundred sperm whales in the PELAGIS survey area (however, this estimate was derived from only nine sightings and had a wide confidence interval).

5.2.8 Cuvier's beaked whale

The predicted distribution of Cuvier's beaked whale was consistent overall with its known preference for deep continental slopes throughout the Mediterranean Sea. Strandings and sightings data indicate that Cuvier's beaked whales occur in the Alborán Sea, the Ligurian Sea (especially the Genoa canyon), the central Tyrrhenian Sea, the southern Adriatic Sea and the Hellenic Trench (Podestà et al. 2016). Other areas of presence include Greek waters, the Levantine Sea and the Balearic region (Podestà et al. 2016).

Depth and slope were the only covariates retained in the final model. Cuvier's beaked whale preferences for waters between 1,000 and 2,000 m were consistent with depth preferences observed in the Ligurian Sea (Podestà et al. 2016) and in the Alborán Sea, where the species occurs in waters of 1,000 m or deeper (Cañadas & Vázquez 2014). However, the preference for gentle slopes was surprising as other studies have pointed out preferences for moderately steep slopes (e.g., Moulins et al. 2007); this matter deserves further investigation. Despite the species known association with canyons and seamounts in some Mediterranean areas (e.g., the Ligurian Sea [Moulins et al. 2008]), distances to the nearest seamount or canyon were not retained in our final model.

Cañadas et al. (2018) developed a basin-wide density model of Cuvier's beaked whale by collating many different surveys in the Mediterranean Sea. It is important to note that perpendicular distances were not available for a significant part of these surveys, so effective

strip widths were extrapolated from similar surveys. Because the authors did not restrict their model to line-transect surveys, the total number of sightings amounted to 507 (it was 68 in our model). Their final model had depth, the coefficient of variation of depth, marine region and longitude as predictors. Their model predicted highest densities in the Alborán Sea, Ligurian Sea, Hellenic Trench, southern Adriatic Sea and eastern Ionian Sea. Two of the areas, the Ligurian Sea and the Hellenic Trench, did not appear as high density areas in our prediction. Thus, it is possible that our model underestimated densities in the Ligurian Sea and the Hellenic Trench. The incorporation of line-transect surveys from the Hellenic Trench and additional line-transect surveys from the Ligurian Sea would increase the reliability of predictions in these potentially important areas. Finally, the 5,799 individuals (CV = 24%) estimated in the entire Mediterranean by the Cañadas et al. (2018) model was about one fourth of our point estimate of abundance. Given the larger amount of sightings incorporated in the Cañadas et al. (2018) model, their abundance estimate is likely to be closer to reality.

5.3 Future Work

Although the habitat-based density models we have developed constitute an important baseline, these models remain exploratory and could be improved in the future. Potential improvements include the following:

Classifying unidentified dolphins to the species level. A substantial number of dolphin sightings were taxonomically ambiguous. For example, for the period 1998–2016, 5,160 dolphin sightings were fully taxonomically resolved to a genus and species while 640 were ambiguous (126 resolved to a pair of species, 514 to three or more). We omitted these ambiguous sightings from our density analysis, which potentially resulted in an underestimation of dolphin densities. A habitat-based classification model, trained on the fully resolved sightings, would assign a species ID to each ambiguous sighting and thus avoid this potential underestimation. This approach is similar to what was done for several species in the AFTT study area.

Exploring extrapolation in multivariate space. For this project, we have primarily explored extrapolation in univariate space based on individual ranges of covariates. In the previous gap analysis for the Mediterranean, we also explored extrapolation in multivariate space based on the convex hull and Gower's distance. Preliminary experiments using the latter metrics revealed computational limitations when calculated from a 5 x 5 km grid and contemporaneous covariates. Our experiments also revealed that multivariate extrapolation was prevalent throughout the Mediterranean Sea. It would be beneficial for future modeling efforts to find a "middle ground" between univariate and multivariate extrapolation based on the convex hull.

Improving uncertainty estimation. Estimation of CVs could be improved by implementing the approach described in Miller et al. 2013 (details in their Appendix S2), which accounts for covariance between monthly predictions. Should statistical tools for incorporating uncertainty in multiple detection functions and g(0)s become available, these could be used to improve CV estimation in the present study.

Quantifying density variations between sub-regions. Quantification of density variations across the Mediterranean Sea could be accomplished by computing mean predicted densities for various geographical sub-regions. A geographical cross-validation, similar to what was done

for the AFTT study area, could be implemented to investigate the sensitivity of density modeling results to heterogeneity in survey coverage. This would involve splitting the available survey data into sub-regions, excluding each region, and examining predictions of the resulting models.

Incorporating survey data from the ACCOBAMS basin-wide survey. A Mediterranean-wide survey is scheduled to take place in the summer 2018 thanks to the long-standing initiative of ACCOBAMS (Agreement on the Conservation of Cetaceans in the Black Sea, Mediterranean Sea and Contiguous Atlantic Area). This survey will be useful for filling existing data gaps and will collect data synoptically with a consistent methodology, which has never been done across the entire Mediterranean Sea. Incorporating data from this survey—should they become available for Navy-funded density modeling—would greatly improve the exploratory density models presented here.

6. References

Azzellino, A., S. Airoldi, S. Gaspari, C. Lanfredi, A. Moulins, M. Podestà, M. Rosso, and P. Tepsich. 2016. Risso's dolphin, *Grampus griseus*, in the Western Ligurian Sea: trends in population size and habitat use. Advances in Marine Biology75:207–234.

Bearzi, G., S. Bonizzoni, N.L. Santostasi, N.B. Furey, L. Eddy, V.D. Valavanis, and O. Gimenez. 2016. Dolphins in scaled-down Mediterranean: the Gulf of Corinth's odontocetes. Advances in Marine Biology75:297–331.

Bearzi, G., R.R. Reeves, G. Notarbartolo Di Sciara, E. Politi, A. Cañadas, A. Frantzis, and B. Mussi. 2003. Ecology, status and conservation of short-beaked common dolphins *Delphinus delphis* in the Mediterranean Sea. Mammal Review 33(3–4):224–252.

Bearzi, G., R.R. Reeves, E. Remonato, N. Pierantonio, and S. Airoldi. 2011. Risso's dolphin *Grampus griseus* in the Mediterranean Sea. Mammalian Biology - Zeitschrift für Säugetierkunde 76(4):385–400.

Becker, J.J., D.T. Sandwell, W.H.F. Smith, J. Braud, B. Binder, J. Depner, D. Fabre, J. Factor, S. Ingalls, S-H. Kim, R. Ladner, K. Marks, S. Nelson, A. Pharaoh, R. Trimmer, J. Von Rosenberg, G. Wallace, and P. Weatherall. 2009. Global bathymetry and elevation data at 30 arc seconds resolution: SRTM30_PLUS. Marine Geodesy 32(4):355–371.

Behrenfeld, M.J., and P.G. Falkowski. 1997. Photosynthetic rates derived from satellite-based chlorophyll concentration. Limnology and Oceanography 42(1):1–20.

Bethoux, JP, and B. Gentili. 1999. Functioning of the Mediterranean Sea: past and present changes related to freshwater input and climate changes. Journal of Marine Systems 20(1):33–47.

Bethoux, J.P., B. Gentili, P. Morin, E. Nicolas, C. Pierre, and D. Ruiz-Pino. 1999. The Mediterranean Sea: a miniature ocean for climatic and environmental studies and a key for the climatic functioning of the North Atlantic. Progress in Oceanography 44(1–3):131–146.

Bosc, E., A. Bricaud, and D. Antoine. 2004. Seasonal and interannual variability in algal biomass and primary production in the Mediterranean Sea, as derived from 4 years of SeaWiFS observations. Global Biogeochemical Cycles 18(1):GB1005.

Brasnett, B. 2008. The impact of satellite retrievals in a global sea-surface-temperature analysis. Quarterly Journal of the Royal Meteorological Society 134(636):1745–1760.

Buckland, S.T., D.R. Anderson, K.P. Burnham, J.L. Laake, D.L. Borchers, and L. Thomas. 2001. Introduction to Distance Sampling: Estimating Abundance of Biological Populations. Oxford University Press, New York.

Cañadas, A. 2011. Beaked Whales and Pilot Whales in the Alboran Sea (SW Mediterranean): Research Towards Improved Science-Based Mitigation Strategies for Risks from Man-Made Sound. DTIC Document. Available from http://oai.dtic.mil/oai/oai?verb=getRecord&metadataPrefix=html&identifier=ADA541598 (accessed 2 September 2014).

Cañadas, A, N. Aguilar de Soto, M. Aissi, A. Arcangeli, M. Azzolin, A. B-Nagy, G. Bearzi, I. Campana, C. Chicote, C. Cotte, R. Crosti, L. David, A. Di Natale, C. Fortuna, A. Frantzis, P. Garcia, M. Gazo, R. Gutierrez-Xarxa, D. Holcer, S. Laran, G. Lauriano, T. Lewis, A. Moulins, B. Mussi, G. Notarbartolo di Sciara, S Panigada, X. Pastor, E. Politi, M. Pulcini, J.A. Raga, L. Rendell, M. Rosso, P. Tepsich, J. Tomás, M. Tringali, and Th. Roger. 2018. The challenge of habitat modelling for threatened low density species using heterogeneous data: the case of Cuvier's beaked whales in the Mediterranean. Ecological Indicators 85:128–136.

Cañadas, A., and P.S. Hammond. 2006. Model-based abundance estimates for bottlenose dolphins off southern Spain: implications for conservation and management. Journal of Cetacean Research and Management 8(1):13–27.

Cañadas, A., and P.S. Hammond. 2008. Abundance and habitat preferences of the short-beaked common dolphin *Delphinus delphis* in the southwestern Mediterranean: implications for conservation. Endangered Species Research 4:309–331.

Cañadas, A., R. Sagarminaga, R. De Stephanis, E. Urquiola, and P.S. Hammond. 2005. Habitat preference modelling as a conservation tool: proposals for marine protected areas for cetaceans in southern Spanish waters. Aquatic Conservation: Marine and Freshwater Ecosystems 15(5):495–521.

Cañadas, A, and J.A. Vázquez. 2014. Conserving Cuvier's beaked whales in the Alboran Sea (SW Mediterranean): identification of high density areas to be avoided by intense man-made sound. Biological Conservation 178:155–162.

Cañadas, A., and J.A. Vázquez. 2017. Common dolphins in the Alboran Sea: facing a reduction in their suitable habitat due to an increase in sea surface temperature. Deep Sea Research Part II: Topical Studies in Oceanography 141:306–318.

Carretta, J.V., M.S. Lowry, C. Stinchcomb, M.S. Lynn, and R.E. Cosgrove. 2000. Distribution and Abundance of Marine Mammals at San Clemente Island and Surrounding Offshore Waters: Results from Aerial and Ground Surveys in 1998 and 1999. National Marine Fisheries Service, Southwest Fisheries Science Center, La Jolla, California.

Department of Navy. 2012. Commander Task Force 20, 4th, and 6th Fleet Navy Marine Species Density Database. (Technical Report). Naval Facilities Engineering Command Atlantic, Norfolk, Virginia.

D'Ortenzio, F., and M. Ribera d'Alcalà. 2009. On the trophic regimes of the Mediterranean Sea: a satellite analysis. Biogeosciences 6(2):139–148.

Drouot, V., A. Gannier, and J.C. Goold. 2004. Diving and feeding behaviour of sperm whales (*Physeter macrocephalus*) in the northwestern Mediterranean Sea. Aquatic Mammals 30(3):419–426.

Druon, J-N. 2017. Ocean Productivity Index for Fish in the Arctic: First Assessment from Satellite-Derived Plankton-to-Fish Favourable Habitats. EUR 29006 EN, Publications Office of the European Union, Luxembourg.

Druon, J-N, S. Panigada, L. David, A. Gannier, P. Mayol, A. Arcangeli, A. Cañadas, S. Laran, N. Di Méglio, and P. Gauffier. 2012. Potential feeding habitat of fin whales in the western Mediterranean Sea: an environmental niche model. Marine Ecology Progress Series 464:289–306.

Elith, J., M. Kearney, and S. Phillips. 2010. The art of modelling range-shifting species. Methods in Ecology and Evolution 1(4):330–342.

Fiori, C., L. Giancardo, M. Aïssi, J. Alessi, and P. Vassallo. 2014. Geostatistical modelling of spatial distribution of sperm whales in the Pelagos Sanctuary based on sparse count data and heterogeneous observations. Aquatic Conservation: Marine and Freshwater Ecosystems 24(3–4):41–49.

Forcada, J., M. Gazo, A. Aguilar, J. Gonzalvo, and M. Fernández-Contreras. 2004. Bottlenose dolphin abundance in the NW Mediterranean: addressing heterogeneity in distribution. Marine Ecology Progress Series 275:275–287.

Forcada, J., and P. Hammond. 1998. Geographical variation in abundance of striped and common dolphins of the western Mediterranean. Journal of Sea Research 39(3–4):313–325.

Foster, S.D., and M.V. Bravington. 2013. A Poisson–Gamma model for analysis of ecological non-negative continuous data. Environmental and Ecological Statistics 20(4):533–552.

Frantzis, A., P. Alexiadou, G. Paximadis, E. Politi, A. Gannier, and M. Corsini-Foka. 2003. Current knowledge of the cetacean fauna of the Greek Seas. Journal of Cetacean Research and Management 5(3):219–232.

Gauffier, P., P. Verborgh, J. Giménez, R. Esteban, JMS Sierra, and R. de Stephanis. 2018. Contemporary migration of fin whales through the Strait of Gibraltar. Marine Ecology Progress Series 588:215–228.

Gomez de Segura, A., E.A. Crespo, S.N. Pedraza, P.S. Hammond, and J.A. Raga. 2006. Abundance of small cetaceans in waters of the central Spanish Mediterranean. Marine Biology 150:149–160.

Harris, P.T., M. Macmillan-Lawler, J. Rupp, and E.K. Baker. 2014. Geomorphology of the oceans. Marine Geology 352:4–24.

Hollander, M., and D. Wolfe. 1975. Nonparametric statistical methods. Biometrical Journal 17(8):526.

Kaschner, K., R. Watson, A.W. Trites, and D. Pauly. 2006. Mapping world-wide distributions of marine mammal species using a relative environmental suitability (RES) model. Marine Ecology Progress Series 316:285–310.

Laake, J., J. Calambokidis, S. Osmek, and D. Rugh. 1997. Probability of detecting harbor porpoise from aerial surveys: estimating g(0). The Journal of Wildlife Management 61(1):63–75.

Laran, S., E. Pettex, M. Authier, A. Blanck, L. David, G. Dorémus, H. Falchetto, P. Monestiez, O. Van Canneyt, and V. Ridoux. 2017. Seasonal distribution and abundance of cetaceans within French waters- Part I: The North-Western Mediterranean, including the Pelagos sanctuary. Deep Sea Research Part II: Topical Studies in Oceanography 141:20–30.

Lauriano, G., N. Pierantonio, G. Donovan, and S. Panigada. 2014. Abundance and distribution of *Tursiops truncatu*s in the Western Mediterranean Sea: an assessment towards the Marine Strategy Framework Directive requirements. Marine Environmental Research 100:86–93.

Lewis, T., O. Boisseau, M. Danbolt, D. Gillespie, C. Lacey, R. Leaper, J.N. Matthews, R. McLanaghan, and A. Moscrop. 2017. Abundance estimates for sperm whales in the Mediterranean Sea from acoustic line-transect surveys. Journal of Cetacean Research and Management. Available from https://ore.exeter.ac.uk/repository/handle/10871/27538 (accessed February 19, 2018).

Longhurst, A.R. 2007. Ecological Geography of the Sea. Academic Press, Oxford.

Mannocci, L., J.J. Roberts, P.N. Halpin, M. Authier, O. Boisseau, M.N. Bradai, A. Cañadas, C. Chicote, L. David, N. Di-Méglio, C.M. Fortuna, A. Frantzis, M. Gazo, T. Genov, P.S.Hammond, D. Holcer, K. Kaschner, D. Kerem, G. Lauriano, T. Lewis, G. Notarbartolo di Sciara, S. Panigada, J.A. Raga, A. Scheinin, V. Ridoux, A. Vella, and J. Vella 2018. Assessing cetacean surveys throughout the Mediterranean Sea: a gap analysis in environmental space. Scientific Reports 8:3126.

Mannocci, L., J.J. Roberts, and P.N. Halpin. 2016. Data gap analysis and data collection for marine species density models in the Mediterranean Sea. Submitted to Naval Facilities Engineering Command Atlantic, prepared for U.S. Fleet Forces Command, prepared by the Duke University Marine Geospatial Ecology Lab, Durham, North Carolina, under Contract N62470-15-D-8006 (TO21) issued to HDR, San Diego, California. August 2016.

Marques, F.F.C., and S.T. Buckland. 2004. Covariate models for the detection function. Pages 31–47 Advanced Distance Sampling. Oxford, New York.

Marques, T.A., L. Thomas, S.G. Fancy, and S.T. Buckland. 2007. Improving estimates of bird density using multiple- covariate distance sampling. The Auk 124(4):1229–1243.

Merow, C., M.J. Smith, T.C. Edwards, A. Guisan, S.M. McMahon, S. Normand, W. Thuiller, R.O. Wüest, N.E. Zimmermann, and J. Elith. 2014. What do we gain from simplicity versus complexity in species distribution models? Ecography 37(12):1267–1281.

Miller, D.L., M.L. Burt, E.A. Rexstad, and L. Thomas. 2013. Spatial models for distance sampling data: recent developments and future directions. Methods in Ecology and Evolution 4(11):1001–1010.

Miller, D.L., and L. Thomas. 2015. Mixture models for distance sampling detection functions. PLoS ONE 10(3):e0118726.

Moulins, A., M. Rosso, M. Ballardini, and M. Würtz. 2008. Partitioning of the Pelagos Sanctuary (north-western Mediterranean Sea) into hotspots and coldspots of cetacean distributions. Journal of the Marine Biological Association of the United Kingdom 88(6):1273–1281.

Moulins, A., M. Rosso, B. Nani, and M. Würtz. 2007. Aspects of the distribution of Cuvier's beaked whale (*Ziphius cavirostris*) in relation to topographic features in the Pelagos Sanctuary (north-western Mediterranean Sea). Journal of the Marine Biological Association of the United Kingdom 87:177–186.

Mussi, B., A. Miragliuolo, A. Zucchini, and D.S. Pace. 2014. Occurrence and spatio-temporal distribution of sperm whale (*Physeter macrocephalus*) in the submarine canyon of Cuma (Tyrrhenian Sea, Italy). Aquatic Conservation: Marine and Freshwater Ecosystems 24(S1):59–70.

Natoli, A., A. Birkun, A. Aguilar, A. Lopez, and A.R. Hoelzel. 2005. Habitat structure and the dispersal of male and female bottlenose dolphins (*Tursiops truncatus*). Proceedings of the Royal Society B: Biological Sciences 272(1569):1217–1226.

Natoli, A., A. Cañadas, C. Vaquero, E. Politi, P. Fernandez-Navarro, and A.R. Hoelzel. 2008. Conservation genetics of the short-beaked common dolphin (*Delphinus delphis*) in the Mediterranean Sea and in the eastern North Atlantic Ocean. Conservation Genetics 9:1479.

Notarbartolo di Sciara, G. 2016. Marine mammals in the Mediterranean Sea: an overview. Academic Press 75:1–36.

Notarbartolo di Sciara, G., M. Castellote, J-N. Druon, and S. Panigada. 2016. Fin whales, *Balaenoptera physalus*: at home in a changing Mediterranean Sea? Advances in Marine Biology 75:75–101.

Panigada, S., G.P. Donovan, J-N. Druon, G. Lauriano, N. Pierantonio, E. Pirotta, M. Zanardelli, A.N. Zerbini, and G. Notarbartolo di Sciara. 2017a. Satellite tagging of Mediterranean fin whales: working towards the identification of critical habitats and the focusing of mitigation measures. Scientific Reports 7:3365.

Panigada, S., G. Lauriano, G. Donovan, N. Pierantonio, A. Cañadas, J.A. Vázquez, and L. Burt. 2017b. Estimating cetacean density and abundance in the Central and Western Mediterranean Sea through aerial surveys: implications for management. Deep Sea Research Part II: Topical Studies in Oceanography 141:41–58.

Pinardi, N., and E. Masetti. 2000. Variability of the large scale general circulation of the Mediterranean Sea from observations and modelling: a review. Palaeogeography, Palaeoclimatology, Palaeoecology 158(3–4):153–173.

Podestà, M., A. Azzellino, A. Cañadas, A. Frantzis, A. Moulins, M. Rosso, P. Tepsich, and C. Lanfredi. 2016. Cuvier's beaked whale, *Ziphius cavirostri*s, distribution and occurrence in the Mediterranean Sea: high-use areas and conservation threats. Advances in Marine Biology 75:103–140.

Pollock, K.H., H.D. Marsh, I.R. Lawler, and M.W. Allderdge. 2006. Estimating animal abundance in heterogeneous environments: an application to aerial surveys for dugongs. Journal of Wildlife Management 70(1):255–262.

Praca, E., and A. Gannier. 2008. Ecological niches of three teuthophageous odontocetes in the northwestern Mediterranean Sea. Ocean Science 4(1):49–59.

Rendell, L., and A. Frantzis. 2016. Mediterranean sperm whales, *Physeter macrocephalus*: the precarious state of a lost tribe. Advances in Marine Biology 75:37–74.

Roberts, J.J., B.D. Best, L. Mannocci, E. Fujioka, P.N. Halpin, D.L. Palka, L.P. Garrison, K.D. Mullin, T.V.N. Cole, C.B. Khan, W.M. McLellan, D.A. Pabst, and G.G. Lockhart. 2016. Habitat-based cetacean density models for the U.S. Atlantic and Gulf of Mexico. Scientific Reports 6:22615.

Roberts, J.J., B.D. Best, D.C. Dunn, E.A. Treml, and P.N. Halpin. 2010. Marine Geospatial Ecology Tools: An integrated framework for ecological geoprocessing with ArcGIS, Python, R, MATLAB, and C++. Environmental Modelling & Software 25(10):1197–1207.

Roberts, J.J., L. Mannocci, and P.N. Halpin. 2015. Marine Mammal Density Models for the U.S. Navy Atlantic Fleet Training and Testing (AFTT) Study Area for the Phase III Navy Marine Species Density Database (NMSDD), Document Version 1.0. Duke University Marine Geospatial Ecology Lab, Durham, NC.

Rovere, M., and M. Würtz. 2015. Atlas of the Mediterranean seamounts and seamount-like structures. Available from https://portals.iucn.org/library/node/45816 (accessed 13 February 2018).

Simoncelli, S., C. Fratianni, N. Pinardi, A. Grandi, M. Drudi, P. Oddo, and S. Dobricic. 2014. Mediterranean Sea physical reanalysis (MEDREA 1987-2015) (Version 1). E.U. Copernicus Marine Service Information. DOI: 10.25423/medsea_reanalysis_phys_006_004.

Tepsich, P., M. Rosso, P.N. Halpin, and A. Moulins. 2014. Habitat preferences of two deep-diving cetacean species in the northern Ligurian Sea. Marine Ecology Progress Series 508:247–260.

Teruzzi, A., G. Cossarini, P. Lazzari, S. Salon, G. Bolzon, A. Crise, and G. Solidoro. 2016. Mediterranean Sea biogeochemical reanalysis (CMEMS MED REA-Biogeochemistry 1999-2015). Copernicus Monitoring Environment Marine Service. DOI: 10.25423/medsea_reanalysis_bio_006_008.

Verborgh, P., R. De Stephanis, S. Pérez, Y. Jaget, C. Barbraud, and C. Guinet. 2009. Survival rate, abundance, and residency of long-finned pilot whales in the Strait of Gibraltar. Marine Mammal Science 25(3):523–536.

Verborgh, P., P. Gauffier, R. Esteban, J. Giménez, A. Cañadas, J.M. Salazar-Sierra, and R. de Stephanis. 2016. Conservation status of long-finned pilot whales, *Globicephala melas*, in the Mediterranean Sea. Advances in Marine Biology 75:173–203..

Wenger, S.J., and J.D. Olden. 2012. Assessing transferability of ecological models: an underappreciated aspect of statistical validation. Methods in Ecology and Evolution 3(2):260–267.

Wood, S. 2014. Mixed GAM Computation Vehicle with GCV/AIC/REML smoothness estimation (mgcv) package Version 1.8-4.

Wood, S.N. 2011. Fast stable restricted maximum likelihood and marginal likelihood estimation of semiparametric generalized linear models. Journal of the Royal Statistical Society: Series B (Statistical Methodology) 73(1):3–36.

This page intentionally left blank.

A

Detection Functions

This page intentionally left blank.

Appendix A: Detection Functions

This appendix provides for each species a detailed summary of detection functions (sightings hierarchies, details of detection functions applied per survey, detection function plots and quantile-quantile plots providing an indication of fit). Depending on available sample size, conventional distance sampling or multiple covariate distance sampling (with one or two covariates) was applied (see Methods).

Striped dolphin

For aerial surveys, there were sufficient sightings to fit survey-specific detection functions. Given the differing altitude of University of Valencia surveys, we preferred survey-specific detection functions (despite the low sample size) to a pooled detection function. For shipboard surveys, there were sufficient sightings to fit separate detection functions for the two configurations of Alnitak surveys and for EcoOcean surveys. IFAW surveys were pooled with EcoOcean surveys that had a similar (slightly higher) observation height.

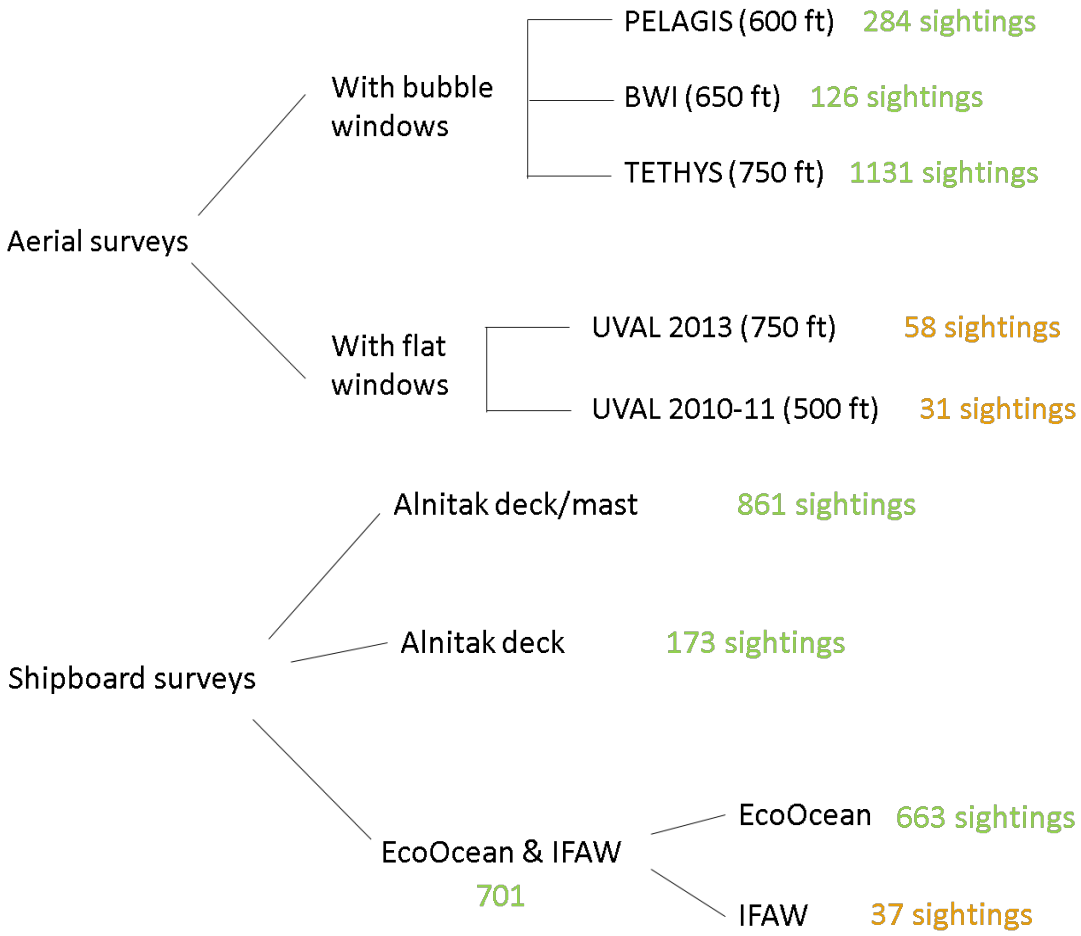

Figure A-1. Sightings hierarchies for aerial and shipboard surveys for striped dolphin. Color coding: ≥60 sightings: green, 31-59 sightings: orange, ≤30 sightings: red. When surveys were conducted by multiple organizations (e.g., TETHYS/ISPRA), only the first survey organization listed in Table was included for brevity. UVAL refers to University of Valencia surveys.

Table A-1. Detection functions applied per survey to striped dolphin sightings. Hn: half normal, Hr: hazard rate, ESHW: effective strip half width. Visibility2 corresponds to the visibility covariate reclassified into a smaller number of classes. SightedBy2 indicates if the sighting was made from the deck or from the mast in Alnitak surveys. When surveys were conducted by multiple organizations (e.g., TETHYS/ISPRA), only the first survey organization listed in Table was included for brevity. UVAL refers to University of Valencia surveys.

Surveys	Surveys used for detection function fitting	Right truncation distance (m)	Left truncation distance (m)	Detection function	Mean ESHW (m)
PELAGIS	PELAGIS	350	0	Hn size	163
BWI	BWI	650	0	Hn size	337
TETHYS	TETHYS	600	0	Hr CloudCover + size	331
UVAL 2013	UVAL 2013	500	124.8	Hn Visibility2	183
UVAL 2010/11	UVAL 2010/11	300	83.2	Hn	107
Alnitak deck/mast	Alnitak deck/mast	2000	0	Hr SightedBy2 + size	621
Alnitak deck	Alnitak deck	900	0	Hr Douglas	216
EcoOcean	EcoOcean	600	0	Hr Douglasfact	84
IFAW	EcoOcean and IFAW	600	0	Hr size	79

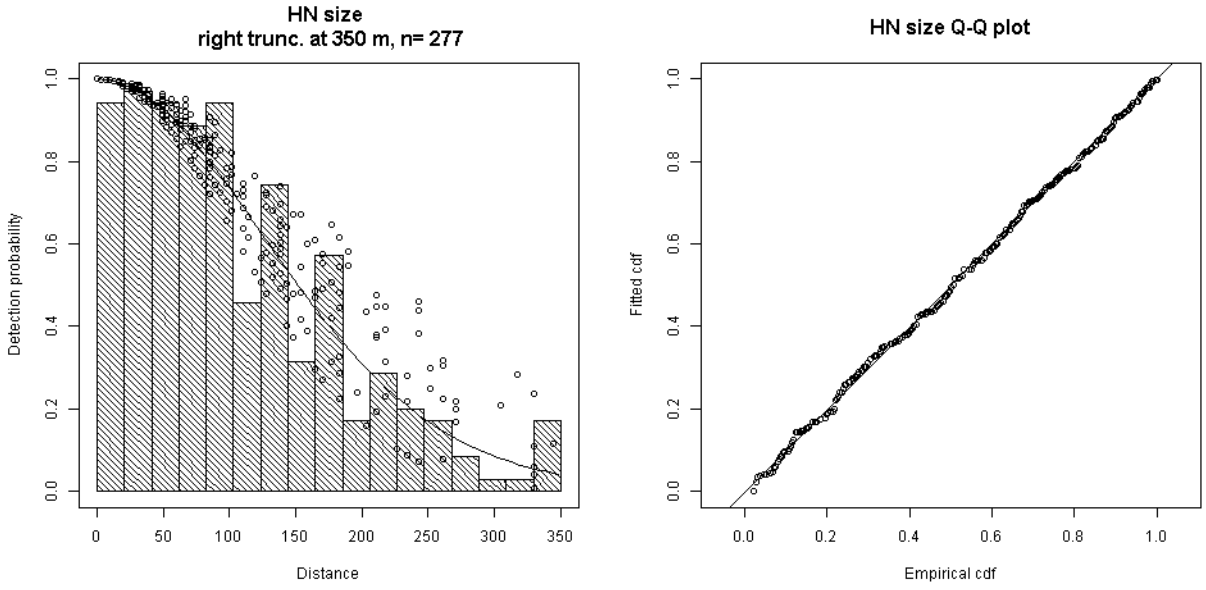

Figure A-2. Selected detection function fitted from PELAGIS surveys

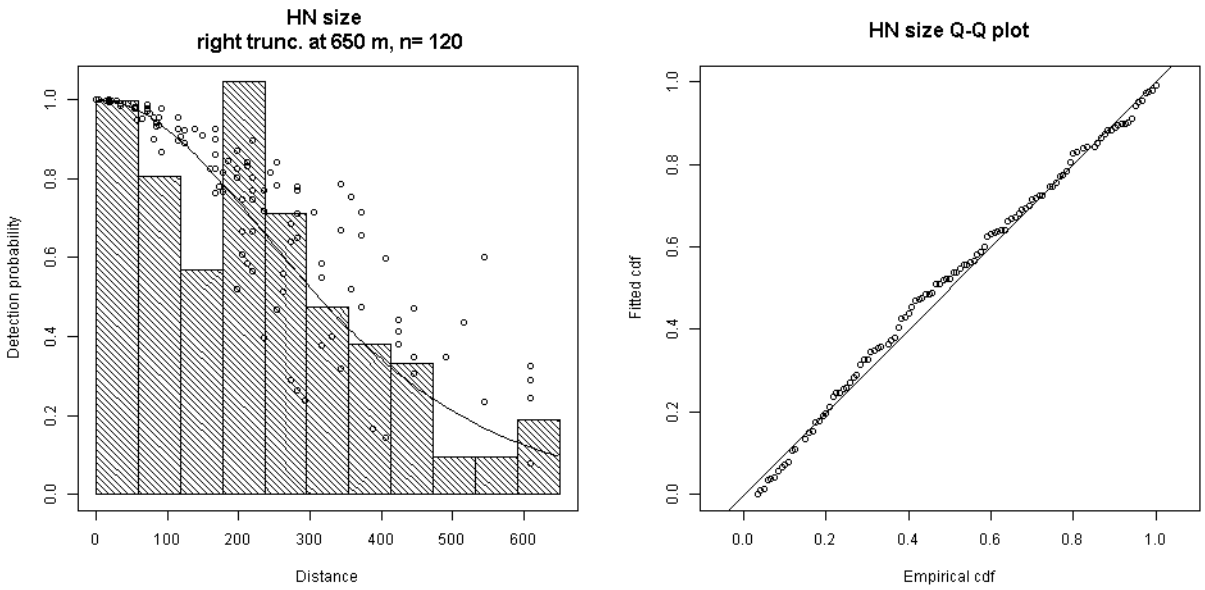

Figure A-3. Selected detection function fitted from BWI surveys

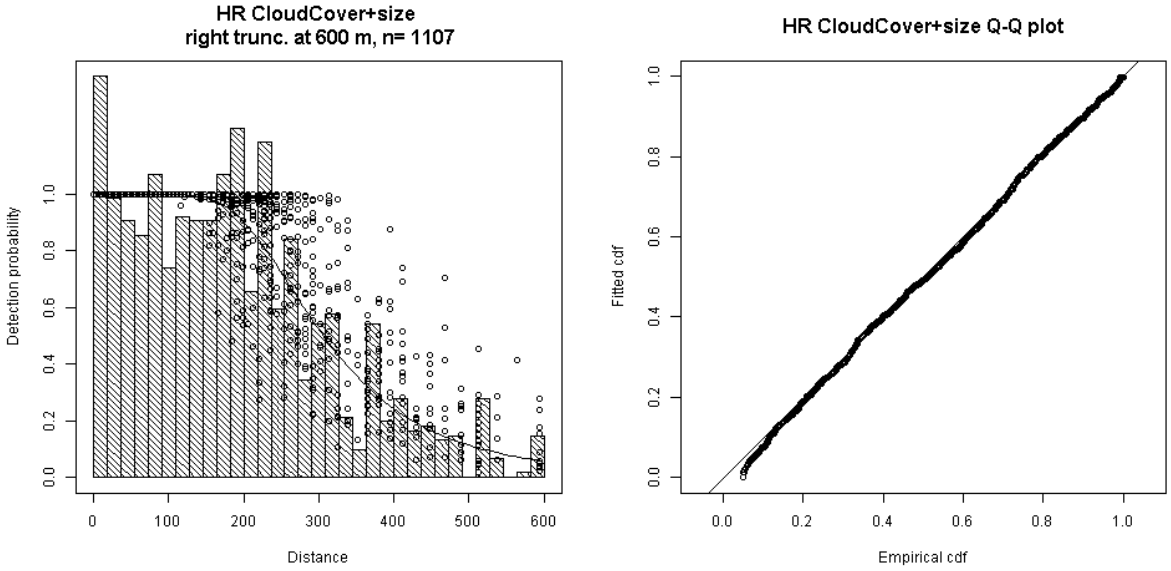

Figure A-4. Selected detection function fitted from TETHYS surveys

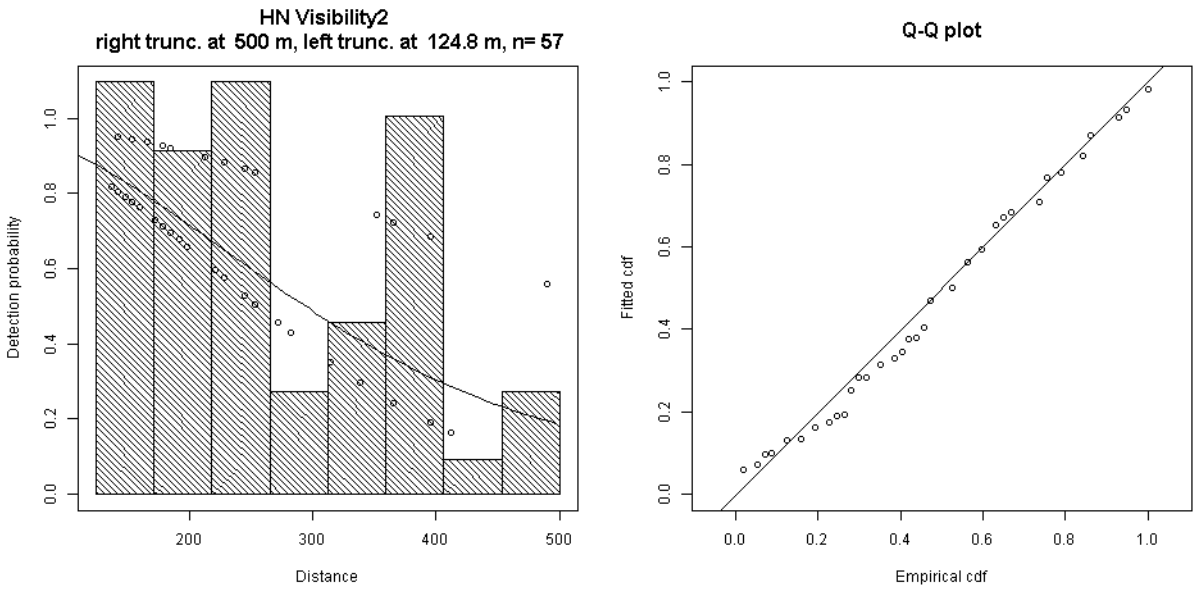

Figure A-5. Selected detection function fitted from UVAL 2013 surveys

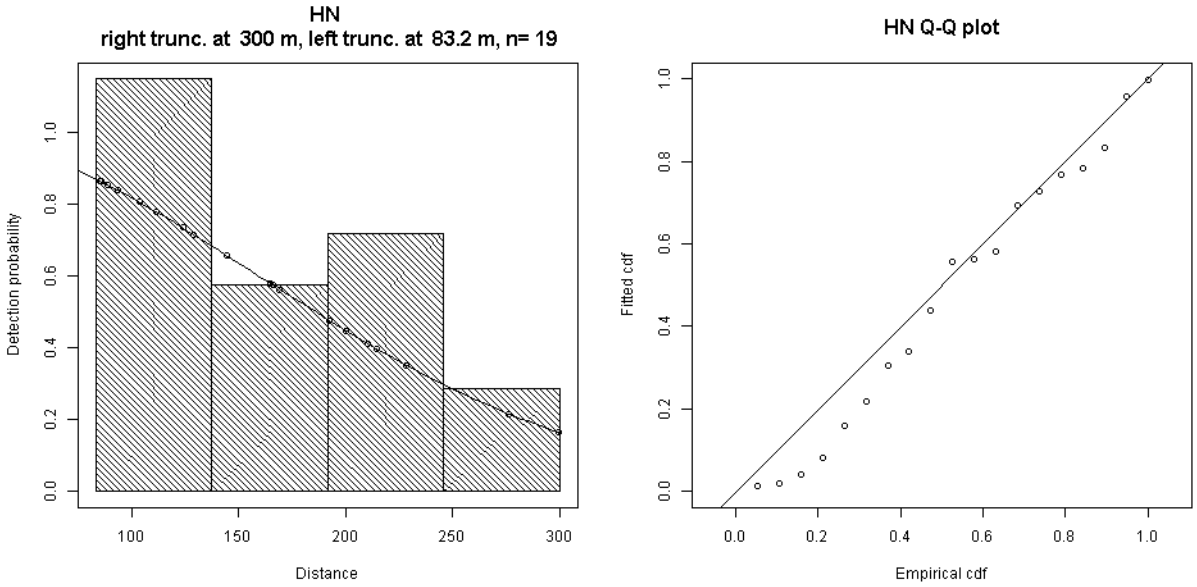

Figure A-6. Selected detection function fitted from UVAL 2010/11 surveys

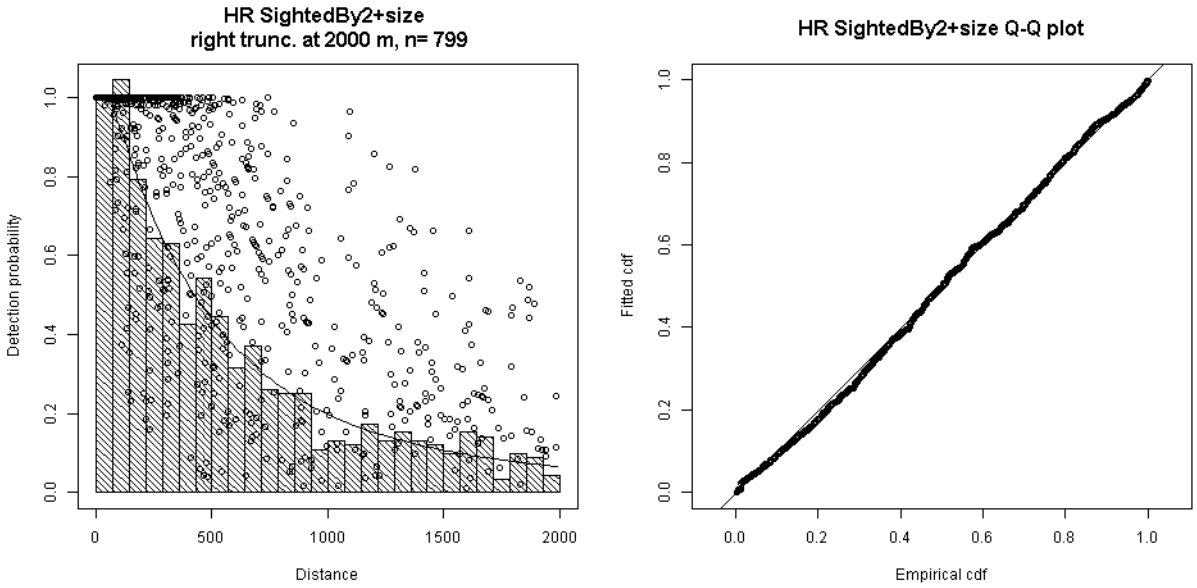

Figure A-7. Selected detection function fitted from Alnitak deck/mast surveys

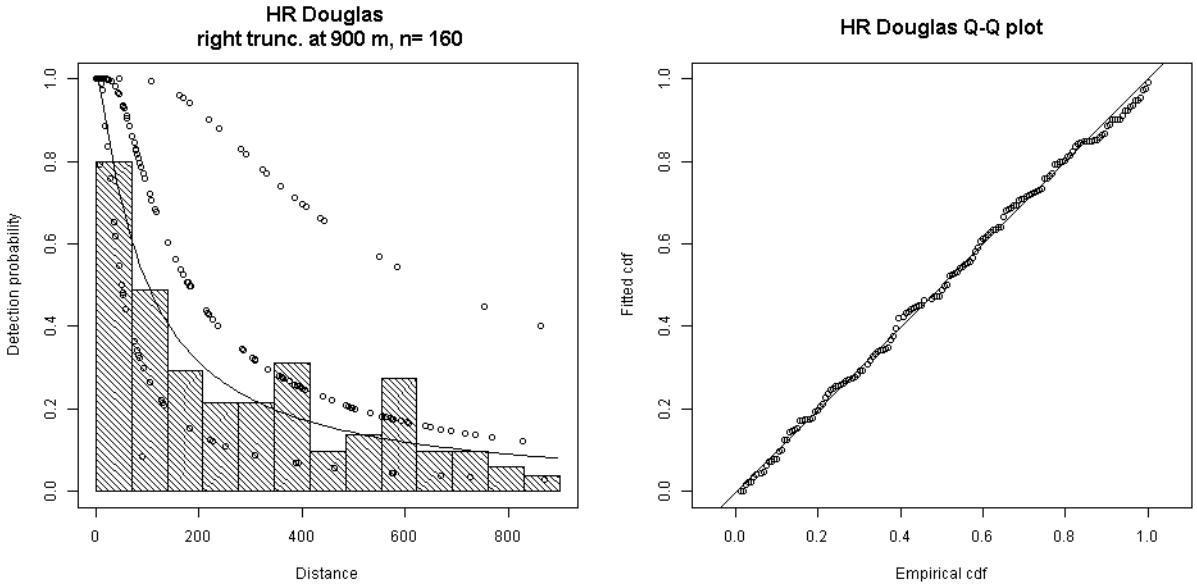

Figure A-8. Selected detection function fitted from Alnitak deck surveys

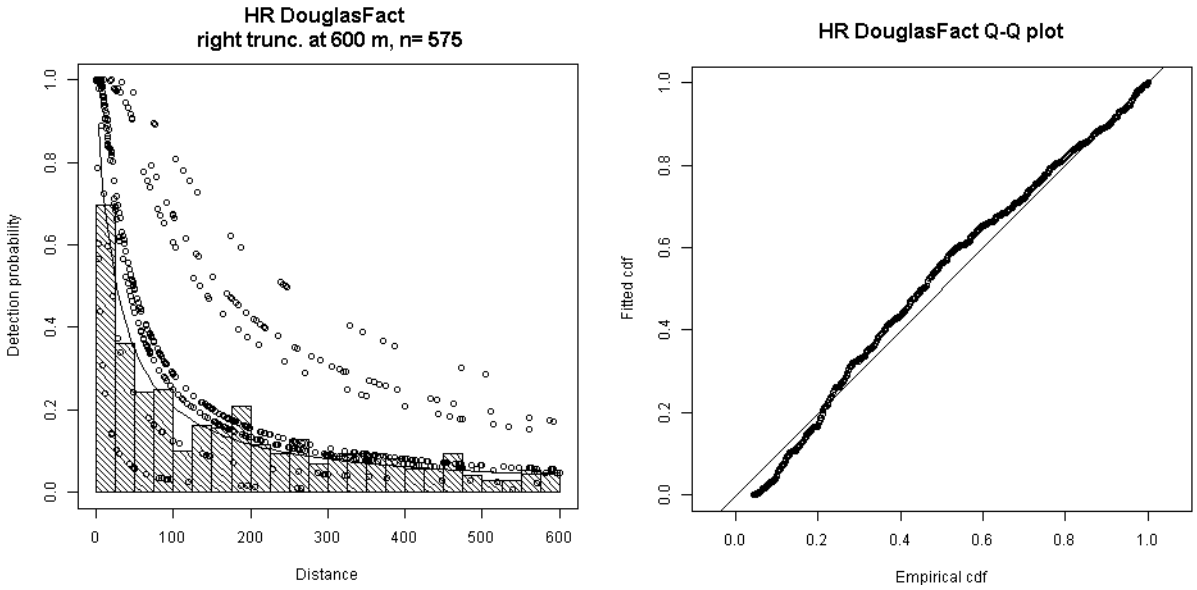

Figure A-9. Selected detection function fitted from EcoOcean surveys

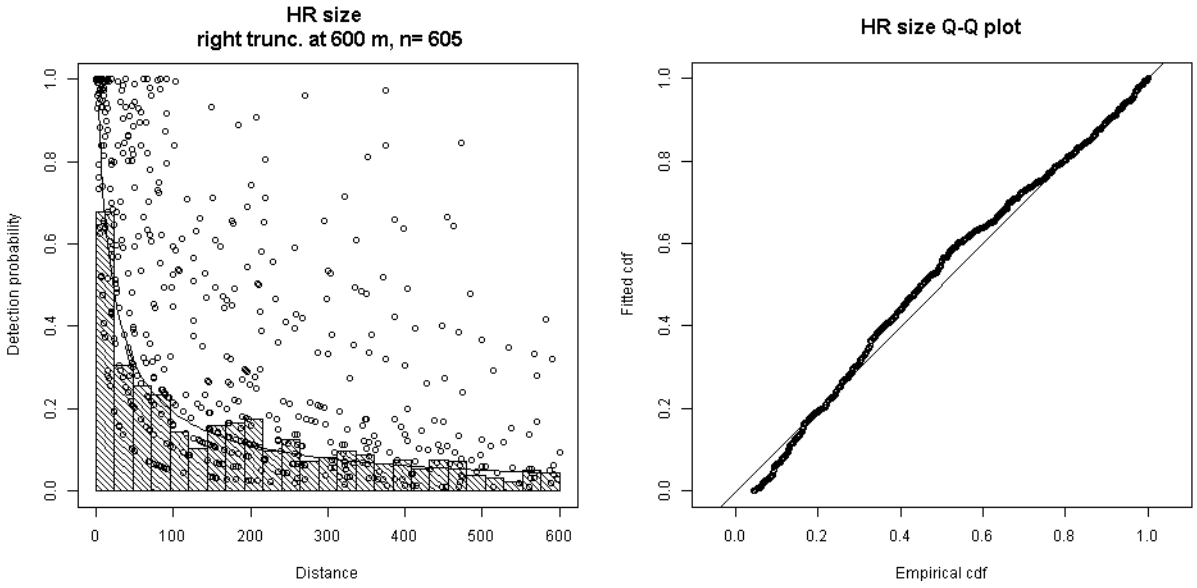

Figure A-10. Selected detection function fitted from IFAW and EcoOcean surveys

Common bottlenose dolphin

For aerial surveys, there were sufficient sightings to fit survey-specific detection functions. There were too few sightings to fit a detection function for University of Valencia surveys so we pooled PELAGIS, BWI and TETHYS surveys and applied the resulting detection function to University of Valencia surveys. Doing so, we assumed detection from the bubble window surveys was a good proxy for detection from the flat window surveys, except for the area not visible from flat windows. For shipboard surveys, there were sufficient sightings to fit separate detection functions for the two configurations of Alnitak surveys, but we had to pool EcoOcean surveys and IFAW surveys.

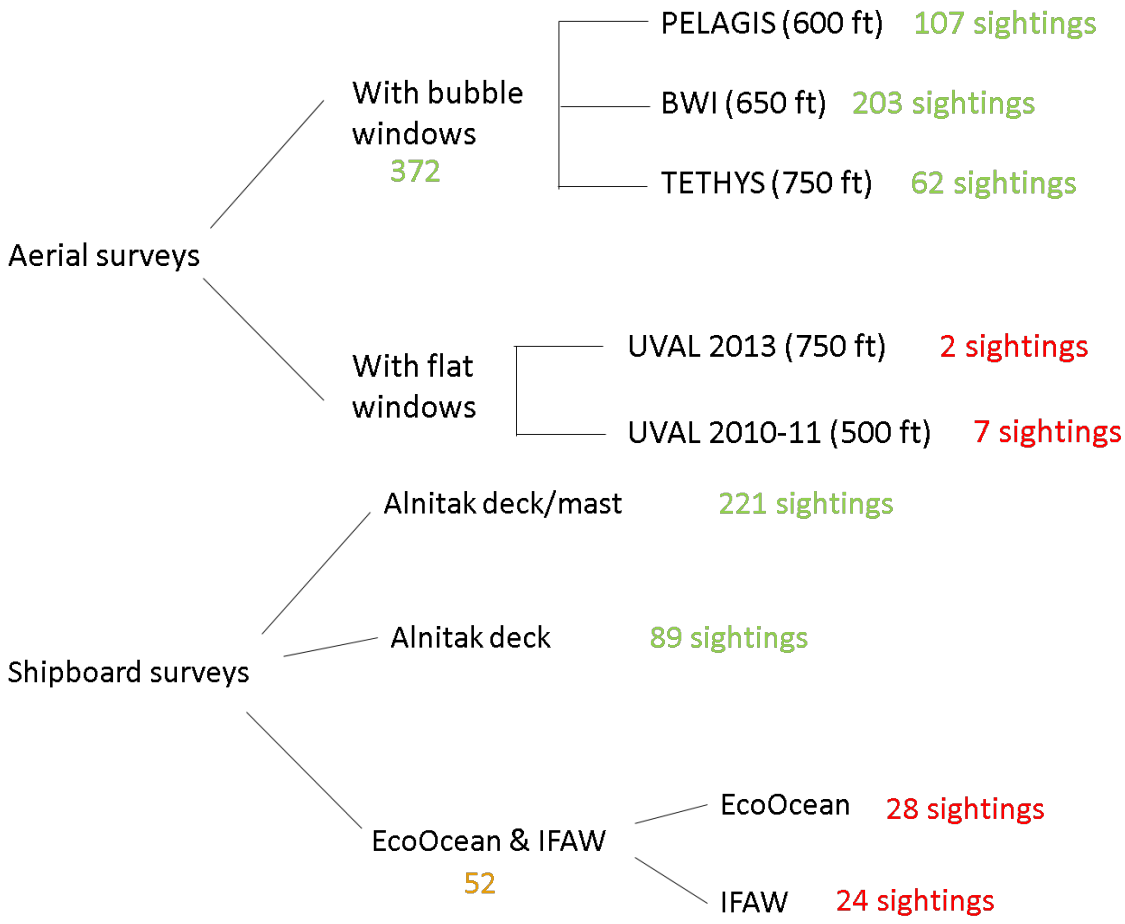

Figure A-11. Sightings hierarchies for aerial and shipboard surveys for bottlenose dolphin. Color coding: ≥60 sightings: green, 31-59 sightings: orange, ≤30 sightings: red. When surveys were conducted by multiple organizations (e.g., TETHYS/ISPRA), only the first survey organization listed in Table was included for brevity. UVAL refers to University of Valencia surveys.

Table A-2. Detection functions applied per survey to bottlenose dolphin sightings. Hn: half normal, Hr: hazard rate, ESHW: effective strip half width. SightedBy2 indicates if the sighting was made from the deck or from the mast in Alnitak surveys. When surveys were conducted by multiple organizations (e.g., TETHYS/ISPRA), only the first survey organization listed in Table was included for brevity. UVAL refers to University of Valencia surveys.

Surveys	Surveys used for detection function fitting	Right truncation distance (m)	Left truncation distance (m)	Detection function applied	Mean ESHW (m)
PELAGIS	PELAGIS	400	0	Hr season	193
BWI	BWI	700	0	Hr	438
TETHYS	TETHYS	400	0	Hr	275
UVAL 2013	PELAGIS, BWI and TETHYS	560	124.8	Hn	297
UVAL 2010/11	PELAGIS, BWI and TETHYS	560	83.2	Hn	297
Alnitak deck/mast	Alnitak deck/mast	200	0	Hr SightedBy2+size	651
Alnitak deck	Alnitak deck	800	0	Hr size	365
EcoOcean	EcoOcean and IFAW	900	0	Hr	78
IFAW	EcoOcean and IFAW	900	0	Hr	78

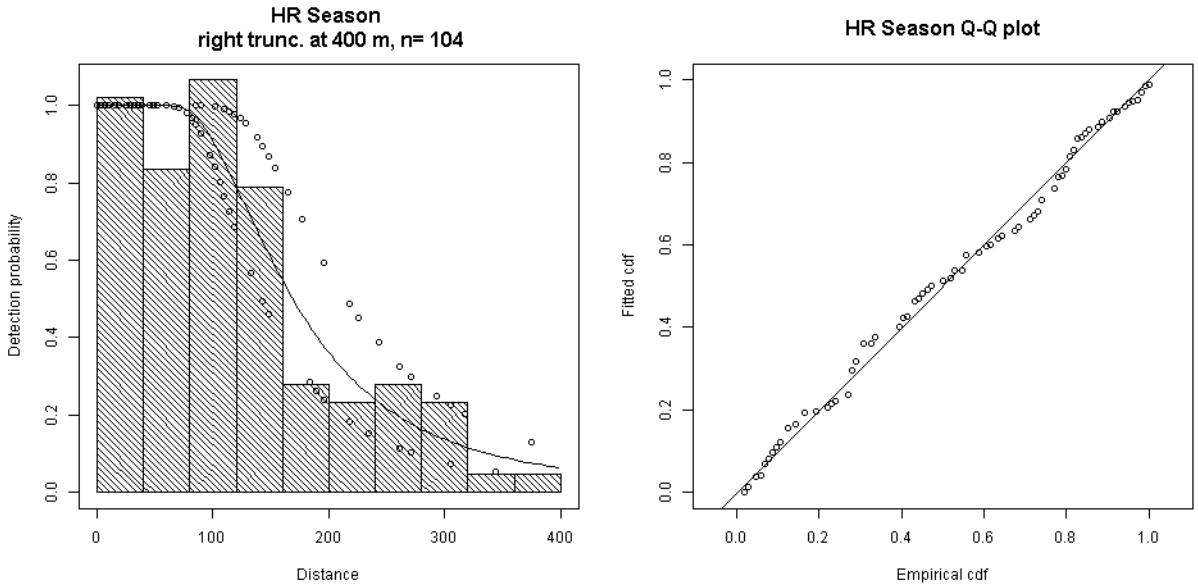

Figure A-12. Selected detection function fitted from PELAGIS surveys

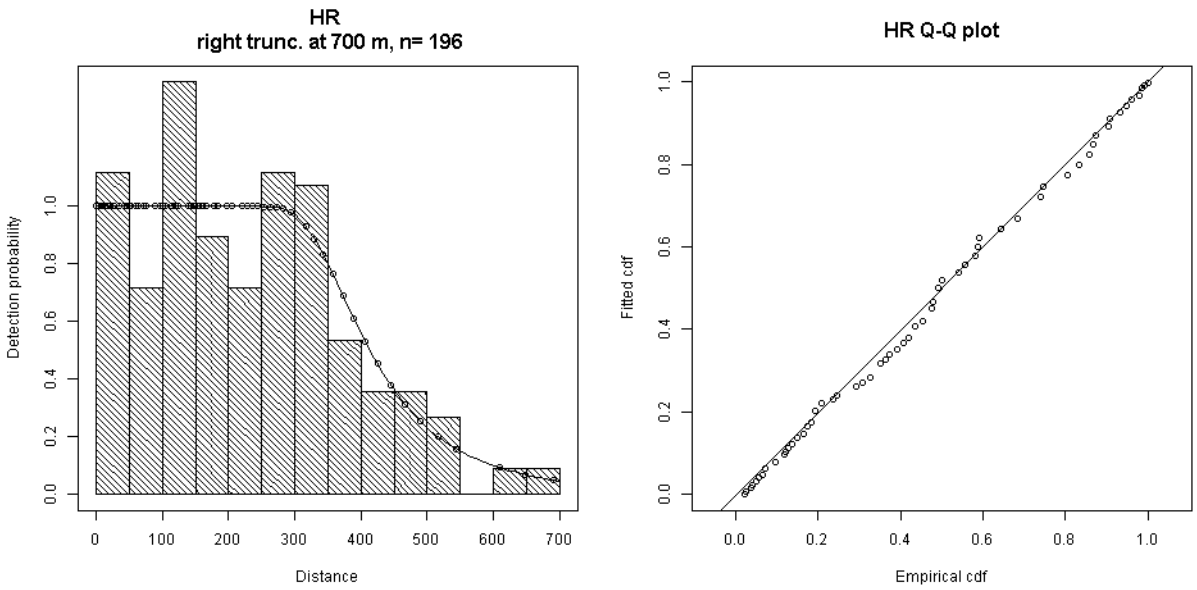

Figure A-13. Selected detection function fitted from BWI surveys

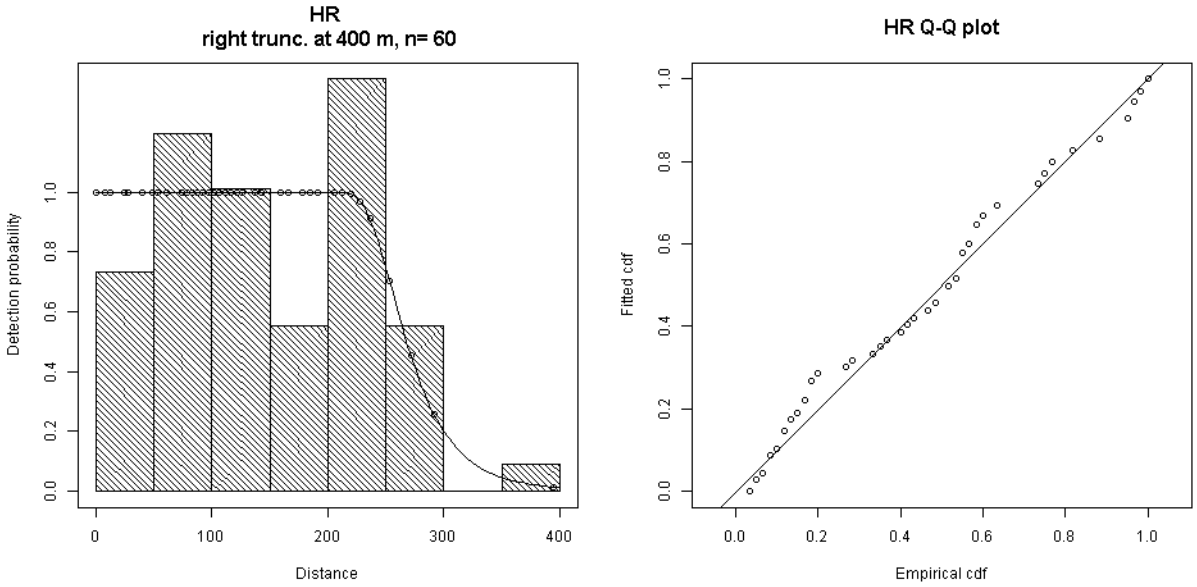

Figure A-14. Selected detection function fitted from TETHYS surveys

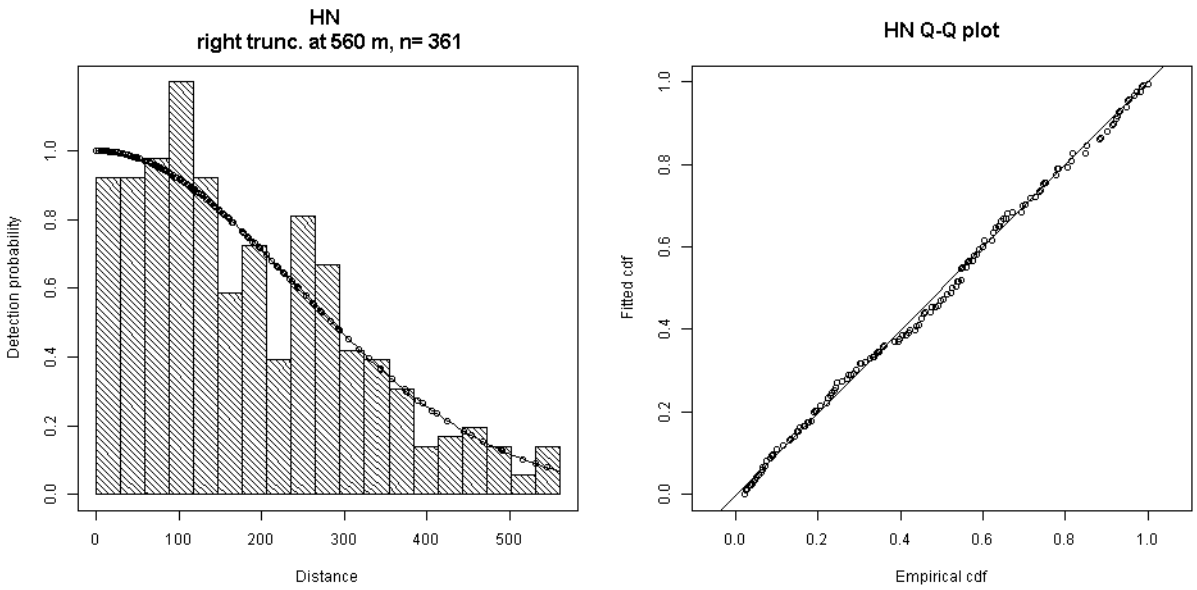

Figure A-15. Selected detection function fitted from PELAGIS, BWI and TETHYS surveys

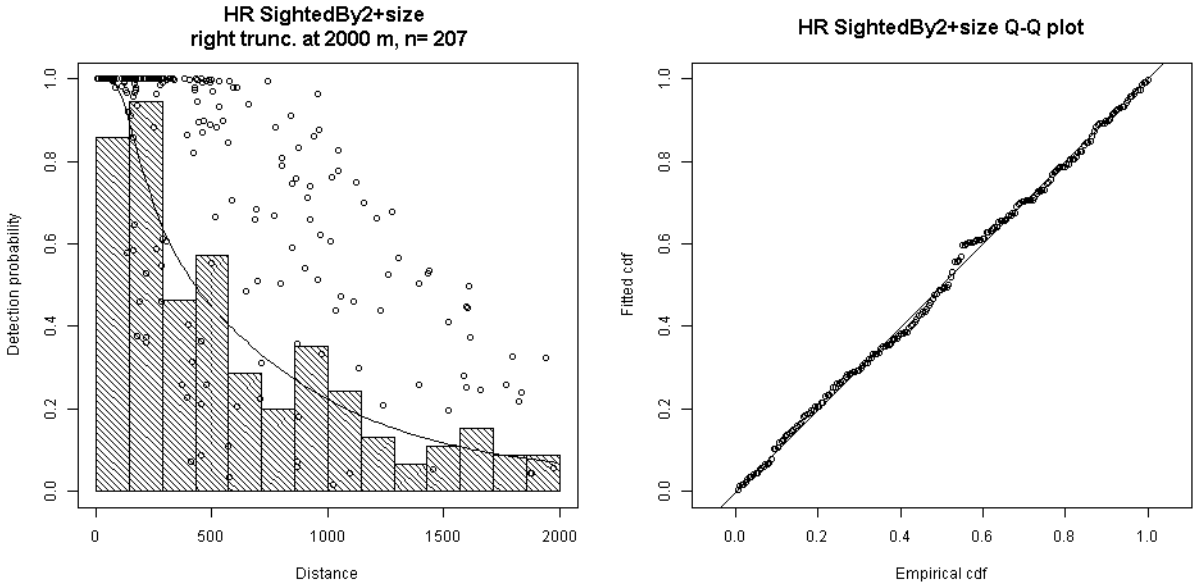

Figure A-16. Selected detection function fitted from Alnitak deck/mast surveys

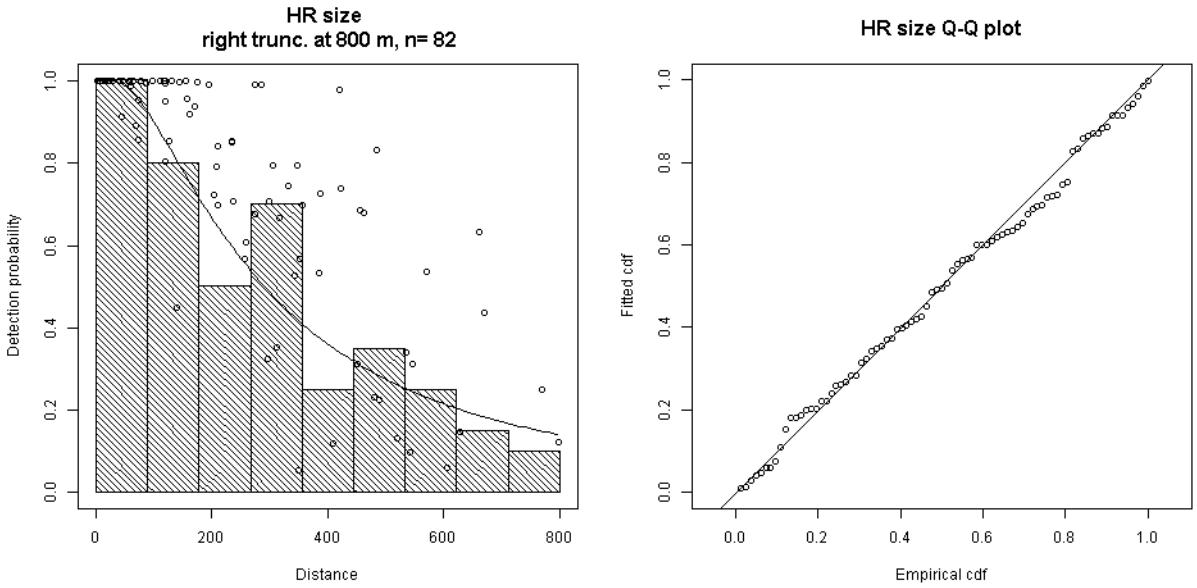

Figure A-17. Selected detection function fitted from Alnitak deck surveys

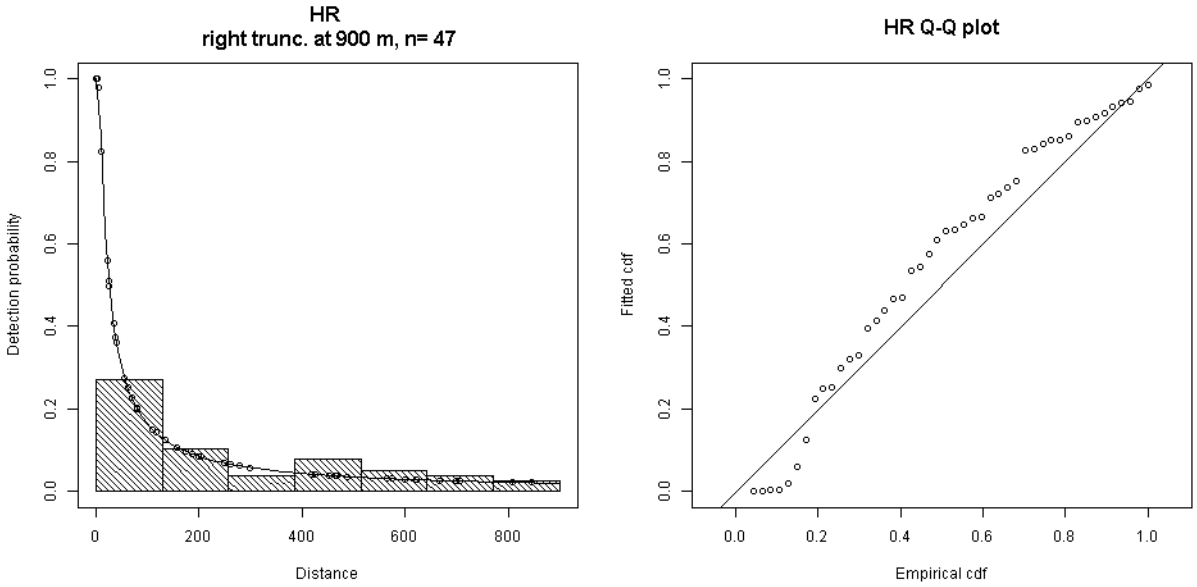

Figure A-18. Selected detection function fitted from EcoOcean and IFAW surveys

Short-beaked common dolphin

Incorporating sightings from PELAGIS aerial surveys in the Atlantic considerably increased sample size and allowed fitting a detection function for PELAGIS surveys. The one sighting of TETHYS surveys was pooled with PELAGIS surveys. For shipboard surveys, there were sufficient sightings to fit separate detection functions for the two configurations of Alnitak surveys. We pooled EcoOcean and IFAW surveys with Alnitak deck surveys.

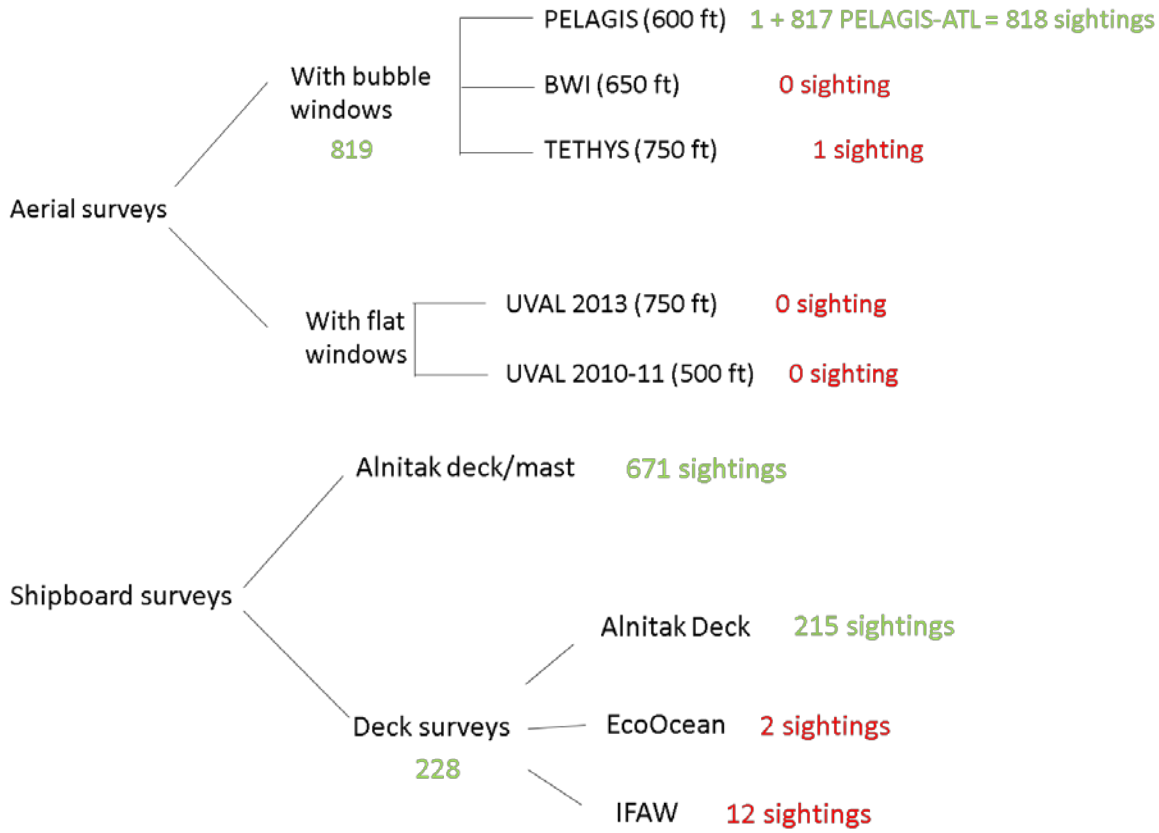

Figure A-19. Sightings hierarchies for aerial and shipboard surveys for short-beaked common dolphin. Color coding: ≥60 sightings: green, 31-59 sightings: orange, ≤30 sightings: red. When surveys were conducted by multiple organizations (e.g., TETHYS/ISPRA), only the first survey organization listed in Table was included for brevity. UVAL refers to University of Valencia surveys. PELAGIS-ATL refers to PELAGIS surveys in the Atlantic Ocean.

Table A-3. Detection functions applied per survey to short-beaked common dolphin sightings. Hn: half normal, Hr: hazard rate, ESHW: effective strip half width. SightedBy2 indicates if the sighting was made from the deck or from the mast in Alnitak surveys. Douglas2 corresponds to the Douglas covariate reclassified into a smaller number of classes. When surveys were conducted by multiple organizations (e.g., TETHYS/ISPRA), only the first survey organization listed in Table was included for brevity. UVAL refers to University of Valencia surveys.

Surveys	Surveys used for detection function fitting	Right truncation distance (m)	Left truncation distance (m)	Detection function applied	Mean ESHW (m)
PELAGIS	PELAGIS	275	0	Hn CloudCover + size	158
BWI	PELAGIS and TETHYS	275	0	Hn CloudCover + size	158
TETHYS	PELAGIS and TETHYS	275	0	Hn CloudCover + size	158
UVAL 2013	PELAGIS and TETHYS	275	124.8	Hn CloudCover + size	158
UVAL 2010/11	PELAGIS and TETHYS	275	83.2	Hn CloudCover + size	158
Alnitak deck/mast	Alnitak deck/mast	2000	0	Hr SightedBy2 + size	516
Alnitak deck	Alnitak deck	900	0	Hr Douglas2	312
EcoOcean	All shipboard deck	900	0	Hr size	279
IFAW	All shipboard deck	900	0	Hr size	279

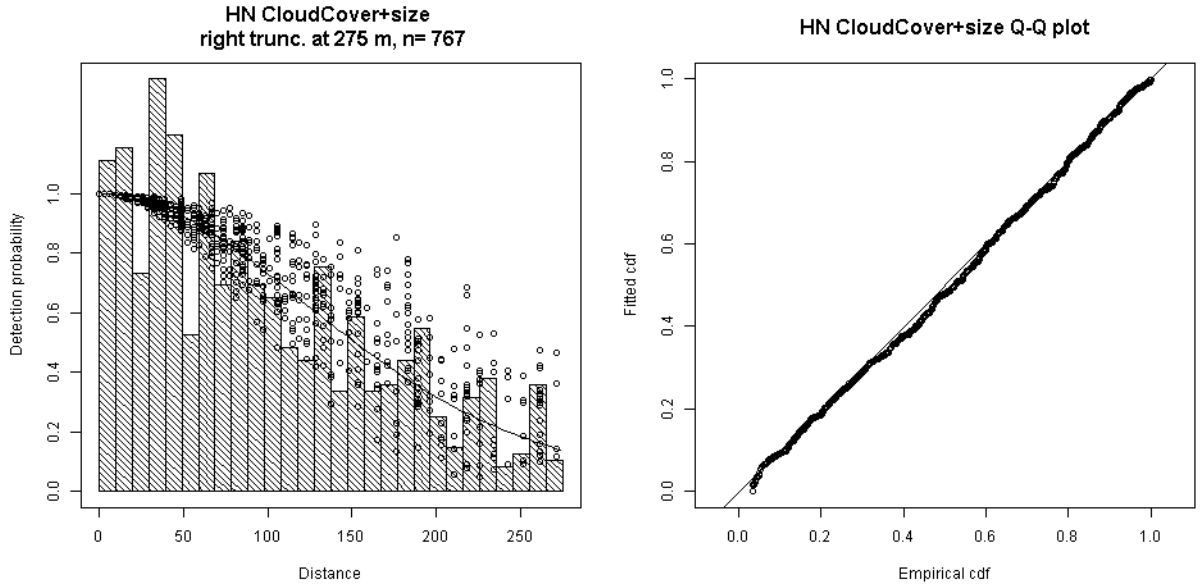

Figure A-20. Selected detection function fitted from PELAGIS surveys

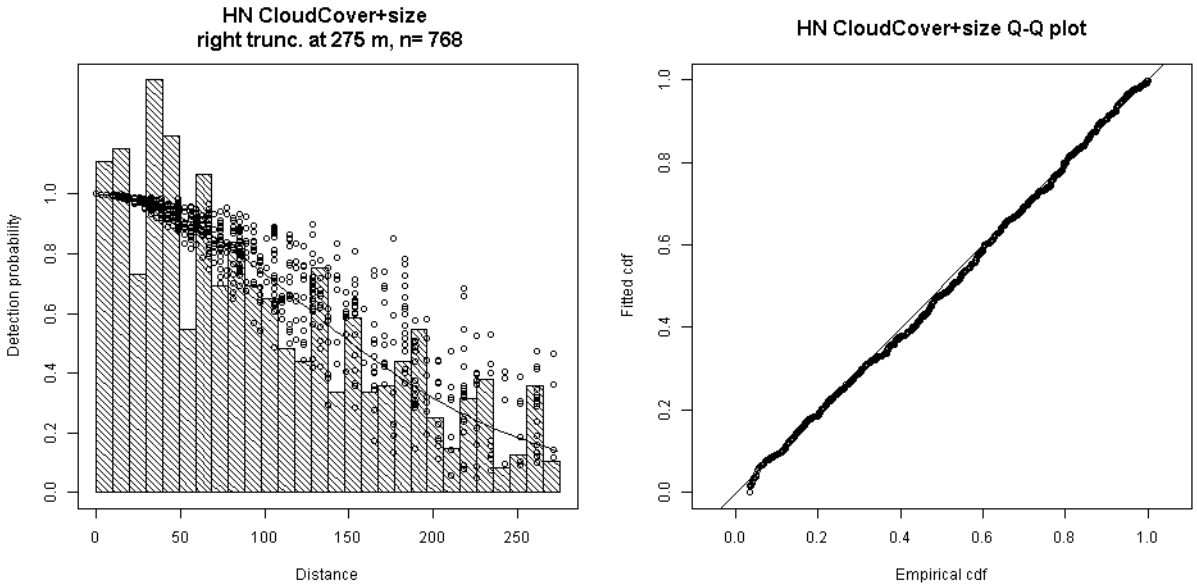

Figure A-21. Selected detection function fitted from PELAGIS and TETHYS surveys

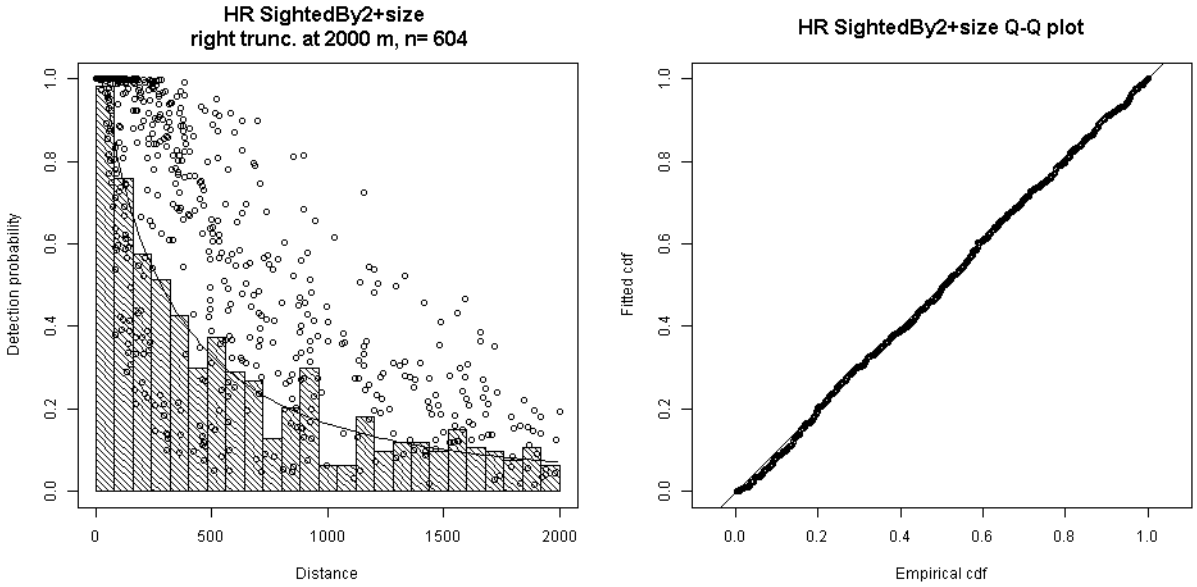

Figure A-22. Selected detection function fitted from Alnitak deck/mast surveys

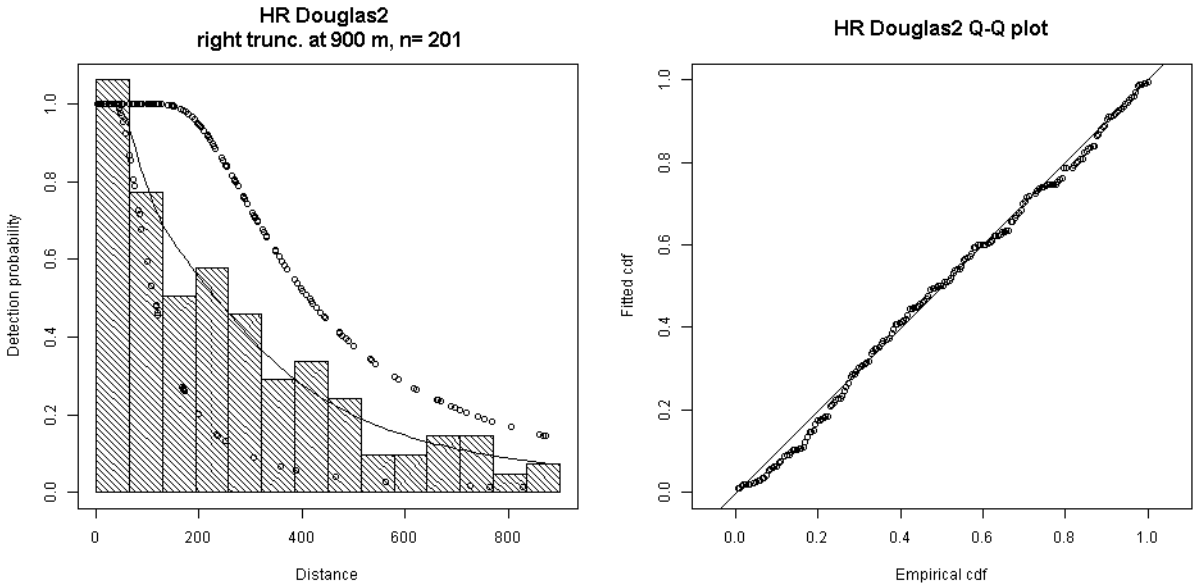

Figure A-23. Selected detection function fitted from Alnitak deck surveys

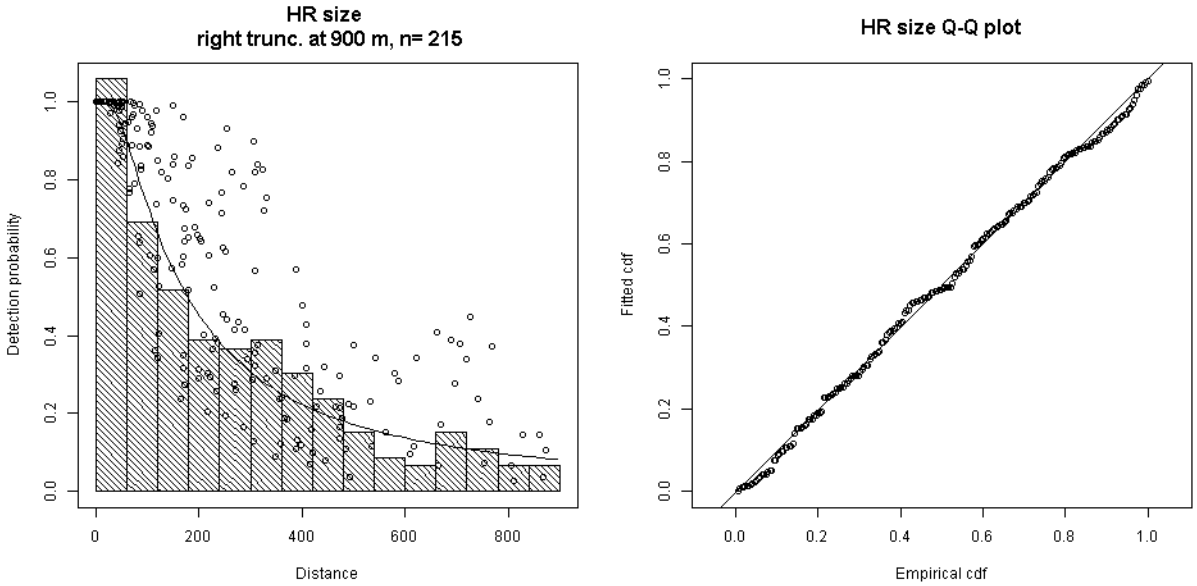

Figure A-24. Selected detection function fitted from all shipboard deck surveys

Risso's dolphin

Incorporating sightings from PELAGIS aerial surveys in the Atlantic increased sample size and allowed fitting a detection function for PELAGIS surveys. BWI surveys were pooled with PELAGIS surveys that flew 50 ft lower. TETHYS surveys were pooled with PELAGIS and BWI surveys that had a slightly lower altitude. There were too few sightings to fit a detection function for University of Valencia surveys so we pooled PELAGIS, BWI and TETHYS surveys and applied the resulting detection function to University of Valencia surveys. Doing so, we assumed detection from the bubble window surveys was a good proxy for detection from the flat window surveys, except for the area not visible from flat windows. Given the low sample sizes, shipboard surveys were pooled, and the presence of a mast observer was used as a covariate for detection function fitting.

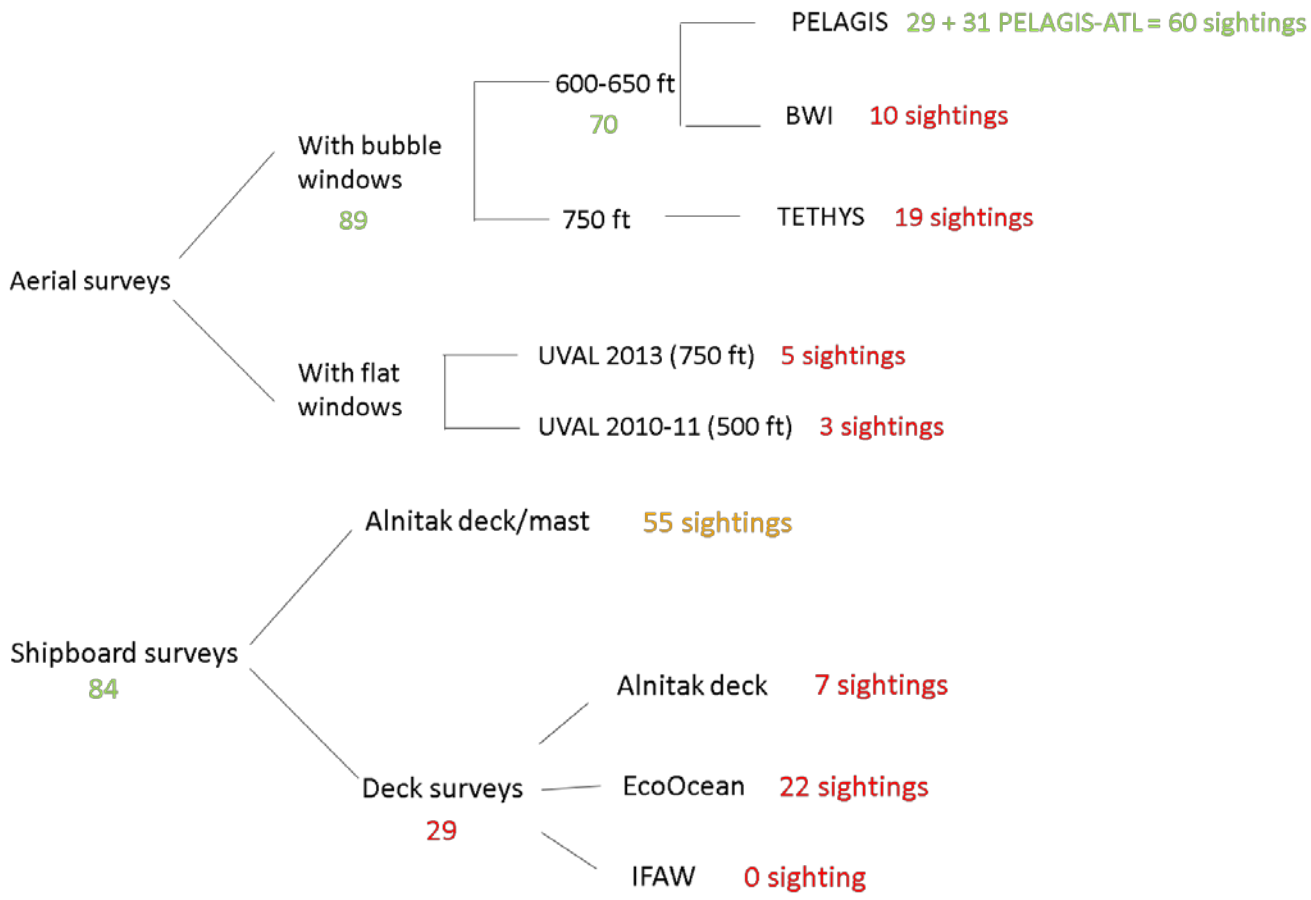

Figure A-25. Sightings hierarchies for aerial and shipboard surveys for Risso's dolphin. Color coding: ≥60 sightings: green, 31-59 sightings: orange, ≤30 sightings: red. When surveys were conducted by multiple organizations (e.g., TETHYS/ISPRA), only the first survey organization listed in Table was included for brevity. UVAL refers to University of Valencia surveys. PELAGIS-ATL refers to PELAGIS surveys in the Atlantic Ocean.

Table A-4. Detection functions applied per survey to Risso's dolphin sightings. Hn: half normal, Hr: hazard rate, ESHW: effective strip half width. Beaufort2 corresponds to the Beaufort covariate reclassified into a smaller number of classes (BeaufortFact2 is the factor version of the covariate). Cloudcover2 corresponds to the Cloudcover covariate reclassified into a smaller number of classes. PresenceMast indicates whether a mast observer was present in shipboard surveys. When surveys were conducted by multiple organizations (e.g., TETHYS/ISPRA), only the first survey organization listed in Table was included for brevity. UVAL refers to University of Valencia surveys.

Surveys	Surveys used for detection function fitting	Right truncation distance (m)	Left truncation distance (m)	Detection function applied	Mean ESHW (m)
PELAGIS	PELAGIS	450	0	Hn BeaufortFact2	230
BWI	PELAGIS and BWI	550	0	Hn Beaufort2	262
TETHYS	PELAGIS, BWI and TETHYS	600	0	Hn Cloudcover2	280
UVAL 2013	PELAGIS, BWI and TETHYS	600	124.8	Hn	285
UVAL 2010/11	PELAGIS, BWI and TETHYS	600	82.3	Hn	285
Alnitak deck/mast	Alnitak deck/mast	2000	0	Hr	667
Alnitak deck	All shipboard	2000	0	Hr PresenceMast	548
EcoOcean	All shipboard	2000	0	Hr PresenceMast	548
IFAW	All shipboard	2000	0	Hr PresenceMast	548

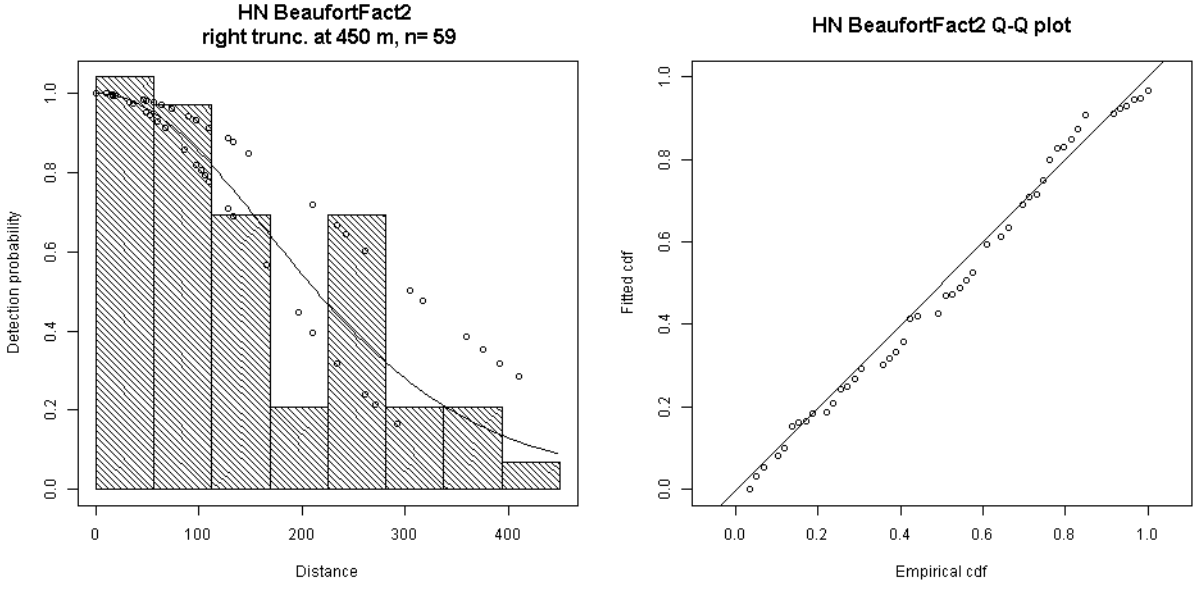

Figure A-26. Selected detection function fitted from PELAGIS surveys

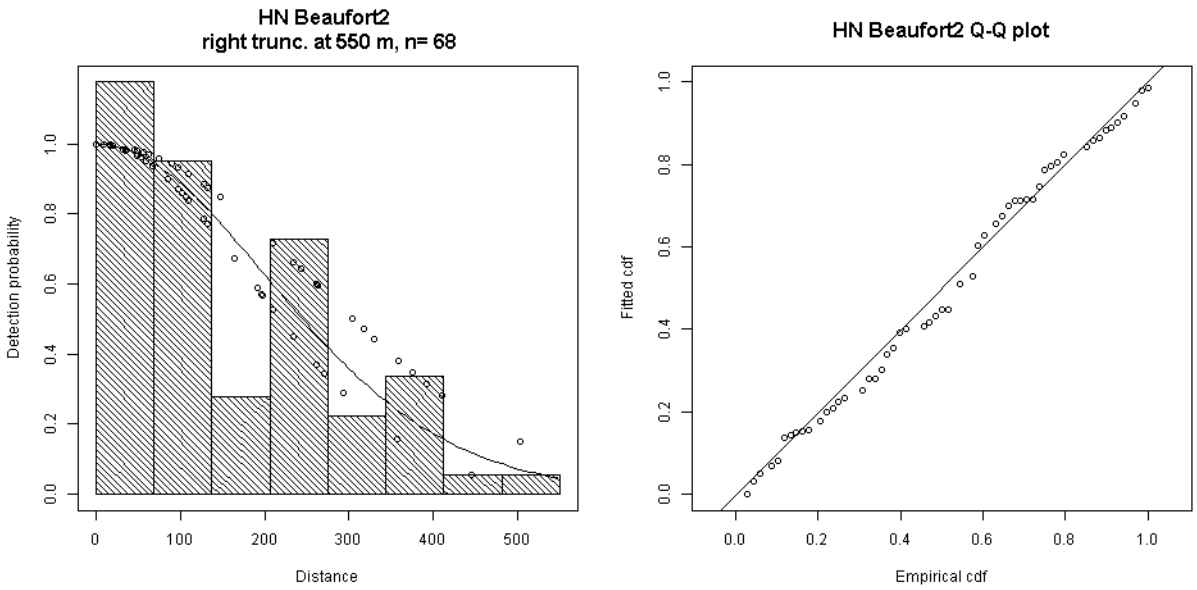

Figure A-27. Selected detection function fitted from PELAGIS and BWI surveys

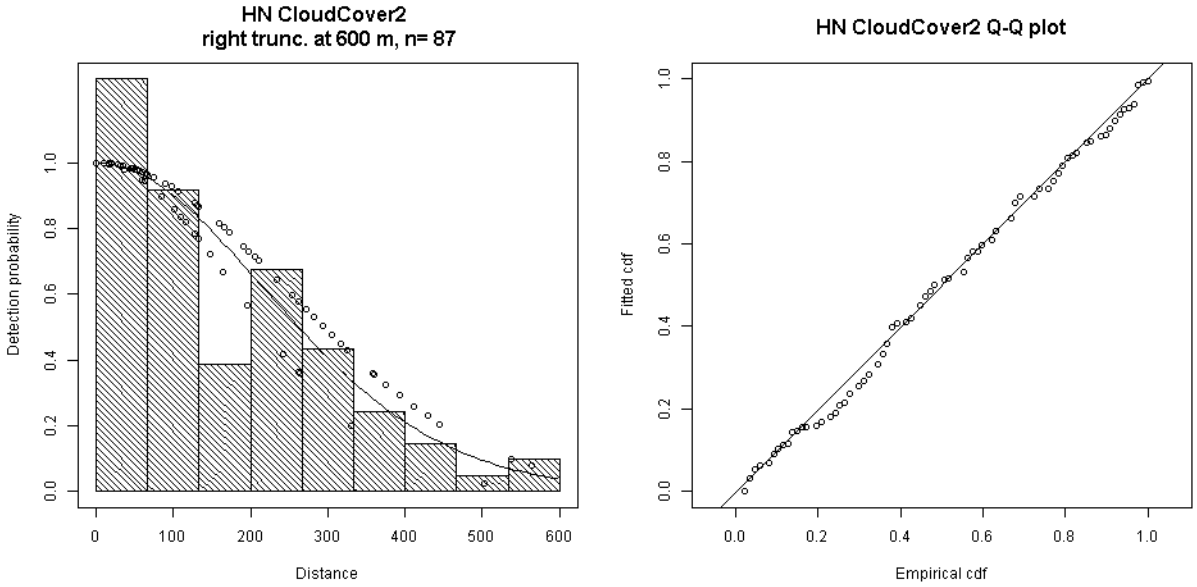

Figure A-28. Selected detection function fitted from PELAGIS, BWI and TETHYS surveys (applied to TETHYS surveys)

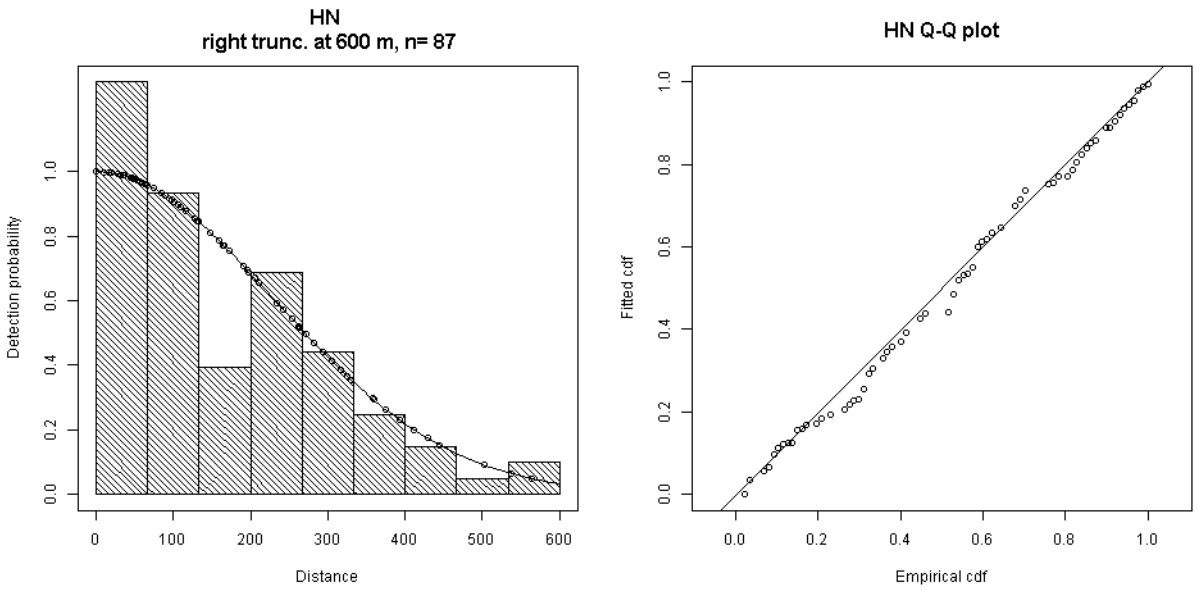

Figure A-29. Selected detection function fitted from PELAGIS, BWI and TETHYS surveys (applied to UVAL 2013 and 2010/11 surveys)

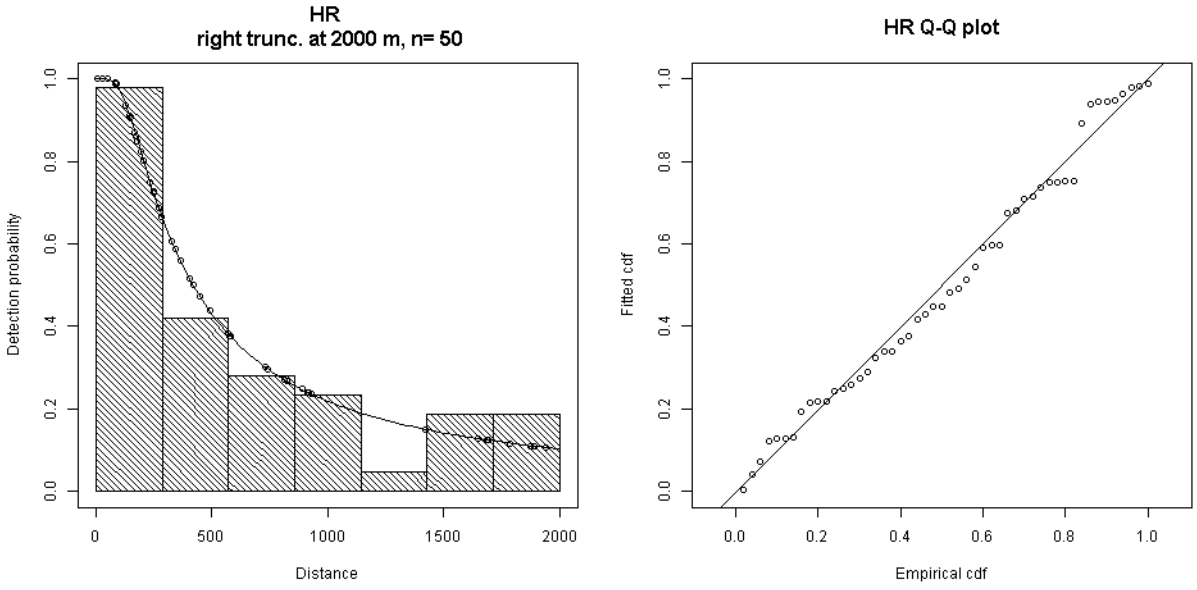

Figure A-30. Selected detection function fitted from Alnitak deck/mast surveys

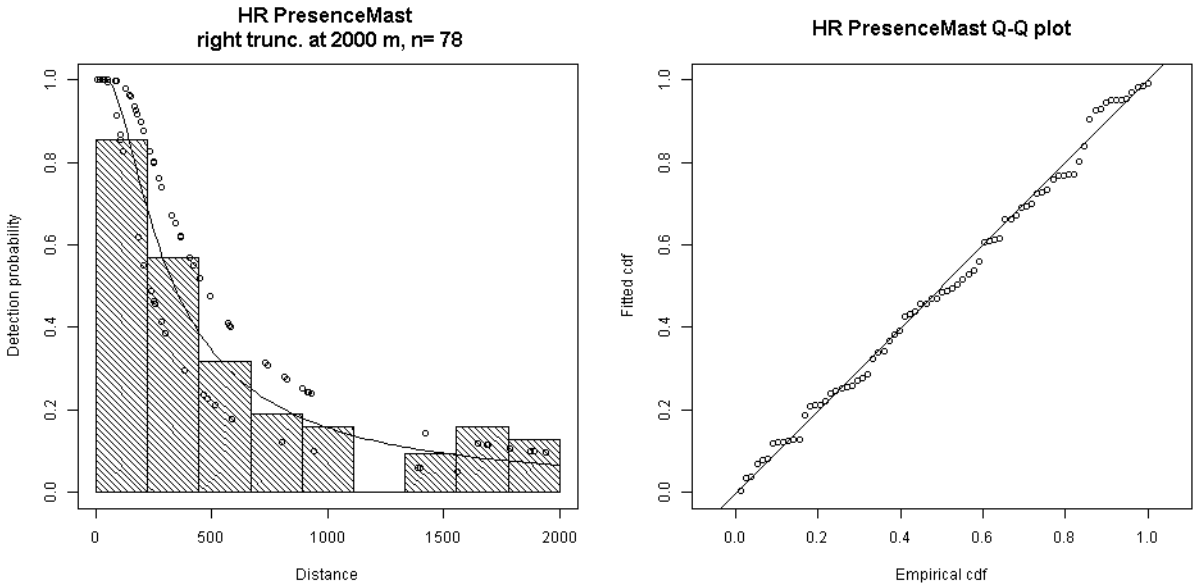

Figure A-31. Selected detection function fitted from all shipboard deck surveys

Long-finned pilot whale

Incorporating sightings from PELAGIS aerial surveys in the Atlantic importantly increased sample size and allowed fitting a detection function for PELAGIS surveys. TETHYS surveys were pooled with PELAGIS surveys that flew 150 ft lower. There were too few sightings to fit a detection function for University of Valencia surveys so we pooled PELAGIS, BWI and TETHYS surveys and applied the resulting detection function to University of Valencia surveys. Doing so, we assumed detection from the bubble window surveys was a good proxy for detection from the flat window surveys, except for the area not visible from flat windows. There were sufficient sightings to fit separate detection functions for the two configurations of Alnitak surveys. IFAW and EcoOcean surveys were pooled with Alnitak deck surveys.

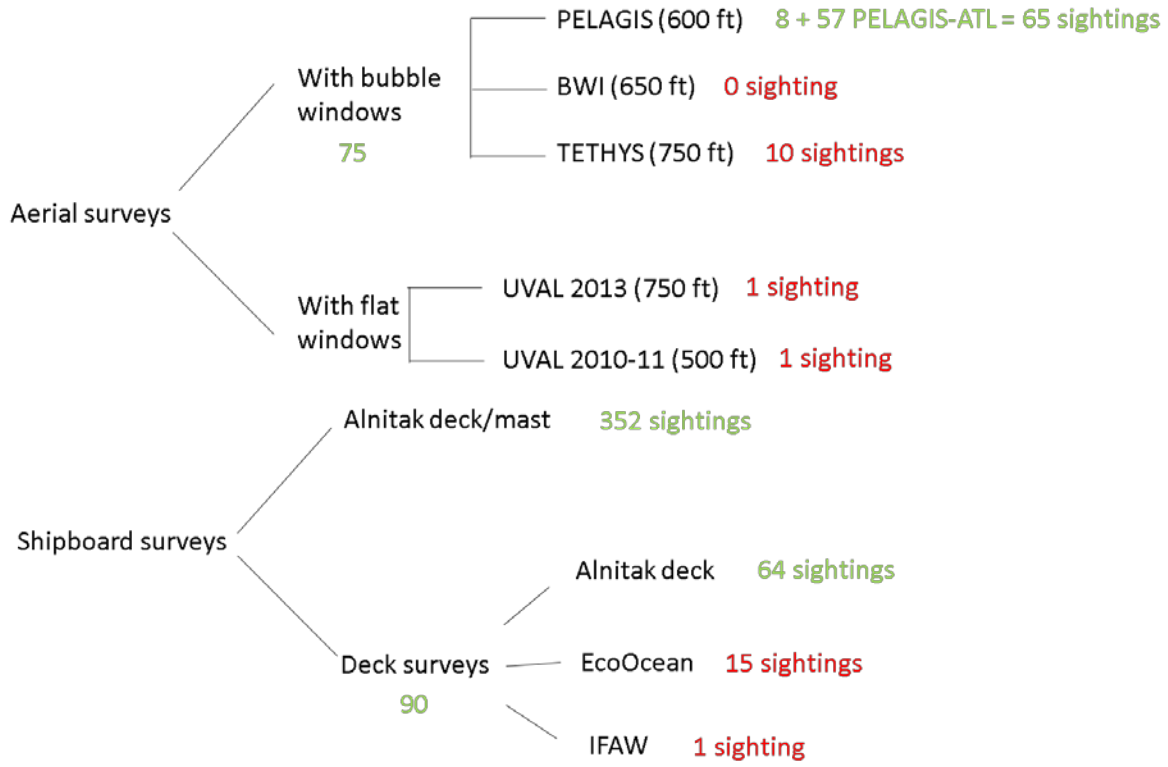

Figure A-32. Sightings hierarchies for aerial and shipboard surveys for pilot whale. Color coding: ≥60 sightings: green, 31-59 sightings: orange, ≤30 sightings: red. When surveys were conducted by multiple organizations (e.g., TETHYS/ISPRA), only the first survey organization listed in Table was included for brevity. UVAL refers to University of Valencia surveys. PELAGIS-ATL refers to PELAGIS surveys in the Atlantic Ocean.

Table A-5. Detection functions applied per survey to pilot whale sightings. Hn: half normal, Hr: hazard rate; Un: uniform, ESHW: effective strip half width. SightedBy2 indicates if the sighting was made from the deck or from the mast in Alnitak surveys. Beaufort2 corresponds to the Beaufort covariate reclassified into a smaller number of classes (BeaufortFact2 is the factor version of the covariate). Douglas2 corresponds to the Douglas covariate reclassified into a smaller number of classes. When surveys were conducted by multiple organizations (e.g., TETHYS/ISPRA), only the first survey organization listed in Table was included for brevity. UVAL refers to University of Valencia surveys.

Surveys	Surveys used for detection function fitting	Right truncation distance (m)	Left truncation distance (m)	Detection function applied	Mean ESHW (m)
PELAGIS	PELAGIS	500	0	Hr season	195
BWI	PELAGIS and TETHYS	600	0	Hr BeaufortFact2	225
TETHYS	PELAGIS and TETHYS	600	0	Hr BeaufortFact2	225
UVAL 2013	PELAGIS and TETHYS	600	124.8	Hr BeaufortFact2	225
UVAL 2010/11	PELAGIS and TETHYS	600	83.2	Hr BeaufortFact2	225
Alnitak deck/mast	Alnitak deck/mast	2500	0	Hn SightedBy2 + YearFact	1147
Alnitak deck	Alnitak deck	1100	0	Hn Douglas2	560
EcoOcean	All shipboard deck	1100	0	Un cos 1	583
IFAW	All shipboard deck	1100	0	Un cos 1	583

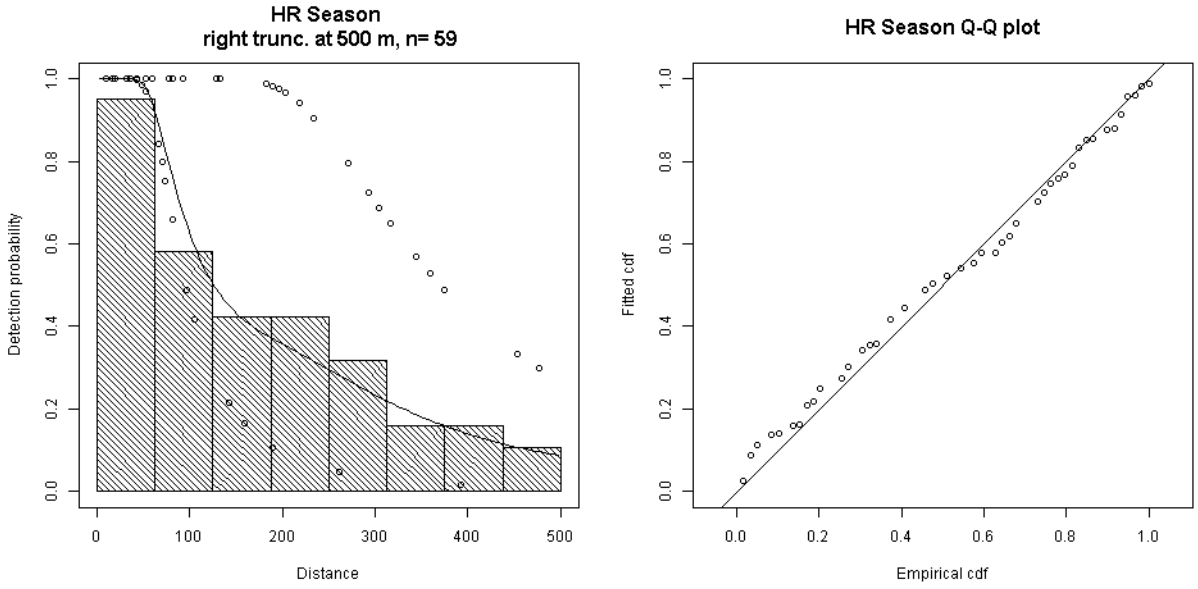

Figure A-33. Selected detection function fitted from PELAGIS surveys

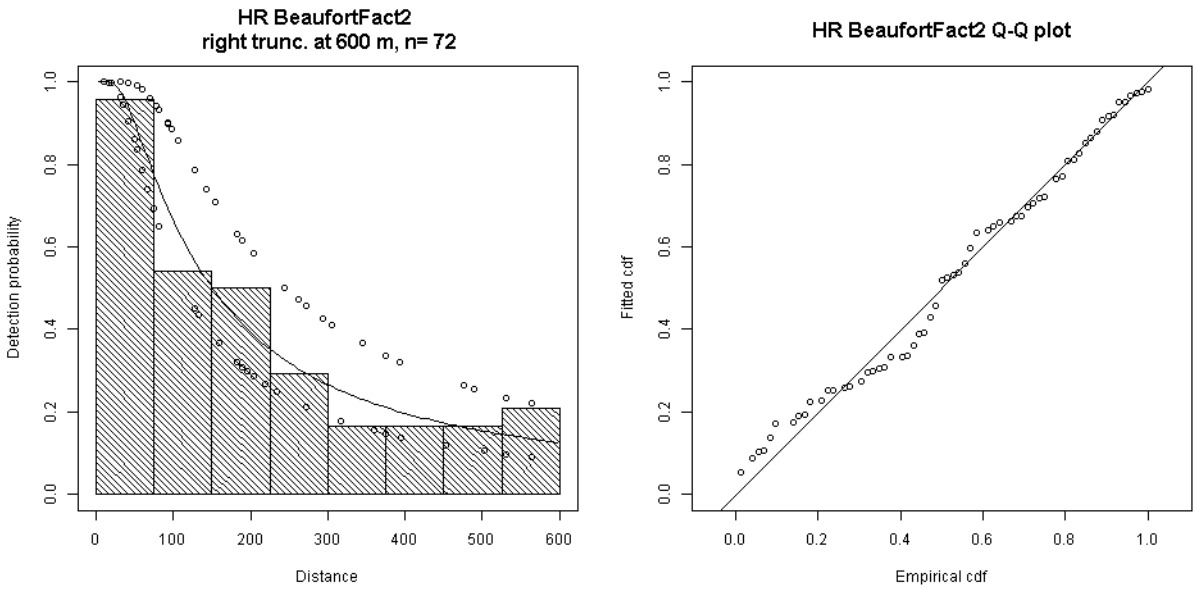

Figure A-34. Selected detection function fitted from PELAGIS and TETHYS surveys

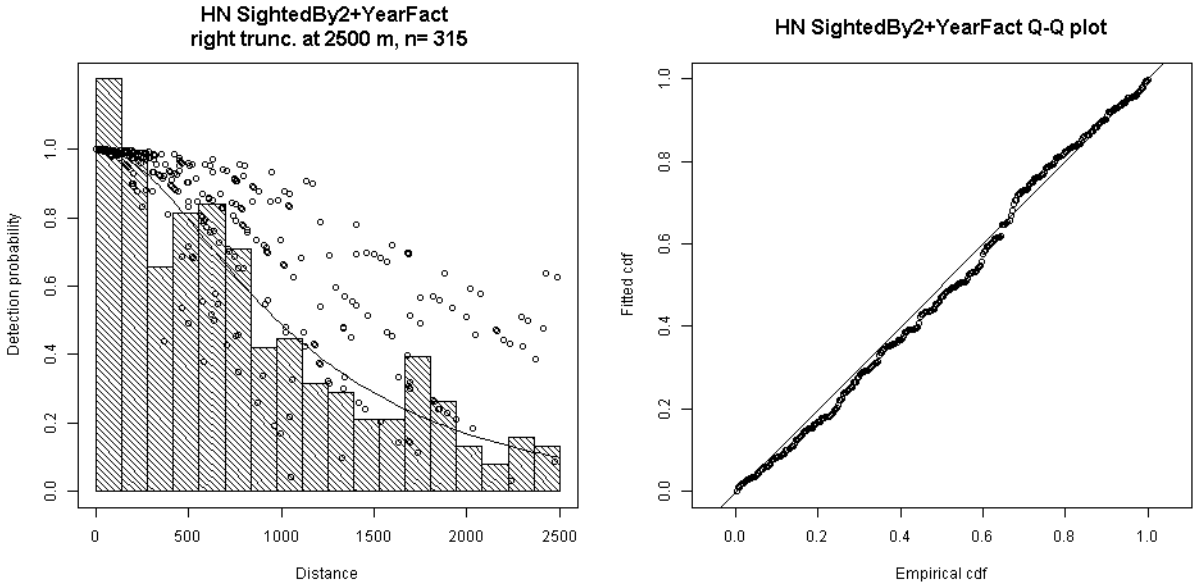

Figure A-35. Selected detection function fitted from Alnitak deck/mast surveys

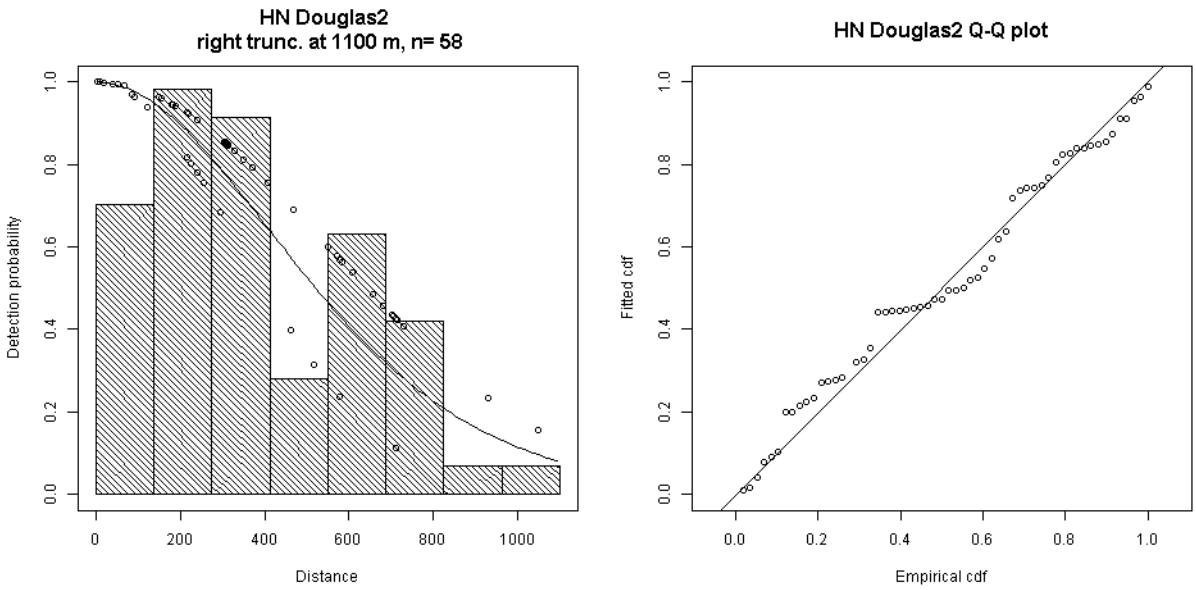

Figure A-36. Selected detection function fitted from Alnitak deck surveys

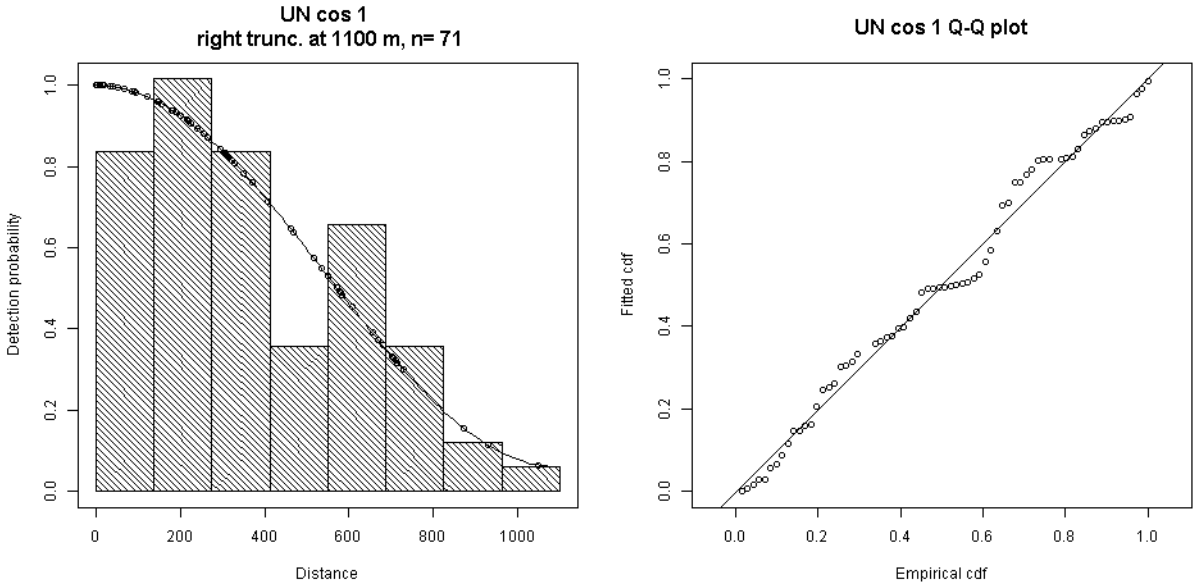

Figure A-37. Selected detection function fitted from all shipboard deck surveys

Fin whale

Incorporating sightings from PELAGIS aerial surveys in the Atlantic increased sample size and allowed fitting a detection function for PELAGIS surveys. BWI surveys were pooled with PELAGIS surveys that flew 50 ft lower. There were sufficient sightings to fit a survey-specific detection function for TETHYS surveys. There were too few sightings to fit a detection function for University of Valencia surveys so we pooled PELAGIS, BWI and TETHYS surveys and applied the resulting detection function to University of Valencia surveys. Doing so, we assumed detection from the bubble window surveys was a good proxy for detection from the flat window surveys, except for the area not visible from flat windows. There were sufficient sightings to fit a survey-specific detection function for EcoOcean surveys. We pooled Alnitak deck surveys with EcoOcean surveys that were a similar observation height. We fitted a detection function for Alnitak deck/mast surveys although sample size was low.

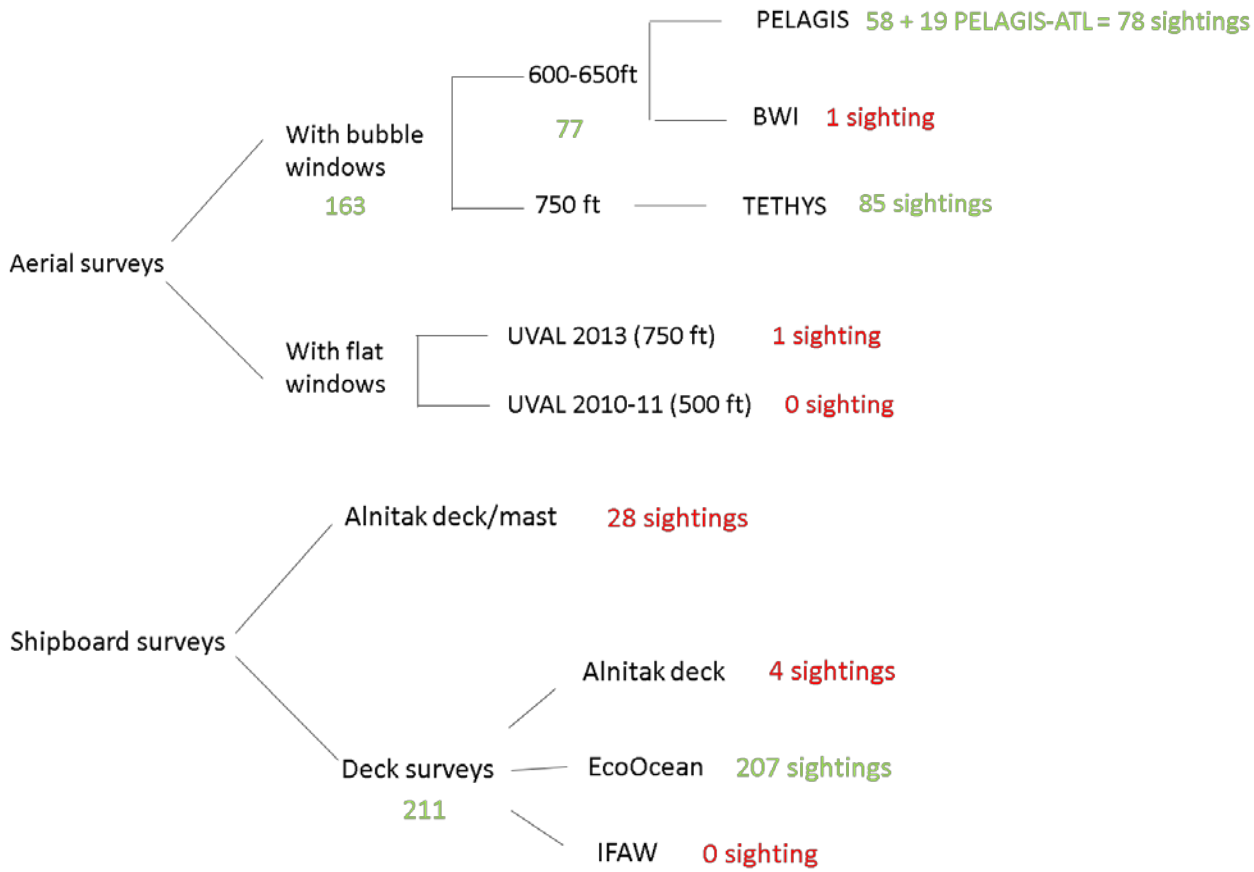

Figure A-38. Sightings hierarchies for aerial and shipboard surveys for fin whale. Color coding: ≥60 sightings: green, 31-59 sightings: orange, ≤30 sightings: red. When surveys were conducted by multiple organizations (e.g., TETHYS/ISPRA), only the first survey organization listed in Table was included for brevity. UVAL refers to University of Valencia surveys. PELAGIS-ATL refers to PELAGIS surveys in the Atlantic Ocean.

Table A-6. Detection functions applied per survey to fin whale sightings. Hn: half normal, Hr: hazard rate, ESHW: effective strip half width. When surveys were conducted by multiple organizations (e.g., TETHYS/ISPRA), only the first survey organization listed in Table was included for brevity. UVAL refers to University of Valencia surveys.

Surveys	Surveys used for detection function fitting	Right truncation distance (m)	Left truncation distance (m)	Detection function applied	Mean ESHW (m)
PELAGIS	PELAGIS and BWI	600	0	Hn	390
BWI	PELAGIS and BWI	600	0	Hn	390
TETHYS	TETHYS	1700	0	Hn cos 3	786
UVAL 2013	PELAGIS, BWI and TETHYS	1500	124.8	Hn cos 2	517
UVAL 2010/11	PELAGIS, BWI and TETHYS	1500	83.2	Hn cos 2	517
Alnitak deck/mast	Alnitak deck/mast	3000	0	Hn	1930
Alnitak deck	Alnitak deck and EcoOcean	1600	0	Hr size	560
EcoOcean	EcoOcean	1600	0	Hr	573
IFAW	Alnitak deck and EcoOcean	1600	0	Hr size	560

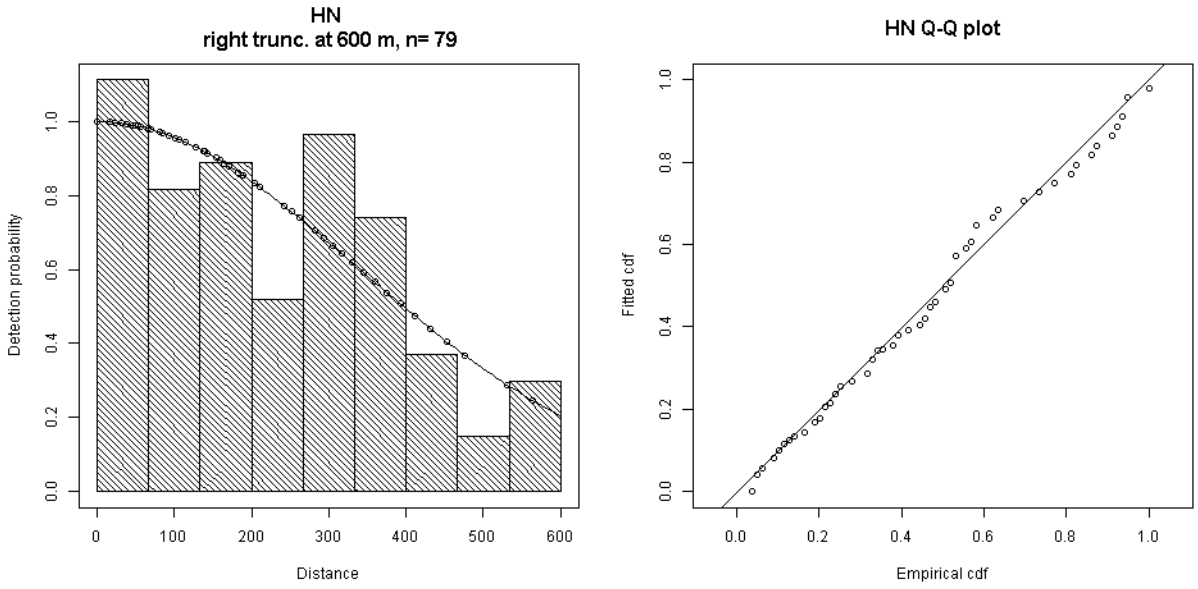

Figure A-39. Selected detection function fitted from PELAGIS and BWI surveys

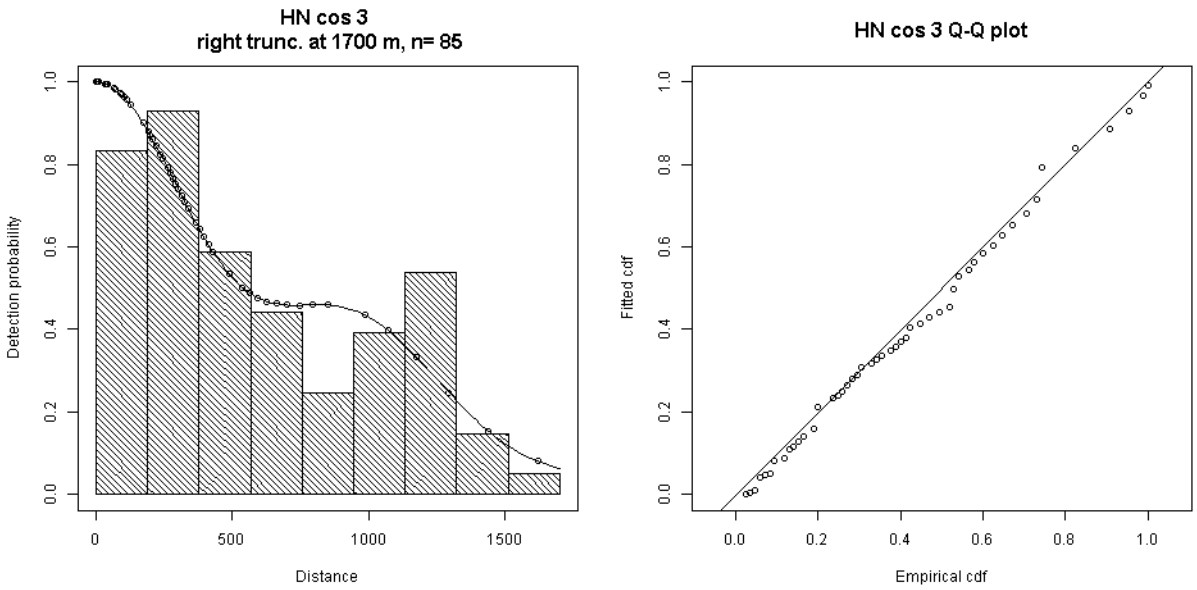

Figure A-40. Selected detection function fitted from TETHYS surveys

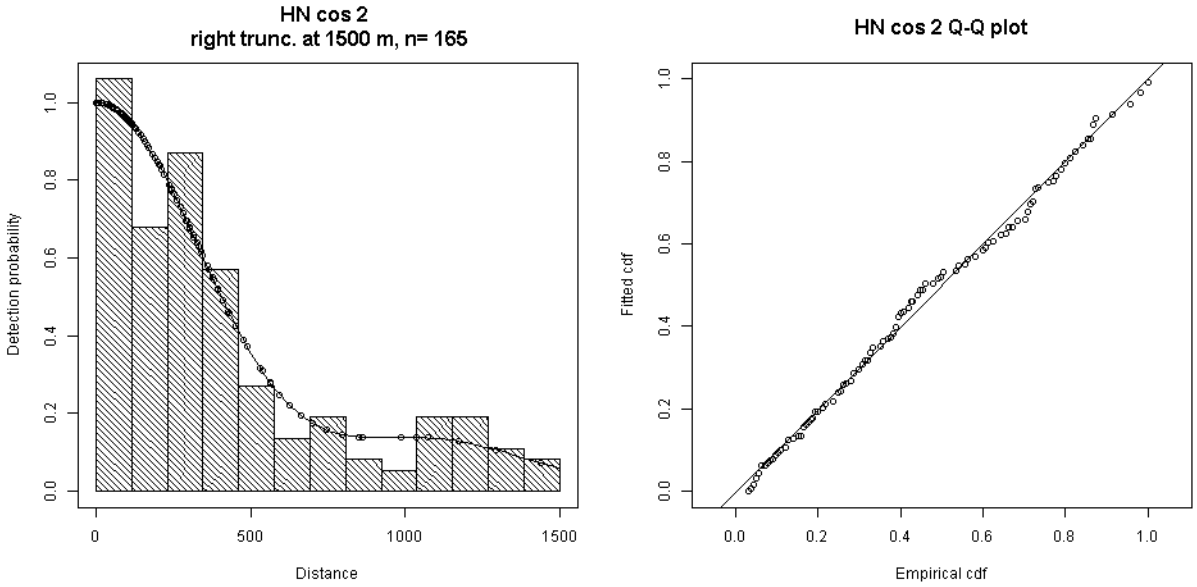

Figure A-41. Selected detection function fitted from PELAGIS, BWI and TETHYS surveys

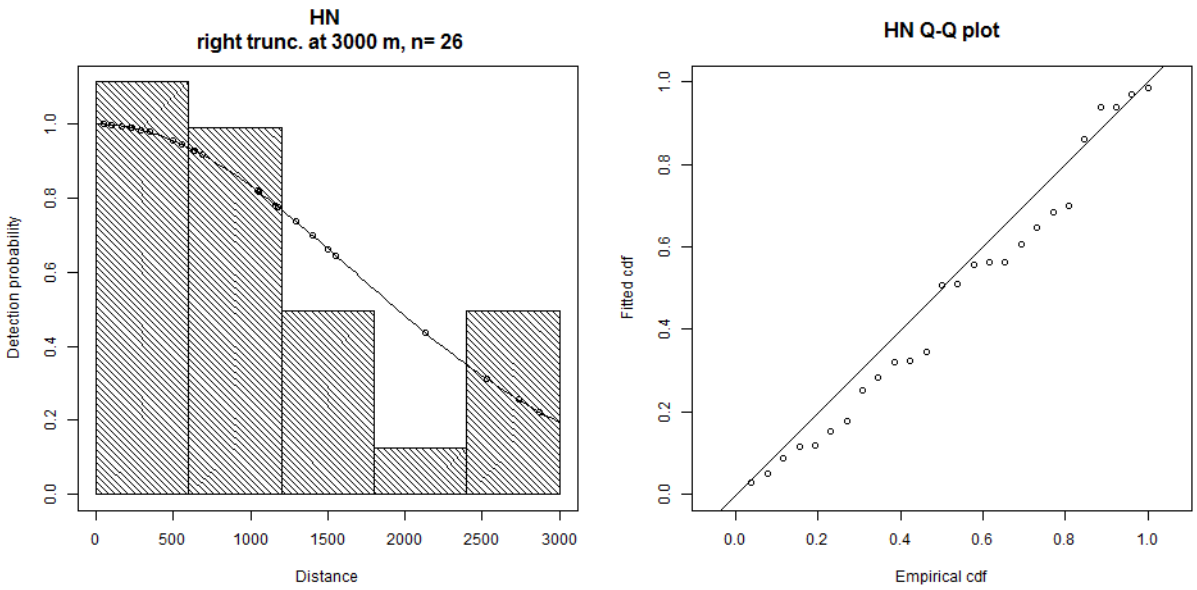

Figure A-42. Selected detection function fitted from Alnitak deck/mast surveys

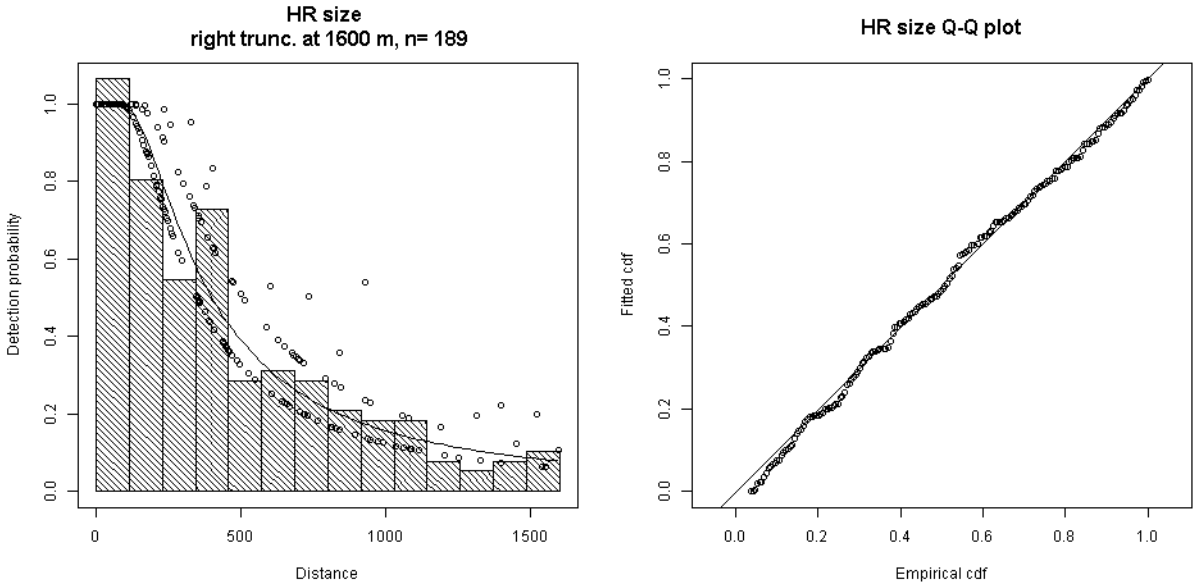

Figure A-43. Selected detection function fitted from Alnitak deck and EcoOcean surveys

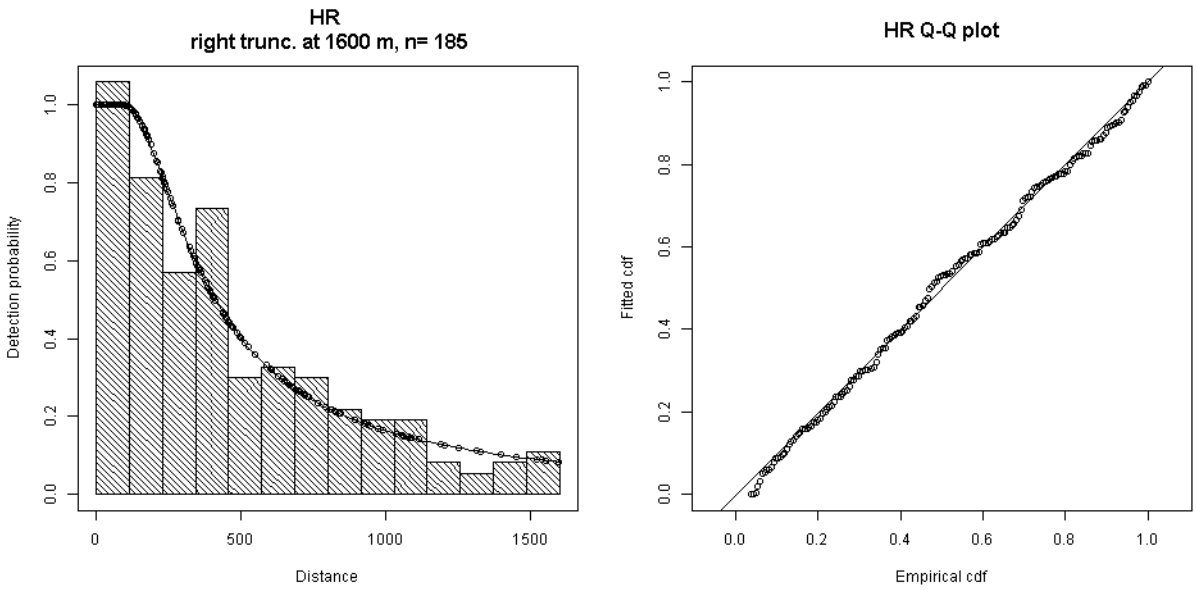

Figure A-44. Selected detection function fitted from EcoOcean surveys

Sperm whale

Despite the incorporation of the PELAGIS Atlantic surveys, there were insufficient sightings to fit survey-specific detection functions so we pooled PELAGIS and TETHYS surveys. We applied the pooled PELAGIS / TETHYS detection function to University of Valencia surveys, assuming detection from these bubble window surveys was a good proxy for detection from the flat window surveys, except for the area not visible from flat windows. For shipboard surveys, there were sufficient sightings to fit a survey-specific detection function for EcoOcean only. For all other shipboard surveys, we had no choice but to pool them, and we used the presence of a mast observer as a covariate.

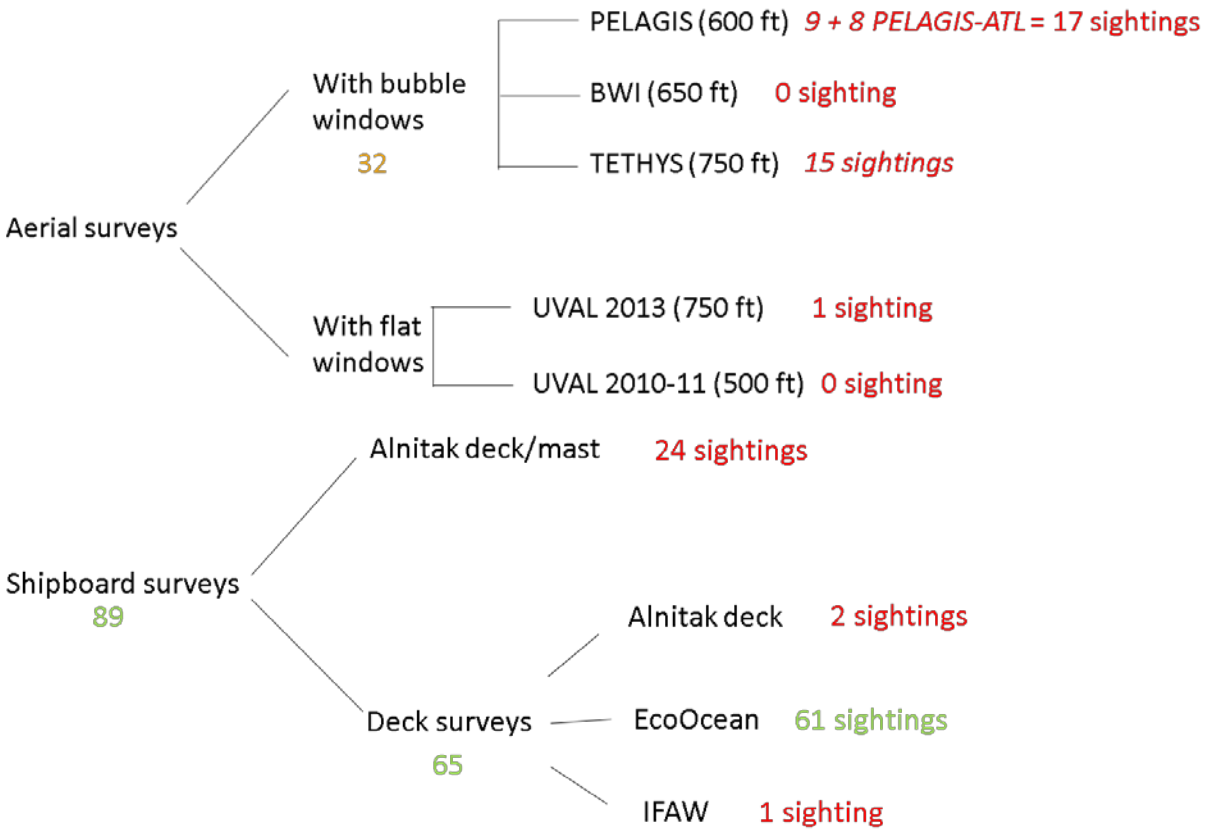

Figure A-45. Sightings hierarchies for aerial and shipboard surveys for sperm whale. Color coding: ≥60 sightings: green, 31-59 sightings: orange, ≤30 sightings: red. When surveys were conducted by multiple organizations (e.g., TETHYS/ISPRA), only the first survey organization listed in Table was included for brevity. UVAL refers to University of Valencia surveys. PELAGIS-ATL refers to PELAGIS surveys in the Atlantic Ocean.

Table A-7. Detection functions applied per survey to sperm whale sightings Hn: half normal, Hr: hazard rate, ESHW: effective strip half width. PresenceMast indicates whether a mast observer was present in shipboard surveys. When surveys were conducted by multiple organizations (e.g., TETHYS/ISPRA), only the first survey organization listed in the Table was included for brevity. UVAL refers to University of Valencia surveys.

Surveys	Surveys used for detection function fitting	Right truncation distance (m)	Left truncation distance (m)	Detection function applied	Mean ESHW (m)
PELAGIS	PELAGIS and TETHYS	1500	0	Hr	352
BWI	PELAGIS and TETHYS	1500	0	Hr	352
TETHYS	PELAGIS and TETHYS	1500	0	Hr	352
UVAL 2013	PELAGIS and TETHYS	1500	124.8	Hr	352
UVAL 2010/11	PELAGIS and TETHYS	1500	83.2	Hr	352
Alnitak deck/mast	All shipboard	2400	0	Hr PresenceMast	443
Alnitak deck	All shipboard	2400	0	Hr PresenceMast	443
EcoOcean	EcoOcean	1500	0	Hr	274
IFAW	All shipboard	2400	0	Hr PresenceMast	443

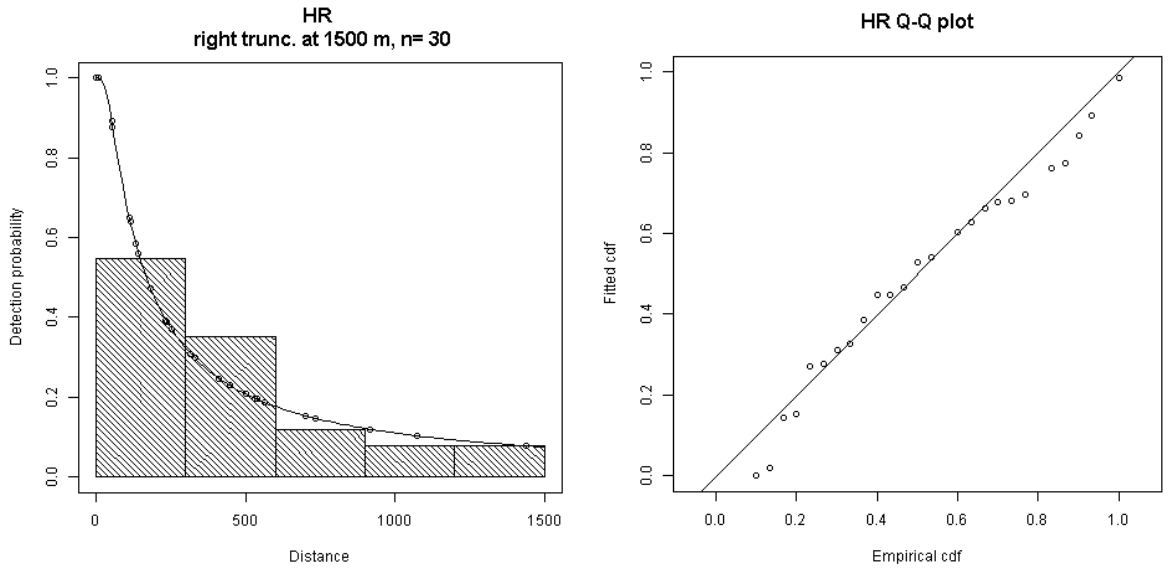

Figure A-46. Selected detection function fitted from PELAGIS and TETHYS surveys

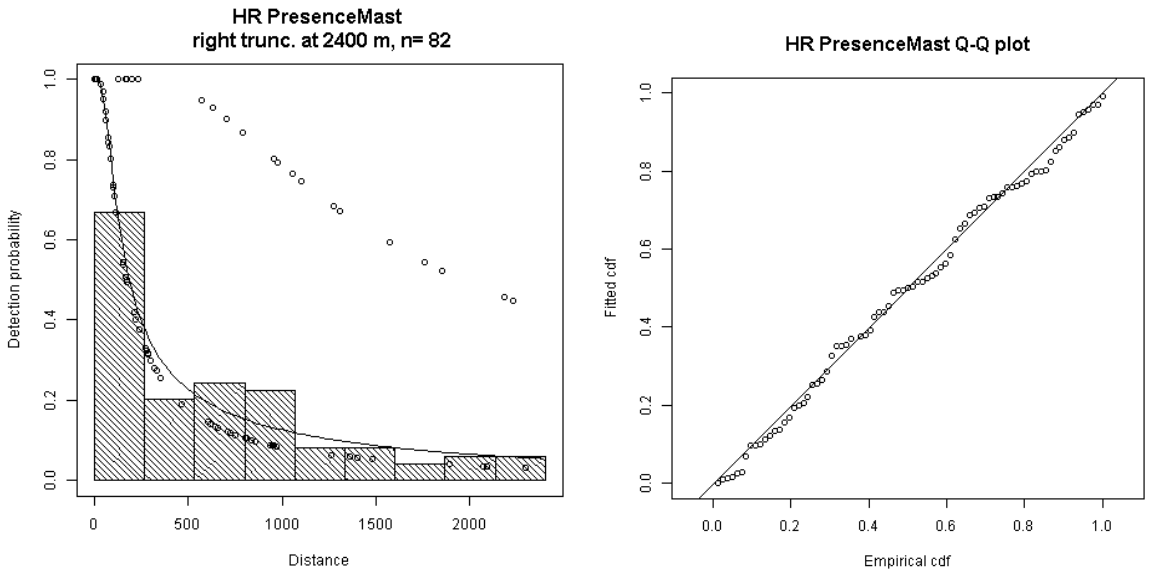

Figure A-47. Selected detection function fitted from all shipboard surveys

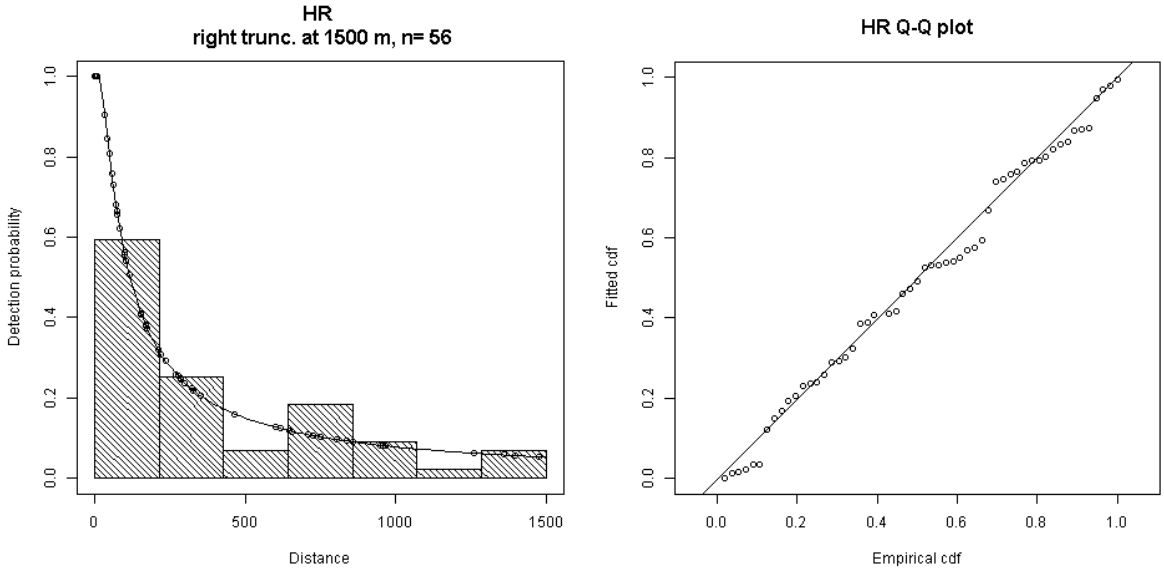

Figure A-48. Selected detection function fitted from EcoOcean surveys

Cuvier's beaked whale

Despite the incorporation of the PELAGIS Atlantic surveys, there were insufficient sightings to fit survey-specific detection functions so we pooled PELAGIS, BWI and TETHYS surveys. We applied the pooled PELAGIS / BWI/ TETHYS detection function to University of Valencia surveys, assuming detection from these bubble window surveys was a good proxy for detection from the flat window surveys, except for the area not visible from flat windows. Despite the modest sample size, we fitted a detection function for Alnitak deck/mast surveys only. We pooled all deck surveys.

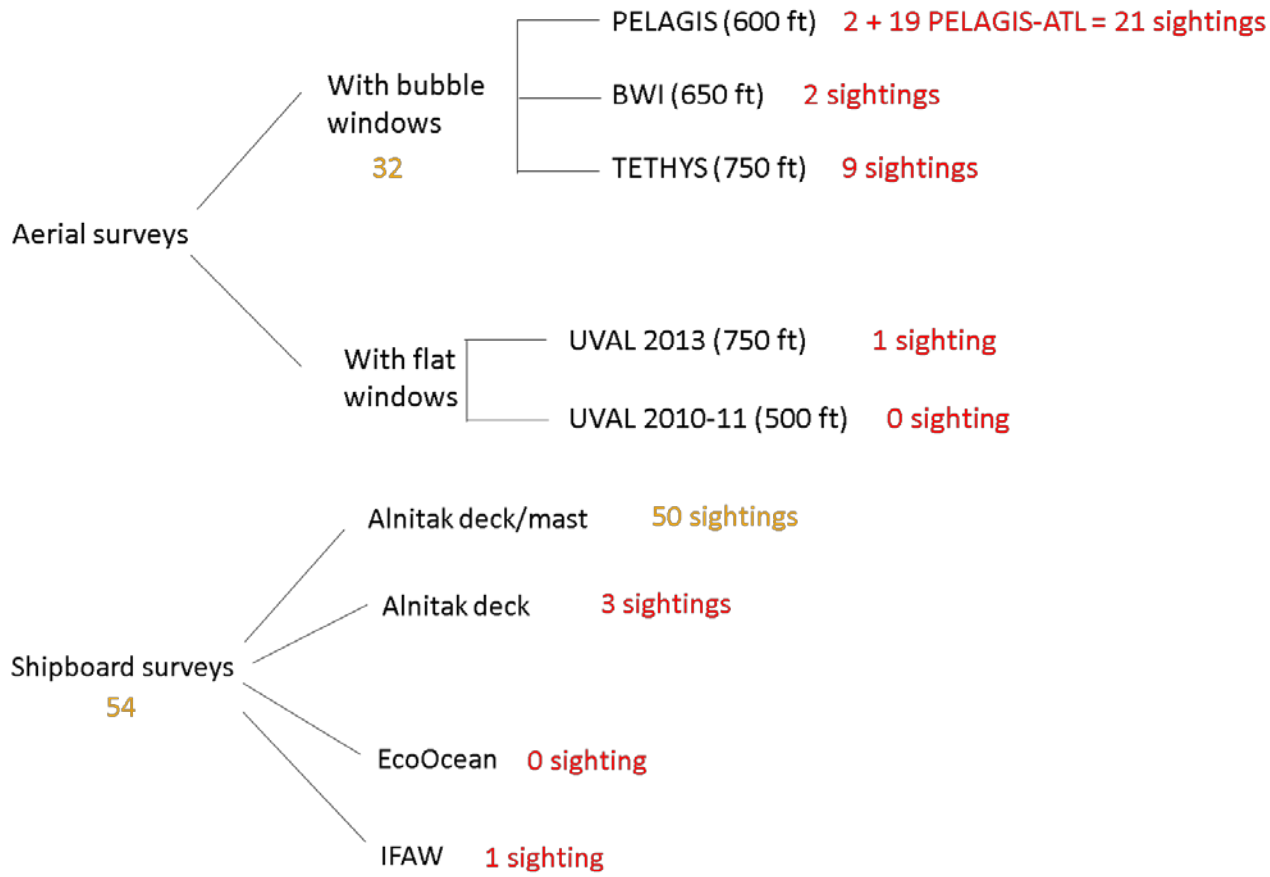

Figure A-49. Sightings hierarchies for aerial and shipboard surveys for Cuvier's beaked whale. Color coding: ≥60 sightings: green, 31-59 sightings: orange, ≤30 sightings: red. When surveys were conducted by multiple organizations (e.g., TETHYS/ISPRA), only the first survey organization listed in Table was included for brevity. UVAL refers to University of Valencia surveys. PELAGIS-ATL refers to PELAGIS surveys in the Atlantic Ocean.

Table A-8. Detection functions applied per survey to Cuvier's beaked whale sightings. Hn: half normal, Hr: hazard rate, ESHW: effective strip half width. SightedBy2 indicates if the sighting was made from the deck or from the mast in Alnitak surveys. PresenceMast indicates whether a mast observer was present in shipboard surveys. When surveys were conducted by multiple organizations (e.g., TETHYS/ISPRA), only the first survey organization listed in Table was included for brevity. UVAL refers to University of Valencia surveys.

Surveys	Surveys used for detection function fitting	Right truncation distance (m)	Left truncation distance (m)	Detection function applied	Mean ESHW (m)
PELAGIS	PELAGIS, BWI and TETHYS	800	0	Hn	403
BWI	PELAGIS, BWI and TETHYS	800	0	Hn	403
TETHYS	PELAGIS, BWI and TETHYS	800	0	Hn	403
UVAL 2013	PELAGIS, BWI and TETHYS	800	124.8	Hn	403
UVAL 2010/11	PELAGIS, BWI and TETHYS	800	83.2	Hn	403
Alnitak deck/mast	Alnitak deck/mast	2400	0	Hn Sightedby2	1083
Alnitak deck	All shipboard	2000	0	Hn PresenceMast	922
EcoOcean	All shipboard	2000	0	Hn PresenceMast	922
IFAW	All shipboard	2000	0	Hn PresenceMast	922

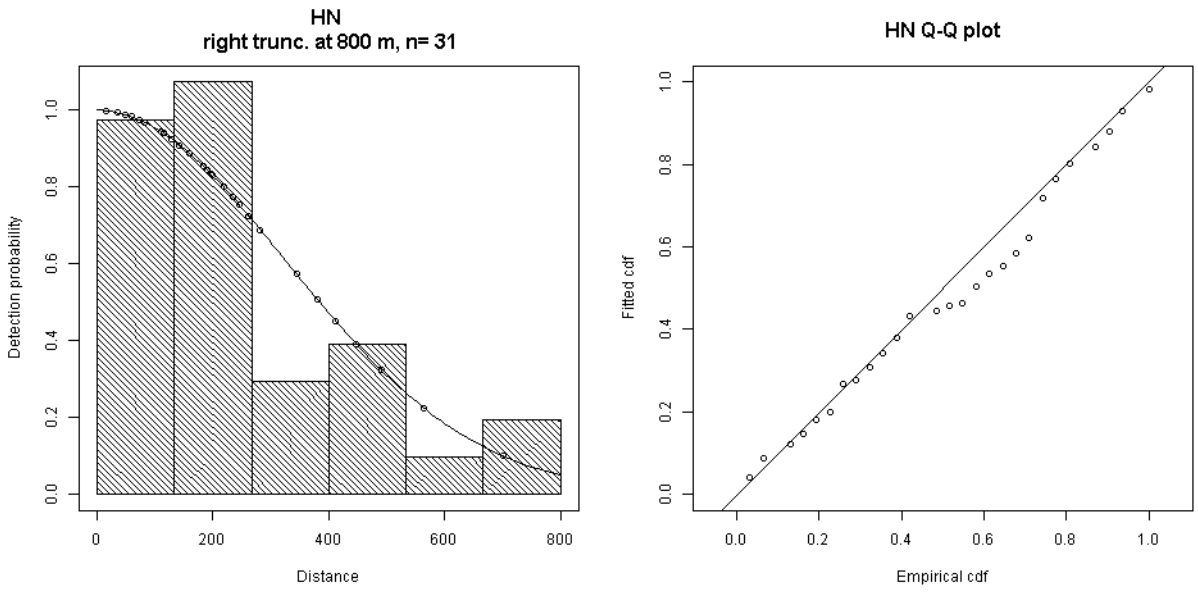

Figure A-50. Selected detection function fitted from PELAGIS, BWI and TETHYS surveys

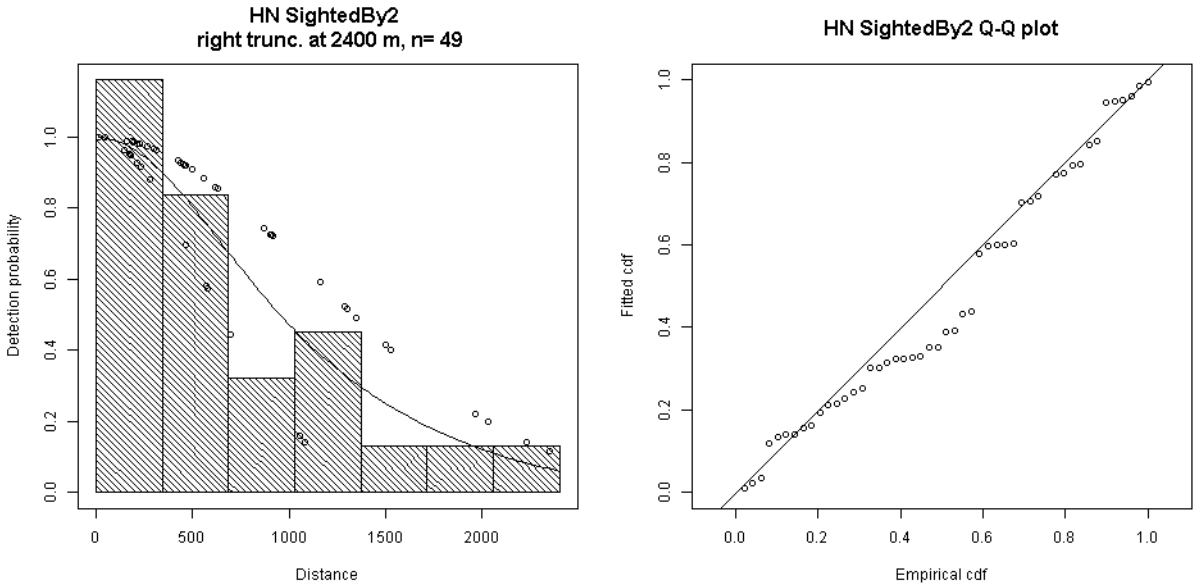

Figure A-51. Selected detection function fitted from Alnitak deck/mast surveys

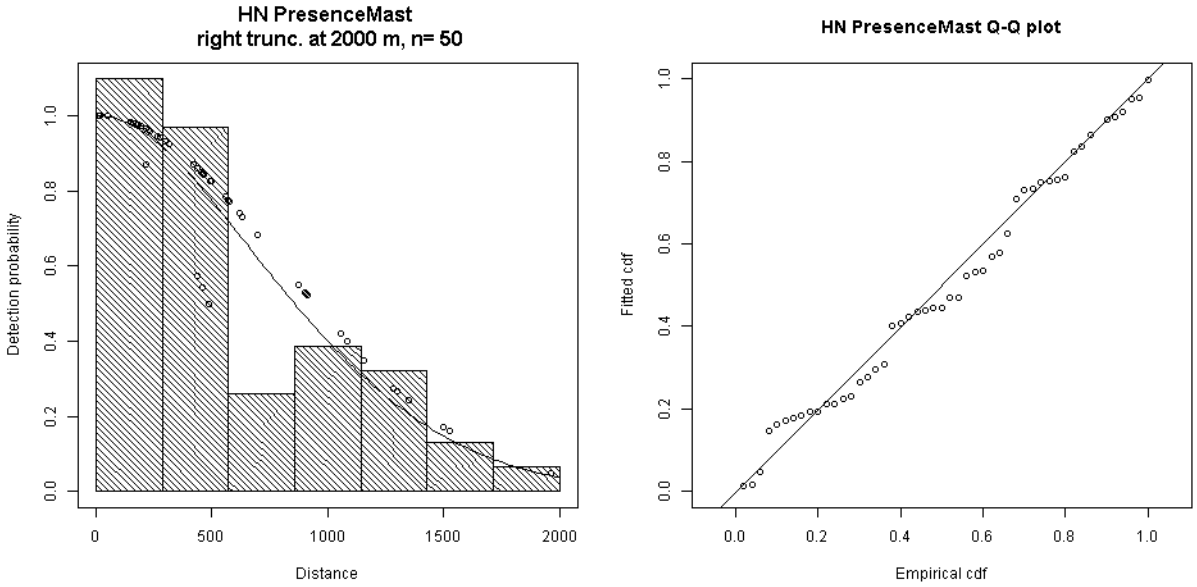

Figure A-52. Selected detection function fitted from all shipboard deck surveys

This page intentionally left blank.

B

Generalized Additive Models

This page intentionally left blank.

Appendix B: Generalized Additive Models

This appendix provides GAM summaries and GAM term plot for each species.

```
Family: Tweedie(p=1.501)
Link function: log

Formula:
Abundance ~ s(Depth, k = 4, bs = "ts") + s(NemoSSTMonthly, k = 4,
    bs = "ts") + s(VGPMMonthly, k = 4, bs = "ts") + s(SalinityMonthly,
    k = 4, bs = "ts") + offset(log(Area))

Parametric coefficients:
            Estimate Std. Error t value Pr(>|t|)
(Intercept) -0.39118    0.03379  -11.57   <2e-16 ***
---
Signif. codes:  0 ‘***’ 0.001 ‘**’ 0.01 ‘*’ 0.05 ‘.’ 0.1 ‘ ’ 1

Approximate significance of smooth terms:
                     edf Ref.df      F p-value
s(Depth)           2.985      3 378.04  <2e-16 ***
s(NemoSSTMonthly)  2.888      3  31.66  <2e-16 ***
s(VGPMMonthly)     2.687      3  30.10  <2e-16 ***
s(SalinityMonthly) 2.770      3  25.13  <2e-16 ***
---
Signif. codes:  0 ‘***’ 0.001 ‘**’ 0.01 ‘*’ 0.05 ‘.’ 0.1 ‘ ’ 1

R-sq.(adj) =  0.0174   Deviance explained = 17.9%
-REML =  21860  Scale est. = 60.727    n = 42631
```

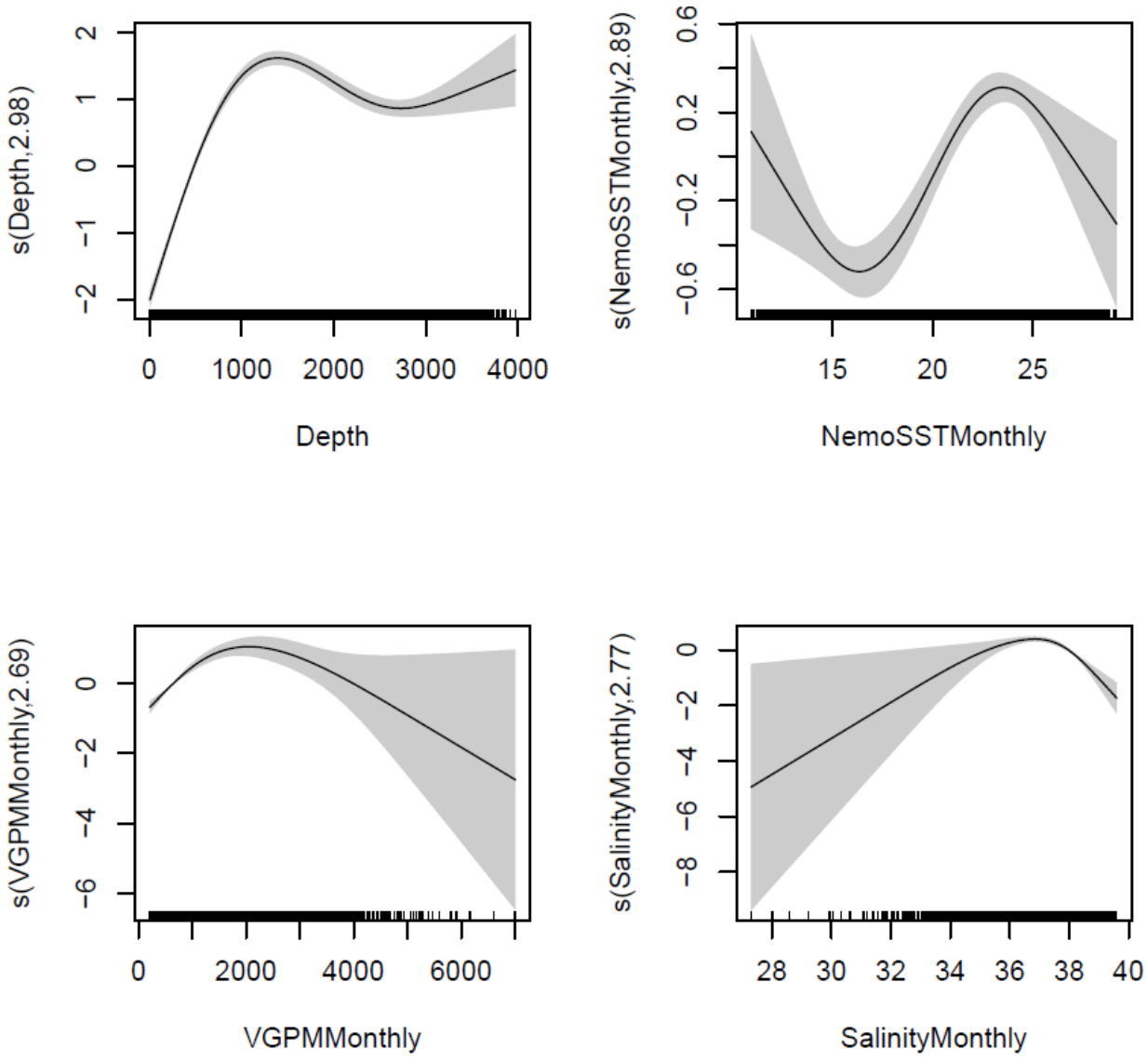

Figure B-1. GAM summary and term plots of the selected striped dolphin model.

```
Family: Tweedie(p=1.521)
Link function: log

Formula:
Abundance ~ s(Depth, k = 4, bs = "ts") + s(Slope, k = 4, bs = "ts") +
    s(SalinityMonthly, k = 4, bs = "ts") + offset(log(Area))

Parametric coefficients:
            Estimate Std. Error t value Pr(>|t|)
(Intercept) -2.72845    0.07164  -38.08   <2e-16 ***
---
Signif. codes:  0 ‘***’ 0.001 ‘**’ 0.01 ‘*’ 0.05 ‘.’ 0.1 ‘ ’ 1

Approximate significance of smooth terms:
                     edf Ref.df      F  p-value
s(Depth)           1.6838      3 45.283  < 2e-16 ***
s(Slope)           2.4691      3  7.820 3.33e-06 ***
s(SalinityMonthly) 0.9319      3  2.695  0.00252 **
---
Signif. codes:  0 ‘***’ 0.001 ‘**’ 0.01 ‘*’ 0.05 ‘.’ 0.1 ‘ ’ 1

R-sq.(adj) =  0.00729   Deviance explained = 17.3%
-REML =   5488  Scale est. = 85.987    n = 42631
```

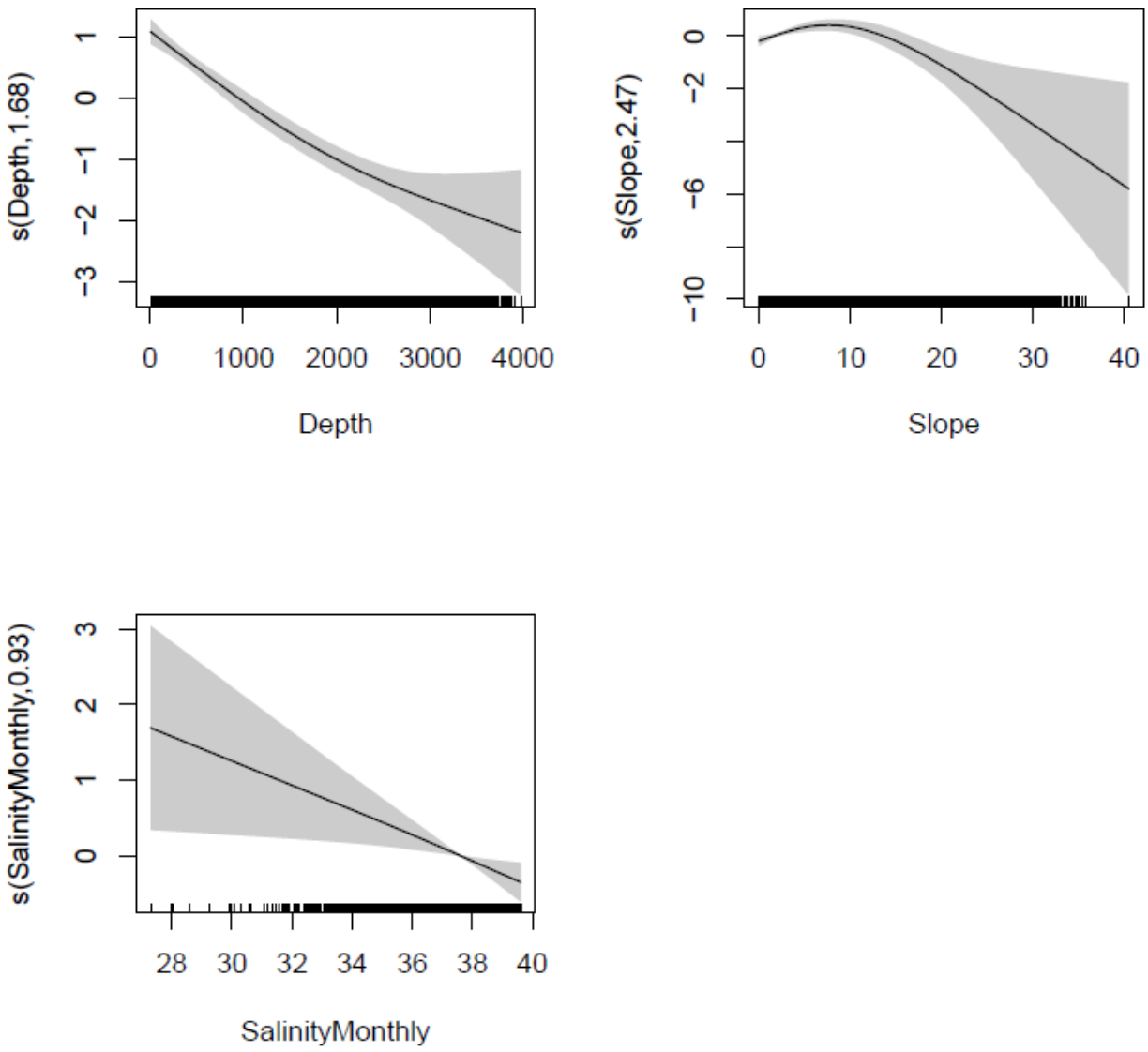

Figure B-2. GAM summary and term plots of the selected common bottlenose dolphin model.

```
Family: Tweedie(p=1.5)
Link function: log

Formula:
Abundance ~ s(Depth, k = 4, bs = "ts") + s(SSTMonthly, k = 4,
    bs = "ts") + s(SalinityMonthly, k = 4, bs = "ts") + s(OPFishMonthly5,
    k = 4, bs = "ts") + offset(log(Area))

Parametric coefficients:
            Estimate Std. Error t value Pr(>|t|)
(Intercept)  -4.2260     0.1697   -24.9   <2e-16 ***
---
Signif. codes:  0 ‘***’ 0.001 ‘**’ 0.01 ‘*’ 0.05 ‘.’ 0.1 ‘ ’ 1

Approximate significance of smooth terms:
                     edf Ref.df       F  p-value
s(Depth)           1.069      3   4.808 8.48e-05 ***
s(SSTMonthly)      2.805      3  19.481 1.89e-13 ***
s(SalinityMonthly) 2.858      3 155.207  < 2e-16 ***
s(OPFishMonthly5)  1.997      3  11.807 4.24e-09 ***
---
Signif. codes:  0 ‘***’ 0.001 ‘**’ 0.01 ‘*’ 0.05 ‘.’ 0.1 ‘ ’ 1

R-sq.(adj) =  0.0145   Deviance explained = 48.3%
-REML =   7380  Scale est. = 106.1     n = 42631
```

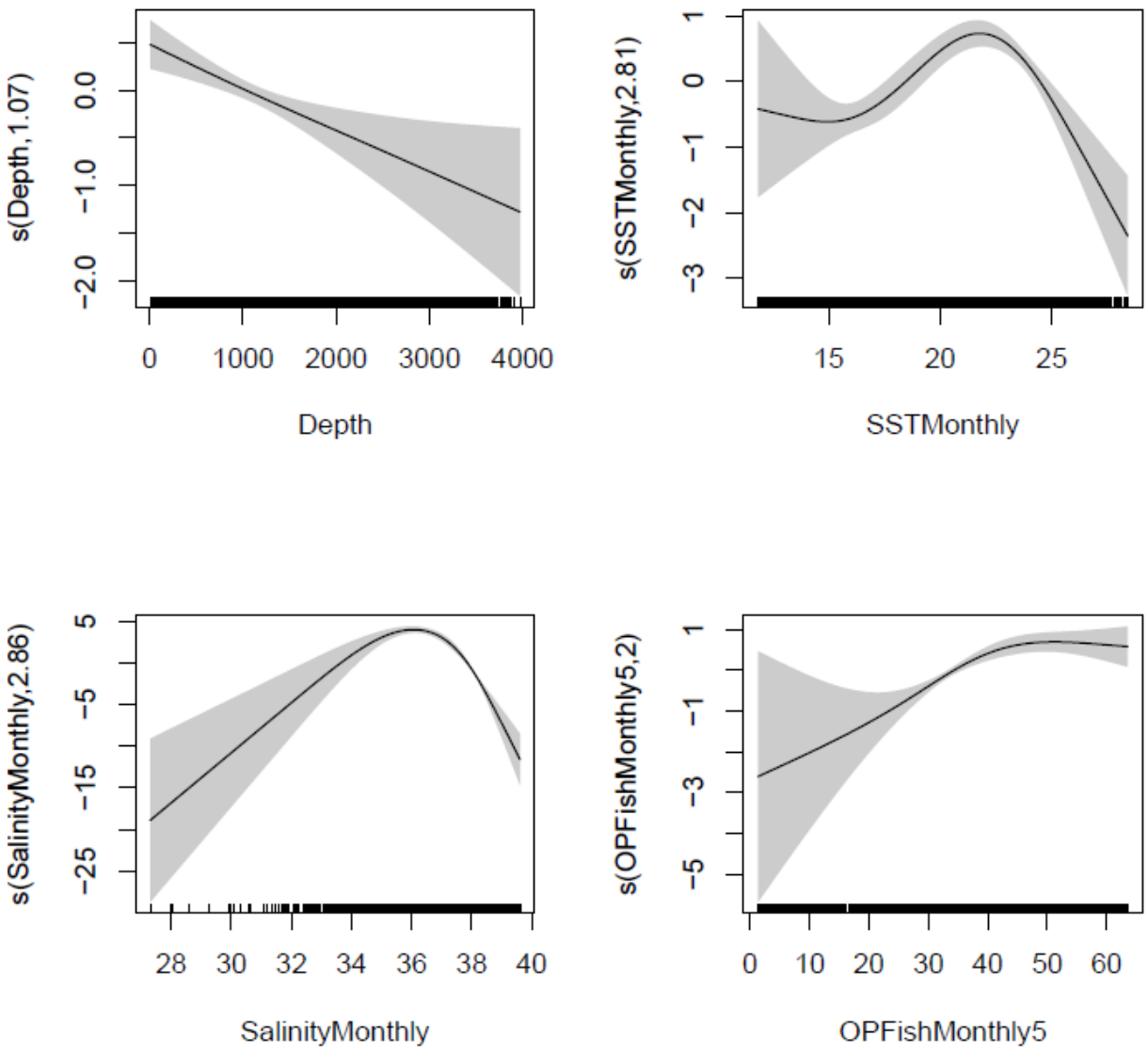

Figure B-3. GAM summary and term plots of the selected short-beaked common dolphin model.

```
Family: Tweedie(p=1.409)
Link function: log

Formula:
Abundance ~ s(Depth, k = 4, bs = "ts") + offset(log(Area))

Parametric coefficients:
            Estimate Std. Error t value Pr(>|t|)
(Intercept)  -4.6370     0.1487  -31.19   <2e-16 ***
---
Signif. codes:  0 ‘***’ 0.001 ‘**’ 0.01 ‘*’ 0.05 ‘.’ 0.1 ‘ ’ 1

Approximate significance of smooth terms:
           edf Ref.df     F  p-value
s(Depth) 2.881      3 24.34 2.53e-16 ***
---
Signif. codes:  0 ‘***’ 0.001 ‘**’ 0.01 ‘*’ 0.05 ‘.’ 0.1 ‘ ’ 1

R-sq.(adj) =  0.00143   Deviance explained = 11.5%
-REML = 1276.6  Scale est. = 132.96    n = 43177
```

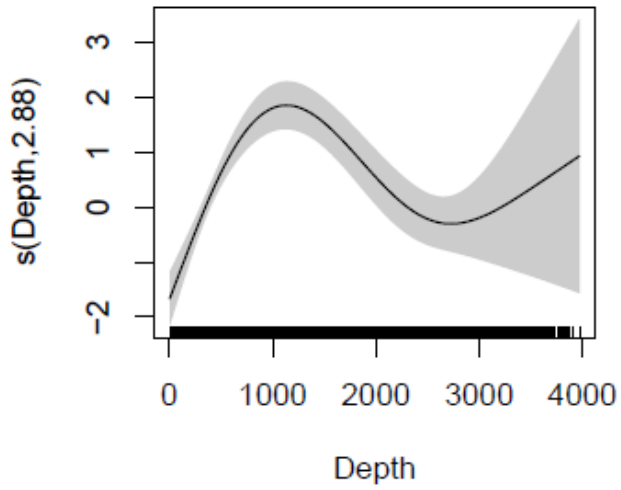

Figure B-4. GAM summary and term plots of the selected Risso's dolphin model.

```
Family: Tweedie(p=1.353)
Link function: log

Formula:
Abundance ~ s(Depth, k = 4, bs = "ts") + s(SSTMonthly, k = 4,
    bs = "ts") + s(VGPMMonthly, k = 4, bs = "ts") + s(SalinityMonthly,
    k = 4, bs = "ts") + offset(log(Area))

Parametric coefficients:
            Estimate Std. Error t value Pr(>|t|)
(Intercept)   -4.978      0.167   -29.8   <2e-16 ***
---
Signif. codes:  0 ‘***’ 0.001 ‘**’ 0.01 ‘*’ 0.05 ‘.’ 0.1 ‘ ’ 1

Approximate significance of smooth terms:
                     edf Ref.df      F  p-value
s(Depth)           2.947      3 87.240  < 2e-16 ***
s(SSTMonthly)      1.110      3  4.879 7.31e-05 ***
s(VGPMMonthly)     2.078      3  6.008 6.54e-05 ***
s(SalinityMonthly) 2.904      3 65.507  < 2e-16 ***
---
Signif. codes:  0 ‘***’ 0.001 ‘**’ 0.01 ‘*’ 0.05 ‘.’ 0.1 ‘ ’ 1

R-sq.(adj) =  0.0152   Deviance explained = 44.5%
-REML = 3246.8  Scale est. = 70.314    n = 42631
```

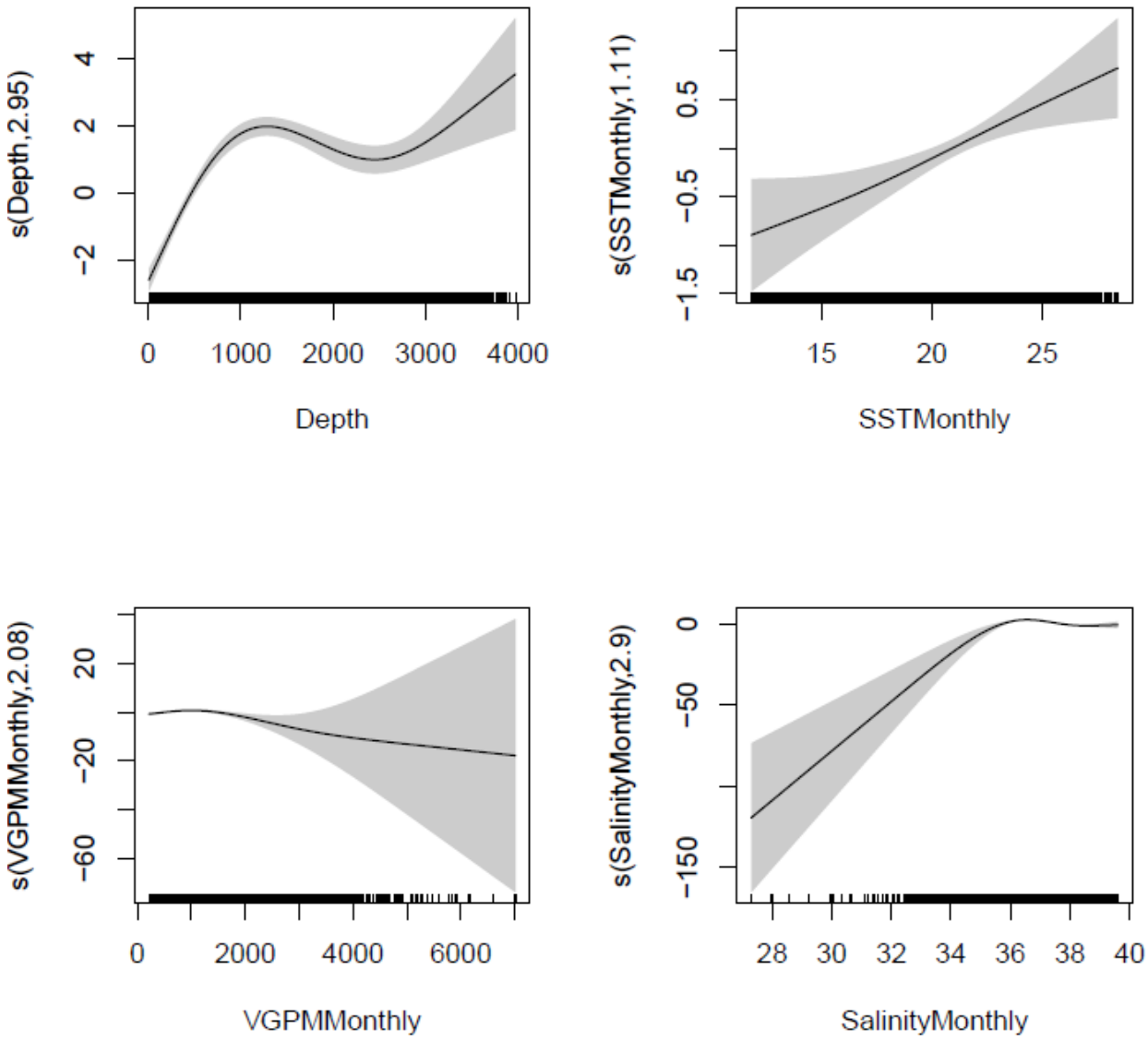

Figure B-5. GAM summary and term plots of the selected long-finned pilot whale.

```
Family: Tweedie(p=1.181)
Link function: log

Formula:
Abundance ~ s(Depth, k = 4, bs = "ts") + s(Slope, k = 4, bs = "ts") +
    s(SalinityMonthly, k = 4, bs = "ts") + s(OPFishMonthly5,
    k = 4, bs = "ts") + offset(log(Area))

Parametric coefficients:
            Estimate Std. Error t value Pr(>|t|)
(Intercept)  -6.1330     0.1062  -57.77   <2e-16 ***
---
Signif. codes:  0 ‘***’ 0.001 ‘**’ 0.01 ‘*’ 0.05 ‘.’ 0.1 ‘ ’ 1

Approximate significance of smooth terms:
                     edf Ref.df      F  p-value
s(Depth)           2.758      3 56.892  < 2e-16 ***
s(Slope)           2.679      3 19.331 7.84e-14 ***
s(SalinityMonthly) 1.001      3  6.366 6.94e-06 ***
s(OPFishMonthly5)  2.487      3 26.969  < 2e-16 ***
---
Signif. codes:  0 ‘***’ 0.001 ‘**’ 0.01 ‘*’ 0.05 ‘.’ 0.1 ‘ ’ 1

R-sq.(adj) =  0.0192   Deviance explained = 23.8%
-REML = 2582.2  Scale est. = 10.805    n = 42631
```

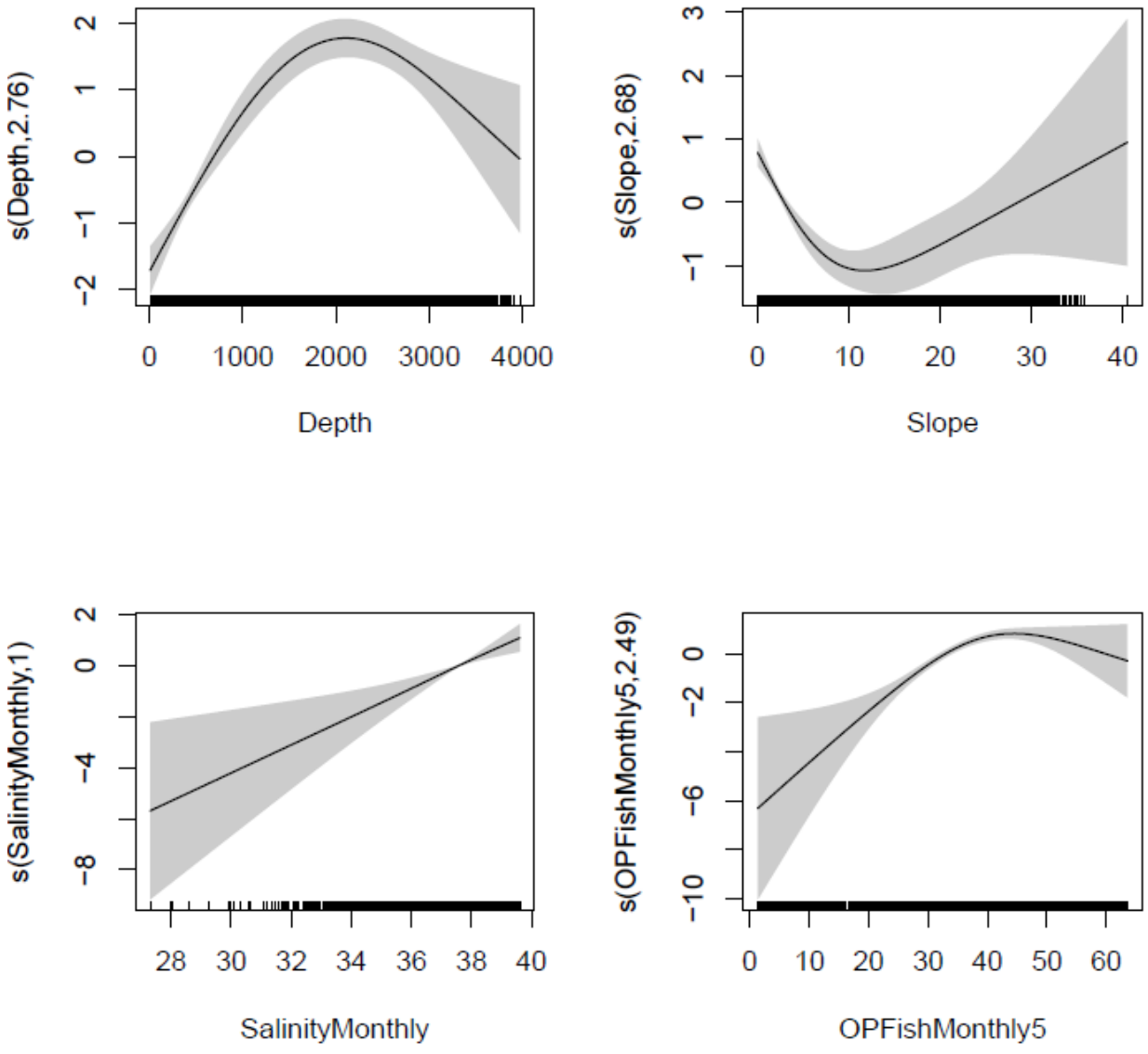

Figure B-6. GAM summary and term plots of the selected fin whale.

```
Family: Tweedie(p=1.366)
Link function: log

Formula:
Abundance ~ s(Depth, k = 4, bs = "ts") + s(NPPMonthly, k = 4,
    bs = "ts") + s(OPFishMonthly3, k = 4, bs = "ts") + offset(log(Area))

Parametric coefficients:
            Estimate Std. Error t value Pr(>|t|)
(Intercept)  -6.3621     0.2241  -28.39   <2e-16 ***
---
Signif. codes:  0 ‘***’ 0.001 ‘**’ 0.01 ‘*’ 0.05 ‘.’ 0.1 ‘ ’ 1

Approximate significance of smooth terms:
                     edf Ref.df      F  p-value
s(Depth)          2.6893      3 20.831 9.59e-15 ***
s(NPPMonthly)     0.9215      3  3.746 0.000426 ***
s(OPFishMonthly3) 2.3759      3  6.570 3.75e-05 ***
---
Signif. codes:  0 ‘***’ 0.001 ‘**’ 0.01 ‘*’ 0.05 ‘.’ 0.1 ‘ ’ 1

R-sq.(adj) =  0.0017   Deviance explained =   22%
-REML = 1018.7  Scale est. = 90.149    n = 42631
```

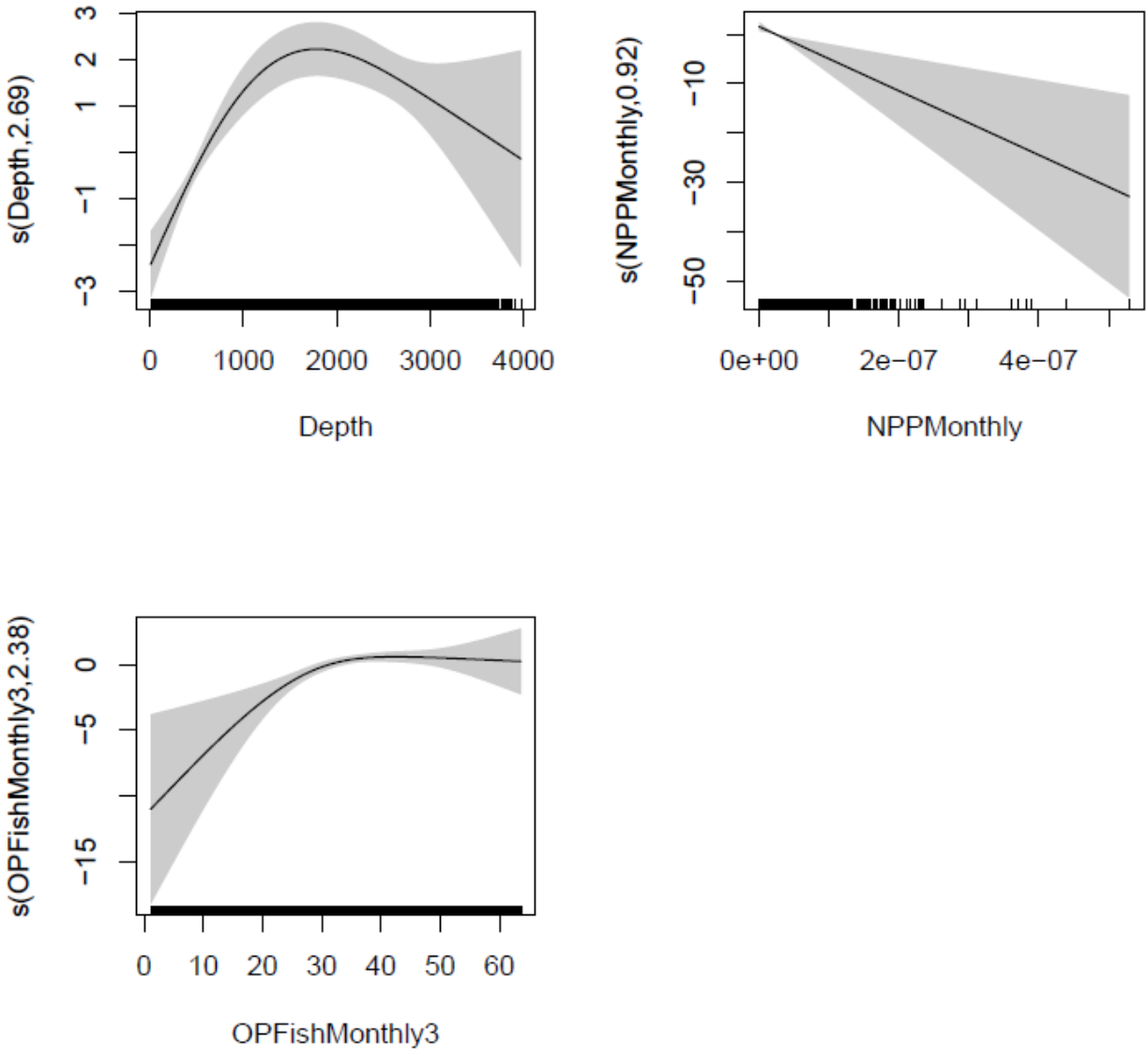

Figure B-7. GAM summary and term plots of the selected sperm whale model

```
Family: Tweedie(p=1.41)
Link function: log

Formula:
Abundance ~ s(Depth, k = 4, bs = "ts") + s(Slope, k = 4, bs = "ts") +
    offset(log(Area))

Parametric coefficients:
            Estimate Std. Error t value Pr(>|t|)
(Intercept)  -8.4662     0.4687  -18.06   <2e-16 ***
---
Signif. codes:  0 ‘***’ 0.001 ‘**’ 0.01 ‘*’ 0.05 ‘.’ 0.1 ‘ ’ 1

Approximate significance of smooth terms:
           edf Ref.df      F  p-value
s(Depth) 2.927      3 32.899  < 2e-16 ***
s(Slope) 1.004      3  6.668 4.65e-06 ***
---
Signif. codes:  0 ‘***’ 0.001 ‘**’ 0.01 ‘*’ 0.05 ‘.’ 0.1 ‘ ’ 1

R-sq.(adj) =  0.00261   Deviance explained = 36.2%
-REML = 652.18  Scale est. = 93.369    n = 43177
```

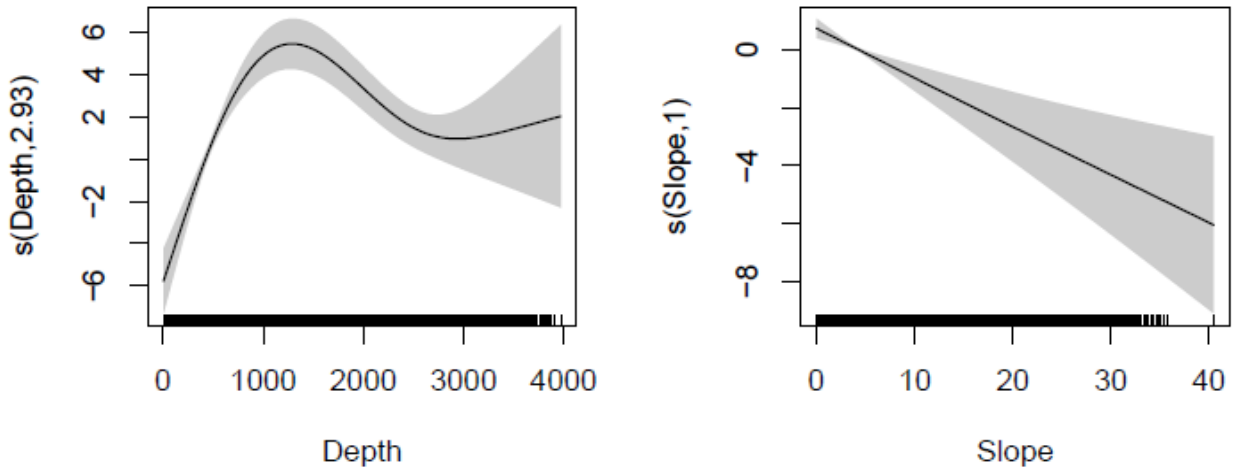

Figure B-8. GAM summary and term plots of the selected Cuvier's beaked whale model.

C

Monthly Densitologies

This page intentionally left blank.

Appendix C: Monthly Densitologies

This appendix shows maps of monthly densitologies and coefficients of variation for each species. Results are not provided for Risso's dolphin or Cuvier's beaked whale as these species were modeled with static covariates only.

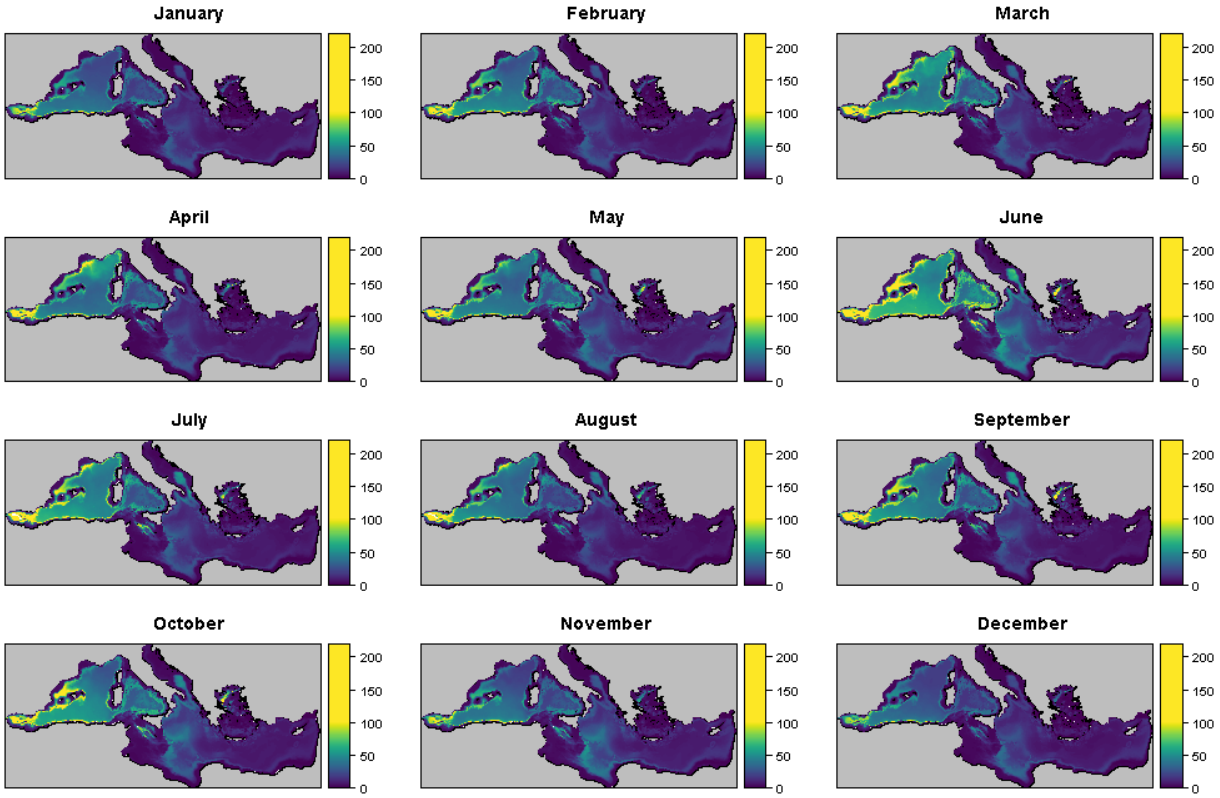

Figure C-1. Maps of monthly densitologies (individuals per 25 km^2) for striped dolphin.

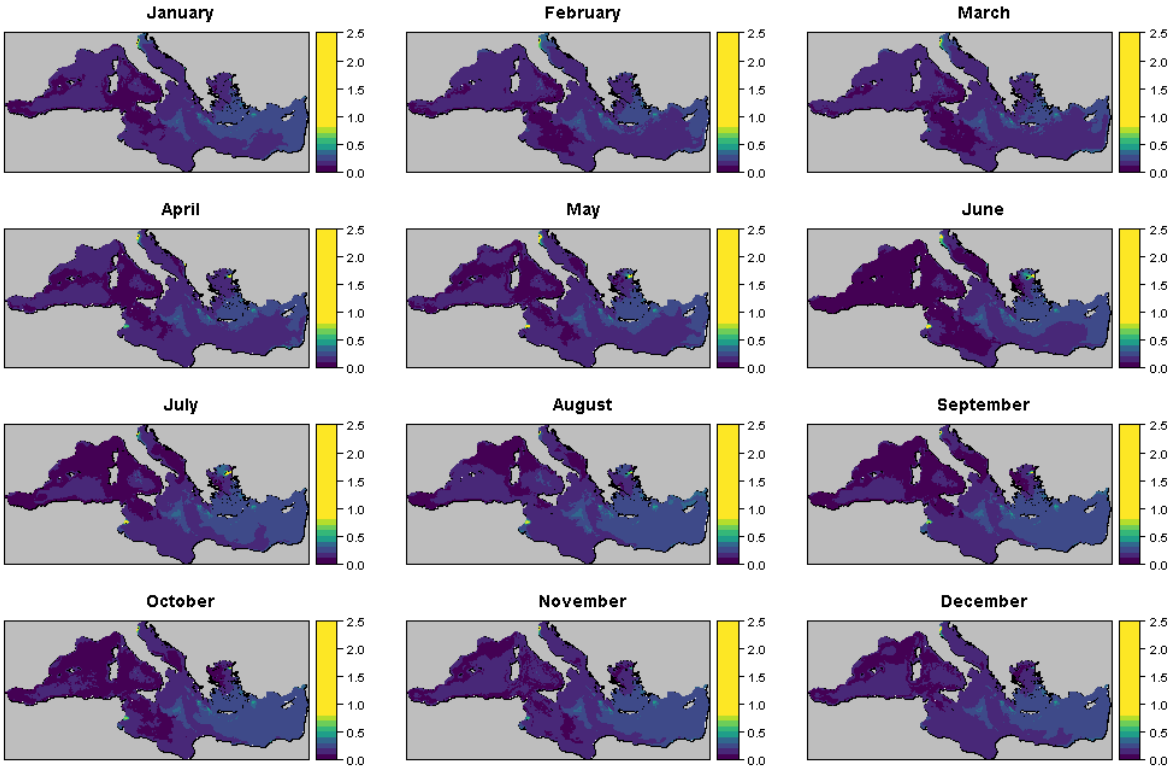

Figure C-2. Maps of monthly predicted CVs for striped dolphin.

Table C-1. Total monthly predicted abundances of striped dolphins and associated CVs in the entire Mediterranean Sea. Note that mean predicted abundances are not corrected for perception bias, and CVs only incorporate spatial uncertainty.

Month	Total predicted abundance (individuals)	CV
January	1,517,636	0.15
February	1,790,534	0.15
March	2,064,045	0.15
April	1,875,025	0.14
May	2,062,345	0.14
June	2,814,166	0.14
July	2,171,980	0.15
August	1,742,655	0.17
September	1,954,178	0.16
October	2,179,204	0.15
November	1,792,995	0.15
December	1,439,381	0.15

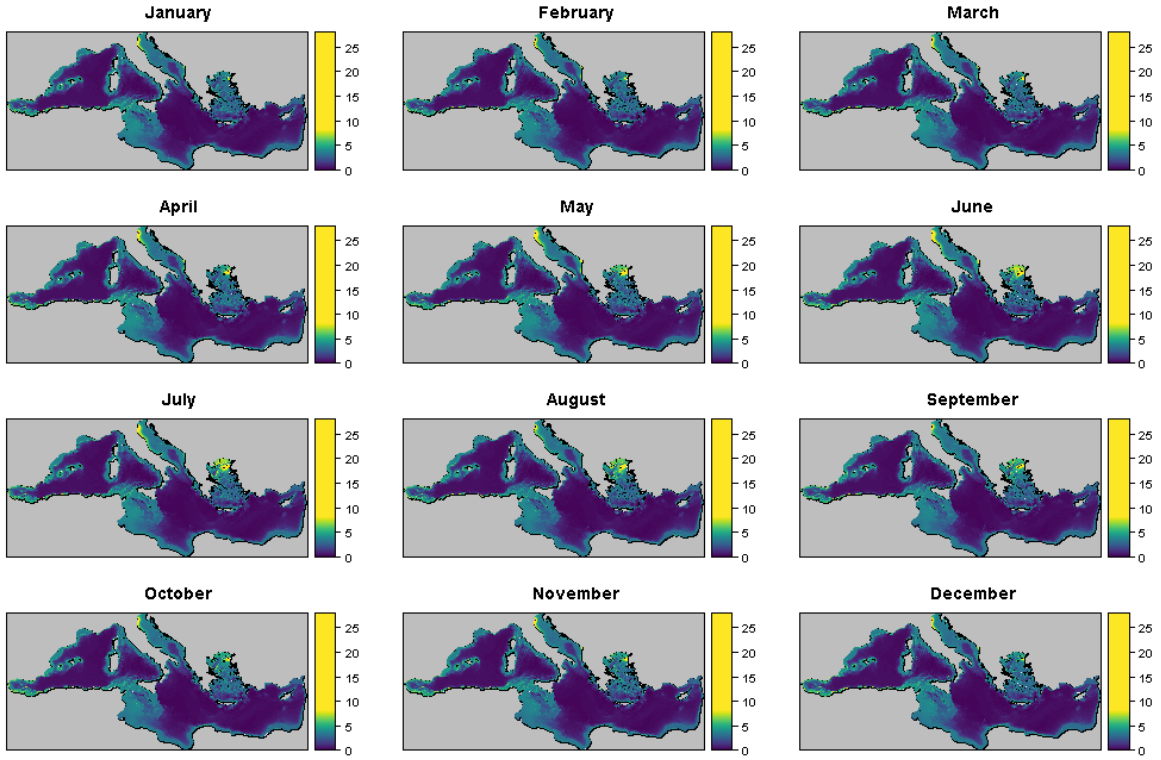

Figure C-3. Maps of monthly densitologies (individuals per 25 km^2) for common bottlenose dolphin.

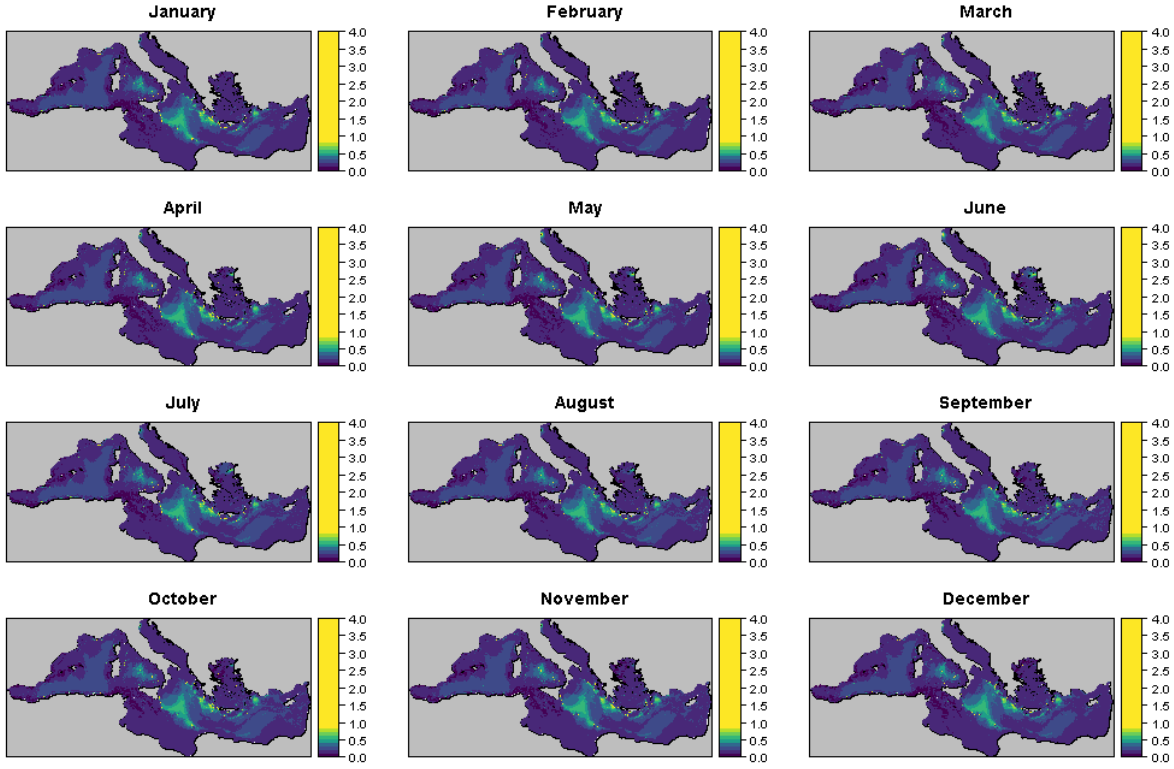

Figure C-4. Maps of monthly predicted CVs for common bottlenose dolphin.

Table C-2. Total monthly predicted abundances of common bottlenose dolphins and associated CVs in the entire Mediterranean Sea. Note that mean predicted abundances are not corrected for perception bias, and CVs only incorporate spatial uncertainty.

Month	Total predicted abundance (individuals)	CV
January	163,269	0.19
February	163,397	0.19
March	164,561	0.19
April	167,095	0.19
May	169,856	0.19
June	170,695	0.19
July	168,004	0.20
August	165,048	0.20
September	163,329	0.20
October	162,928	0.20
November	162,849	0.19
December	162,803	0.19

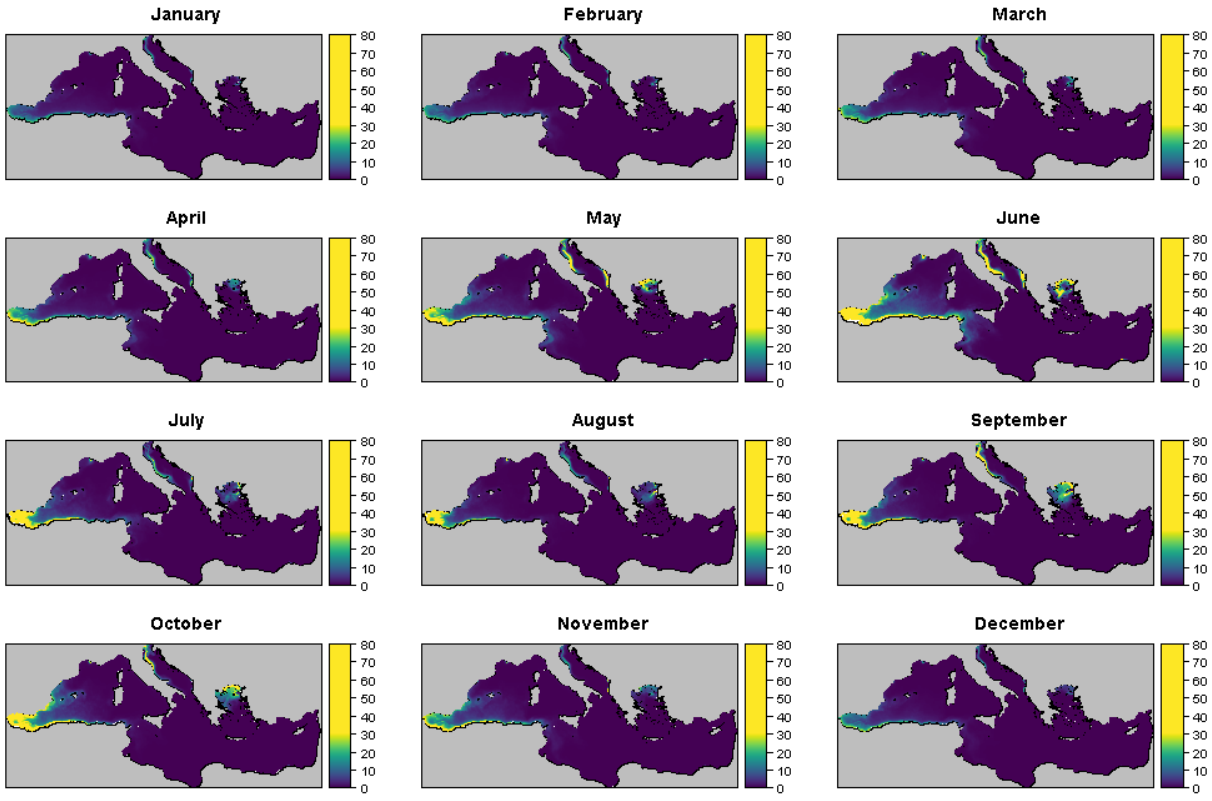

Figure C-5. Maps of monthly densitologies (individuals per 25 km^2) for short-beaked common dolphin.

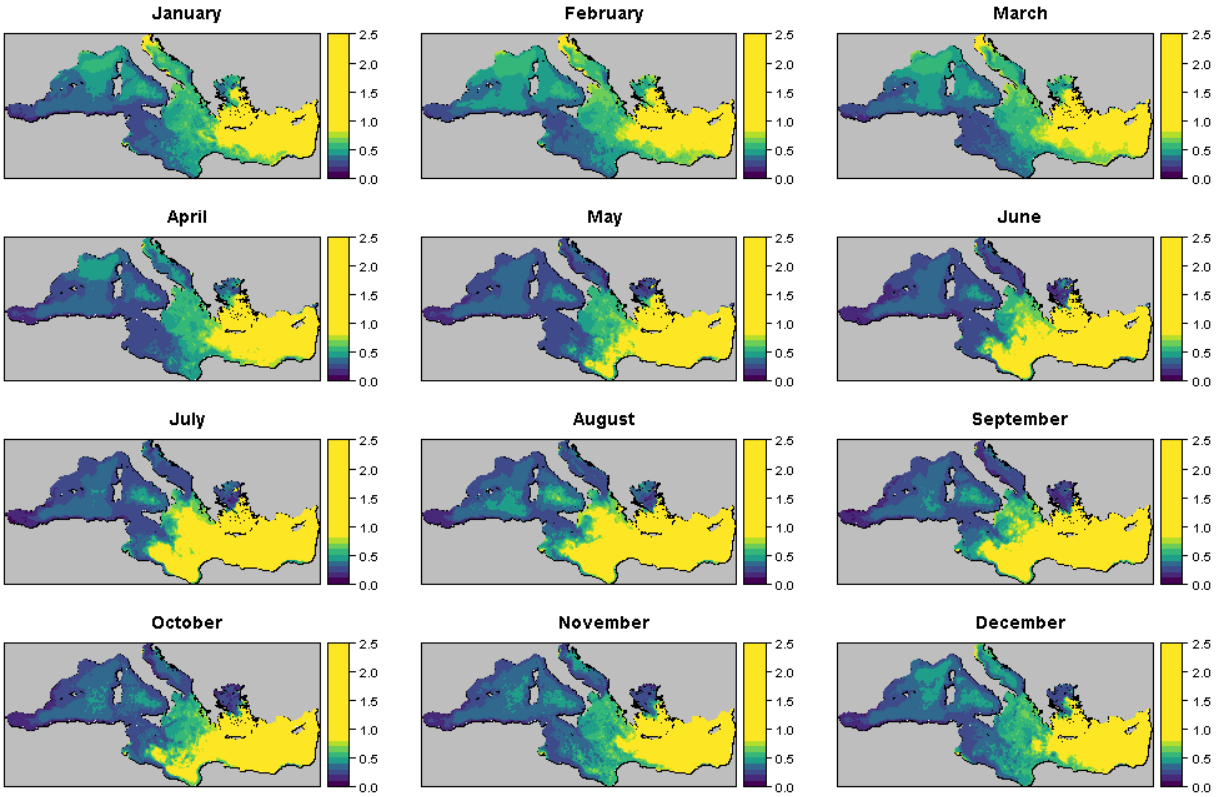

Figure C-6. Maps of monthly predicted CVs for short-beaked common dolphin.

Table C-3: Total monthly predicted abundances of short-beaked common dolphins and associated CVs in the entire Mediterranean Sea. Note that mean predicted abundances are not corrected for perception bias, and CVs only incorporate spatial uncertainty.

Month	Total predicted abundance (individuals)	CV
January	63,744	0.59
February	73,477	0.60
March	92,611	0.58
April	113,965	0.54
May	211,876	0.61
June	371,702	0.72
July	216,318	0.82
August	147,117	0.86
September	221,112	0.81
October	247,242	0.71
November	138,985	0.61
December	75,991	0.59

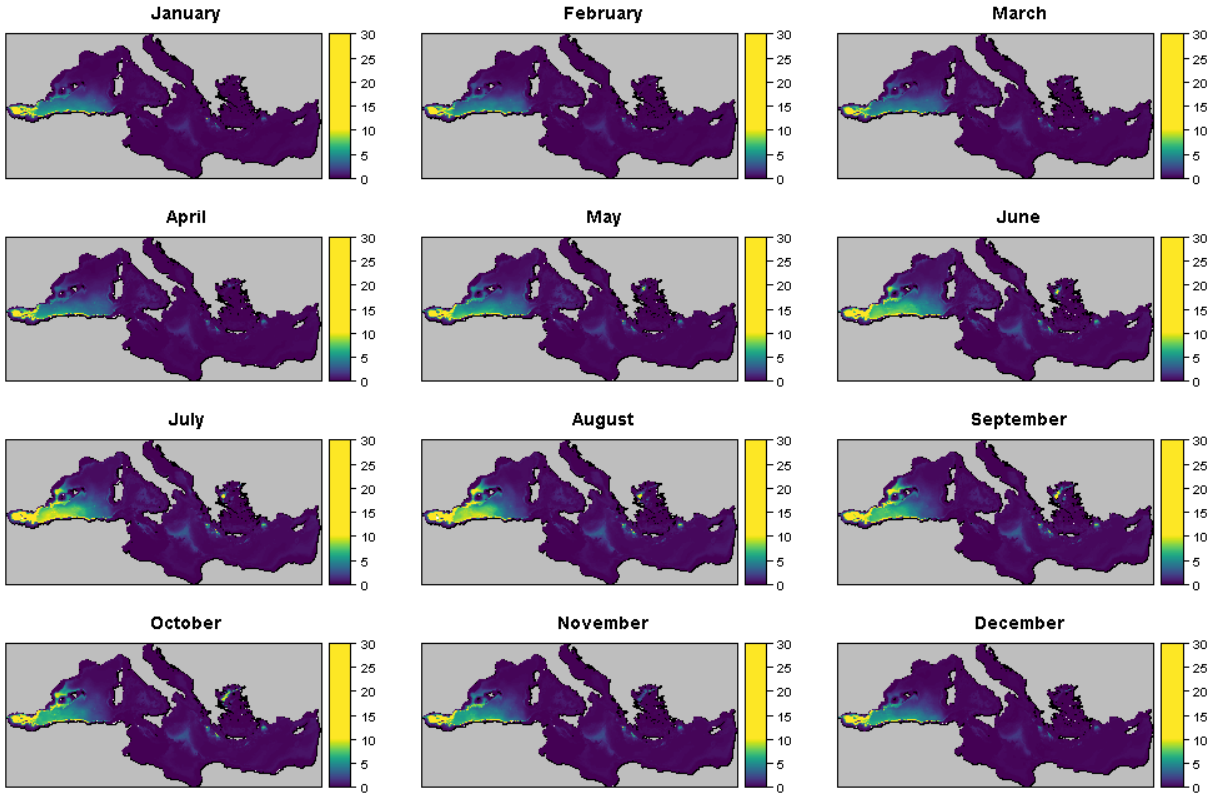

Figure C-7. Maps of monthly densitologies (individuals per 25 km^2) for long-finned pilot whale.

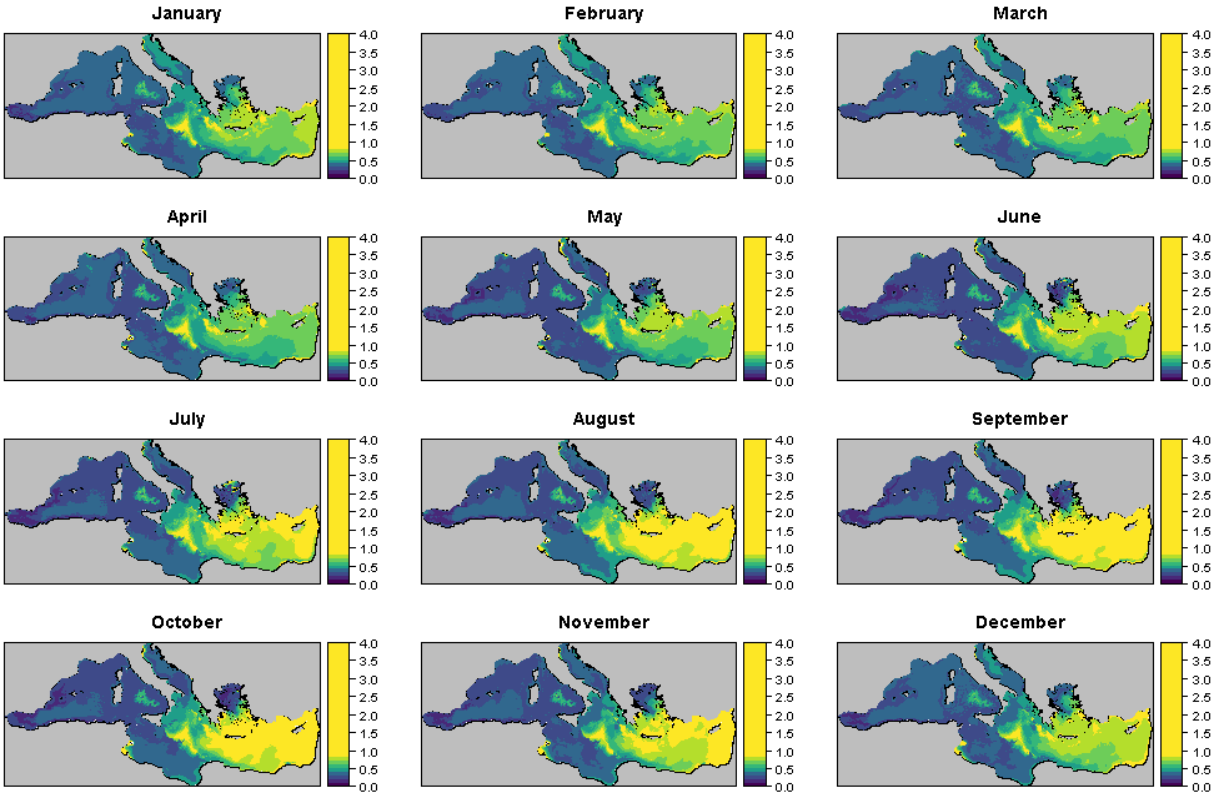

Figure C-8. Maps of monthly predicted CVs for long-finned pilot whale.

Table C-4. Total monthly predicted abundances of long-finned pilot whale and associated CVs in the entire Mediterranean Sea. Note that mean predicted abundances are not corrected for perception bias, and CVs only incorporate spatial uncertainty.

Month	Total predicted abundance (individuals)	CV
January	61,081	0.47
February	60,004	0.46
March	59,489	0.46
April	64,517	0.46
May	82,081	0.48
June	104,391	0.47
July	113,201	0.50
August	109,622	0.52
September	98,284	0.52
October	87,366	0.50
November	76,819	0.49
December	65,099	0.48

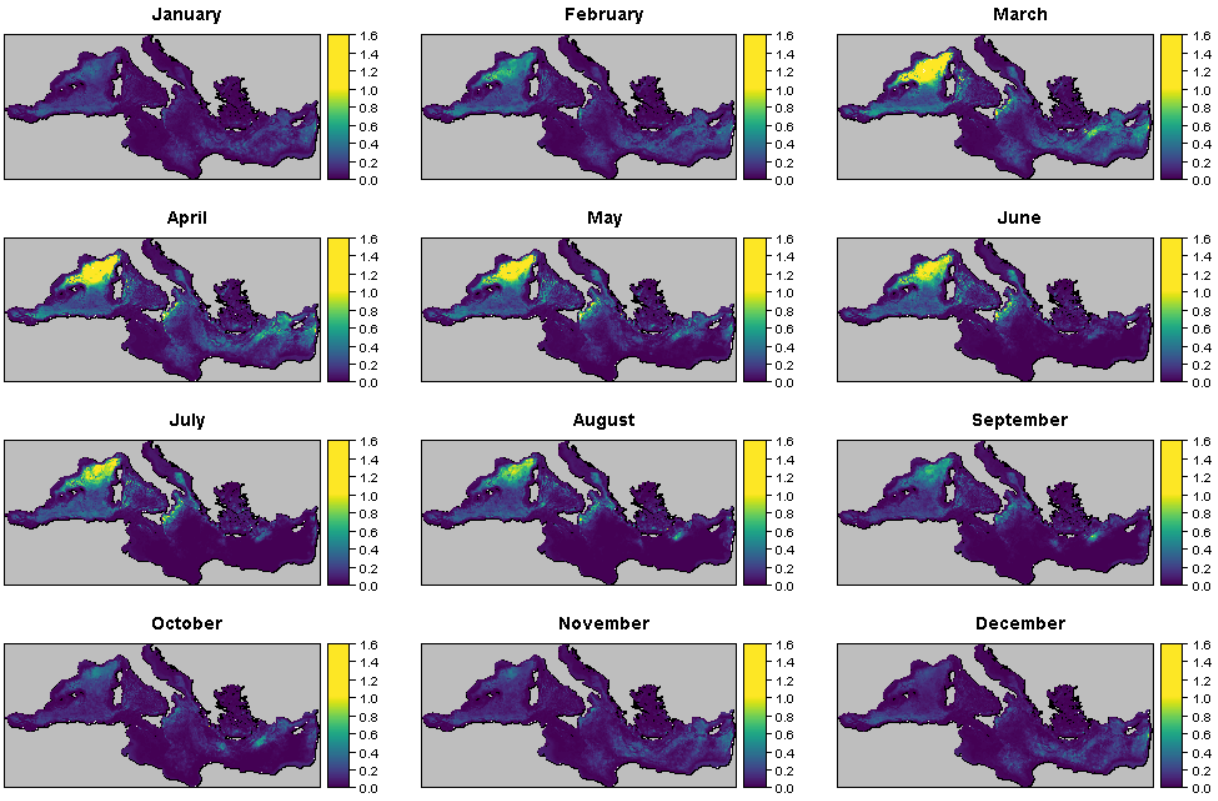

Figure C-9. Maps of monthly densitologies (individuals per 25 km^2) for fin whale.

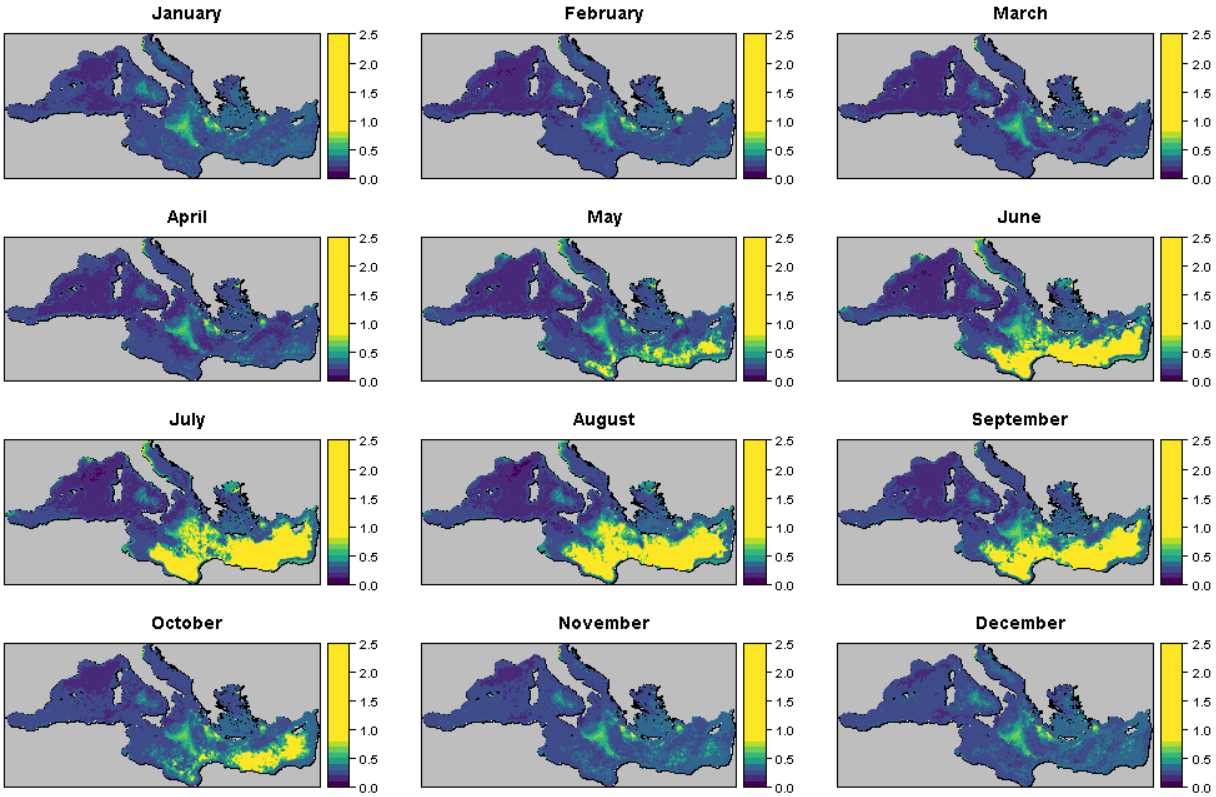

Figure C-10 Maps of monthly predicted CVs for fin whale.

Table C-5. Total monthly predicted abundances of fin whale and associated CVs in the entire Mediterranean Sea. Note that mean predicted abundances are not corrected for perception bias, and CVs only incorporate spatial uncertainty.

Month	Total predicted abundance (individuals)	CV
January	7,652	0.28
February	11,472	0.26
March	19,086	0.24
April	18,274	0.25
May	14,703	0.31
June	12,212	0.45
July	11,153	0.53
August	9,489	0.52
September	7,805	0.48
October	6,908	0.35
November	7,552	0.29
December	7,050	0.29

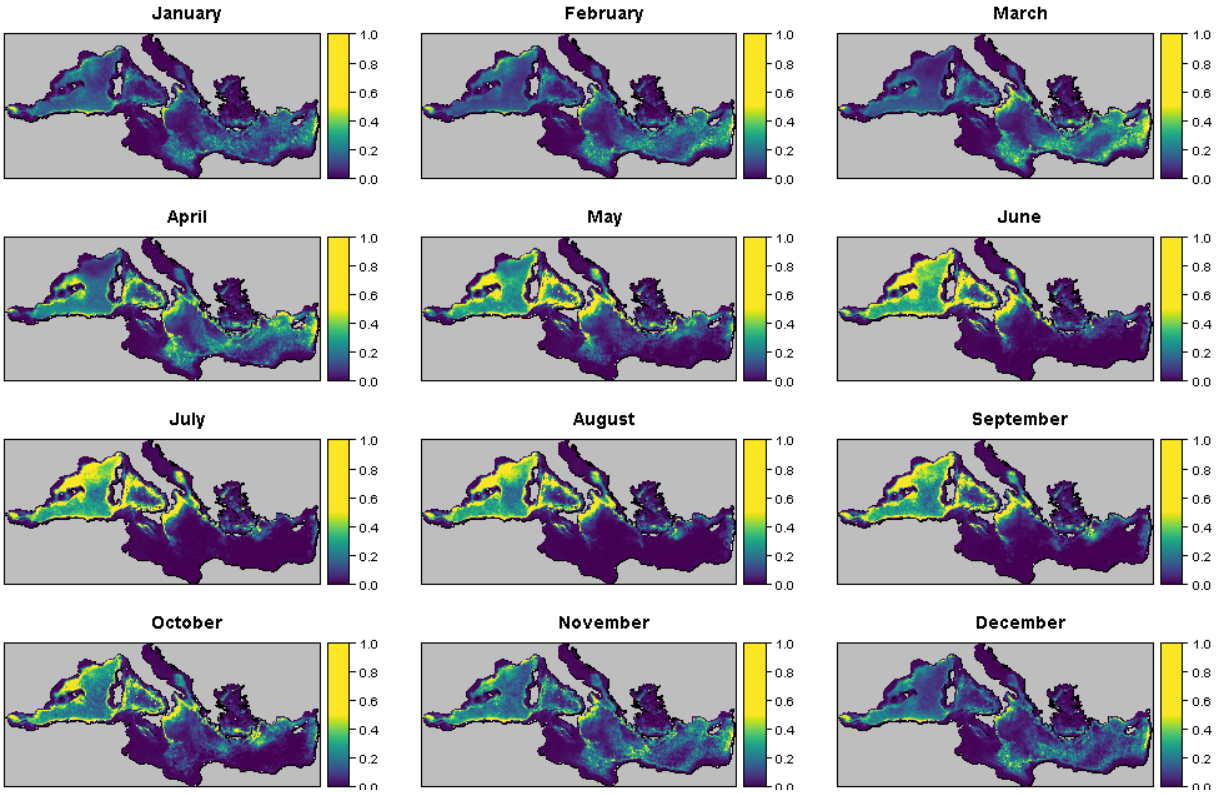

Figure C-11. Maps of monthly densitologies (individuals per 25 km^2) for sperm whale.

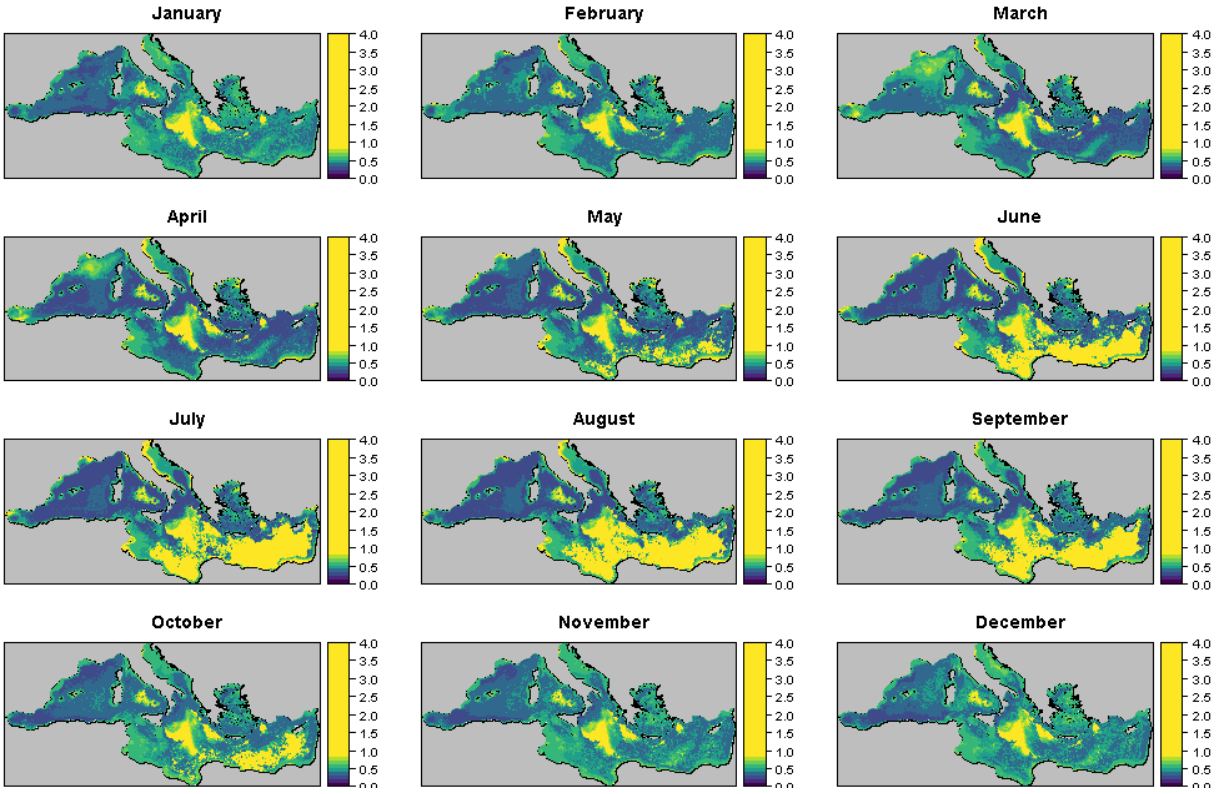

Figure C-12. Maps of monthly predicted CVs for sperm whale.

Table C-6. Total monthly predicted abundances of sperm whale and associated CVs in the entire Mediterranean Sea. Note that mean predicted abundances are not corrected for perception bias, and CVs only incorporate spatial uncertainty.

Month	Total predicted abundance (individuals)	CV
January	9,888	0.47
February	10,968	0.45
March	12,071	0.45
April	13,939	0.43
May	15,007	0.47
June	14,301	0.67
July	13,696	0.81
August	12,922	0.77
September	13,209	0.74
October	12,902	0.53
November	13,128	0.46
December	10,422	0.47